Geodesy and Geospatial Engineering

GNSS & Positionning

Earth Observation

Reality Capture

Data Science, Informatics

Forschung in Geodäsie und Geoinformatik an der Uni.lu

Prof. Dr.-Ing. Felix Norman Teferle

Geodesy and Geospatial Engineering
Civil and Environmental Engineering
Department of Engineering
University of Luxembourg

uni.lu UNIVERSITÉ DU LUXEMBOURG

Geodesy is …

Fundamental for monitoring climate change

Dr. Rajendra Pachauri, Chairman of the Intergovernmental Panel on Climate Change, commented about geodesy at a recent climate symposium in Ny-Ålesund, Svalbard.

PHOTO: IPCC

ARCTIC: IPCC Chairman Dr. Rajendra Pachauri supports the work on a draft UN resolution on global geodesy

"Geodetic Earth observation contributes significantly to strengthen the study of our changing planet and provides valuable information to policy makers who are exploring ways to address climate change," Dr. Pachauri said.

The geodesists around the globe measure and define the Earth's shape, rotation and gravitation and changes to these. Geodetic Earth observation provides a coordinate reference frame for the whole planet, which is fundamental for monitoring changes to the Earth.

Dr. Pachauri said UN-GGIM and the Global Geodetic Reference Frame Working Group are making important contributions to scientific understanding.

"I was gratified to learn about their work on a draft UN resolution on global geodesy," he said. "Their work is making a vital contribution to our understanding of climate change."

Geodesy and Geospatial Engineering

Prof. Dr.-Ing. Felix Norman TEFERLE

Dr. Addisu HUNEGNAW (FNR PDR 1/2023)
Dr. Abdul Awal MD NURUNNABI (FEDER PDR 3/2023)
Ms. Arghavan AKBARIEH (FEDER PhD <2/2023)

Mr. Eshetu Nega ERKIHUNE (UL PhD 2020-2024)
Mr. Peter MARX (self-funded PhD 2020-2024)
Mr. Shahoriar PARVAZ (FNR PhD 2022-2026)
Mr. Haseeb UR REHMAN (FNR PhD 2022-2026)

High-Precision Monitoring, 3D Data Capture, Data Science and AI, and Construction Informatics in Geoscience and Engineering

GNSS & Positionning

Earth Observation

Reality Capture

Data Science, Informatics

Technologies/Methods Development/Application

- GNSS Positioning
- Terrestrial Surveying
- Laser Scanning and Digital Photogrammetry
- SAR Remote Sensing
- Construction Informatics
- Geographical Information Systems
- High Performance Computing
- Machine Learning and Statistical Analyses
- Numerical Weather Prediction Modelling

Current Scientific Applications

- GNSS global crustal deformation monitoring for sea level and geodynamic studies
- GNSS meteorology for severe weather and climate change monitoring
- BIM and information model exchange in civil engineering, architecture and cultural heritage
- Digital models (terrain, built assets, cities …) for hazard modelling and resources management
- Deep Learning for classification, segmentation and modelling in geospatial data analyses

GNSS global crustal deformation monitoring for sea level and geodynamic studies

Geodesy and Geospatial Engineering

We operate a Network of GNSS Stations in the South Atlantic Ocean

- at GLOSS tide gauges:
  - South Georgia and the South Sandwich Islands
  - Republic of Namibia (Walvis Bay and Lüderitz);
  - Ascension, St Helena and Tristan da Cunha

- to further knowledge of sea level change, geodynamics and atmospheric sciences

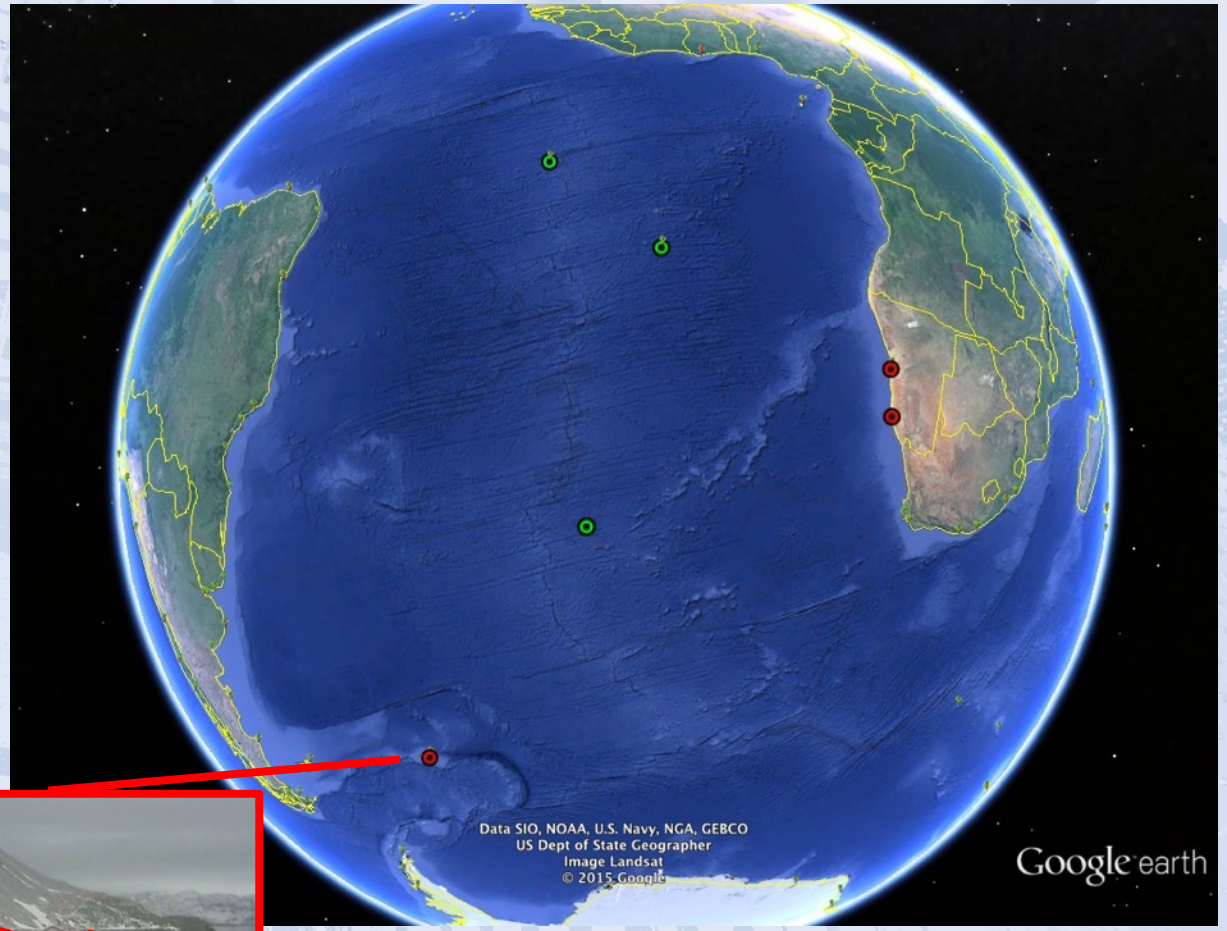

Geodesy and Geospatial Engineering

UNIVERSITÉ DU LUXEMBOURG

National Oceanography Centre
NATURAL ENVIRONMENT RESEARCH COUNCIL

UTIG

THE UNIVERSITY OF MEMPHIS
Center for Earthquake Research and Information

NSF

Vertical Land Movements and Sea Level Changes on South Georgia, South Atlantic Ocean: Results from 7 Years of Geodetic and Oceanographic Observations on a Remote Island

F.N. Teferle[1], A. Hunegnaw[1], A. Hibbert[2],

S.D.P. Williams[2] , P.L. Woodworth[2], I.W.D. Dalziel[3],

R. Smalley[4] and L. Lawver[3]

[1]*University of Luxembourg, Geodesy and Geospatial Engineering, Department of Engineering, Luxembourg*

[2]*National Oceanography Centre, Liverpool, United Kingdom*

[3]*University of Texas at Austin, Jackson School of Geosciences, USA*

[4]*University of Memphis, Center for Earthquake Research and Information, USA*

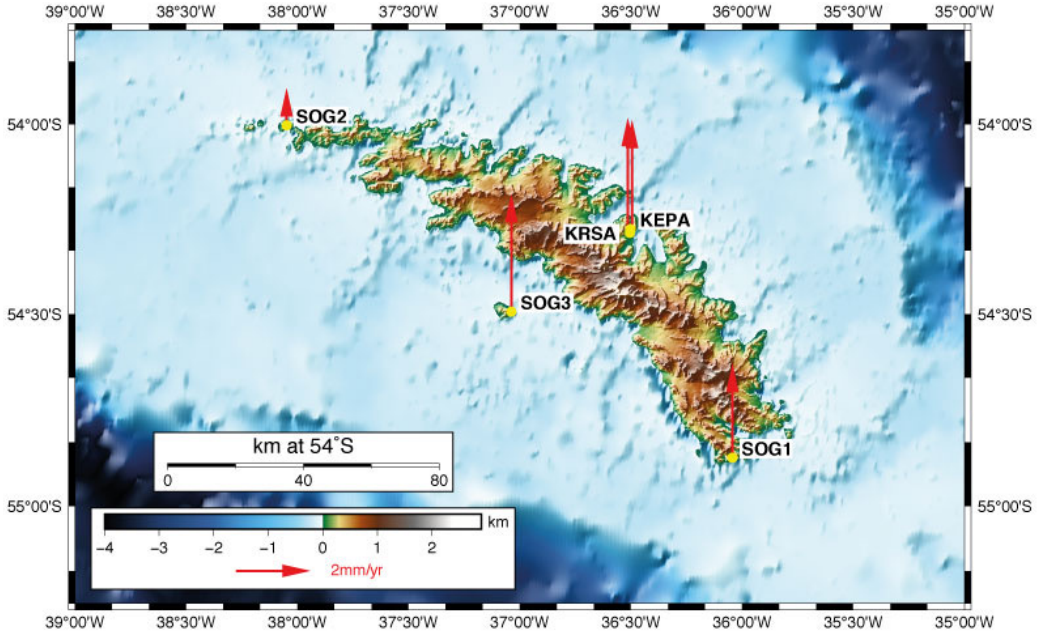

AGU FALL MEETING
Online Everywhere | 1–17 December 2020

Abstract ID: 743158, **Final Paper Number:** G022-04
Session Date and Time: Wednesday, 16 December 2020, 05:30 – 06:30 PST (UTC -8)
Session Number and Title: G022: The Global Geodetic Observing System: Resilient Infrastructure for Sustainable Scientific Activities

UK South Atlantic Tide Gauge (TG) Network

- Established since 1985
- British Overseas Territories (BOTs) and Antarctica
- Affords long sea level records from an under-sampled region
- Used for:
  - Monitoring Antarctic Circumpolar Current (ACC) variability
  - ‘Ground truthing’ satellite altimetry
  - Understanding climate variability on various timescales incl. longer term changes
  - Design and testing of tide gauge (TG) equipment for remote and hostile locations
- GNSS @ TG to provide vertical land movement corrections for MSL!

South Georgia is a subantarctic island between the South Atlantic and Southern Ocean, which is largely covered by glaciers with only its northeast coastal areas being snow-free during the Austral summer.

- Size approximately 170 km x 45 km
- Uninhabited expect for personnel at two research stations:
  - King Edward Point (KEP)
  - Bird Island
- Marine environment is extremely rich in nutrients and supports incredible and uniq biodiversity

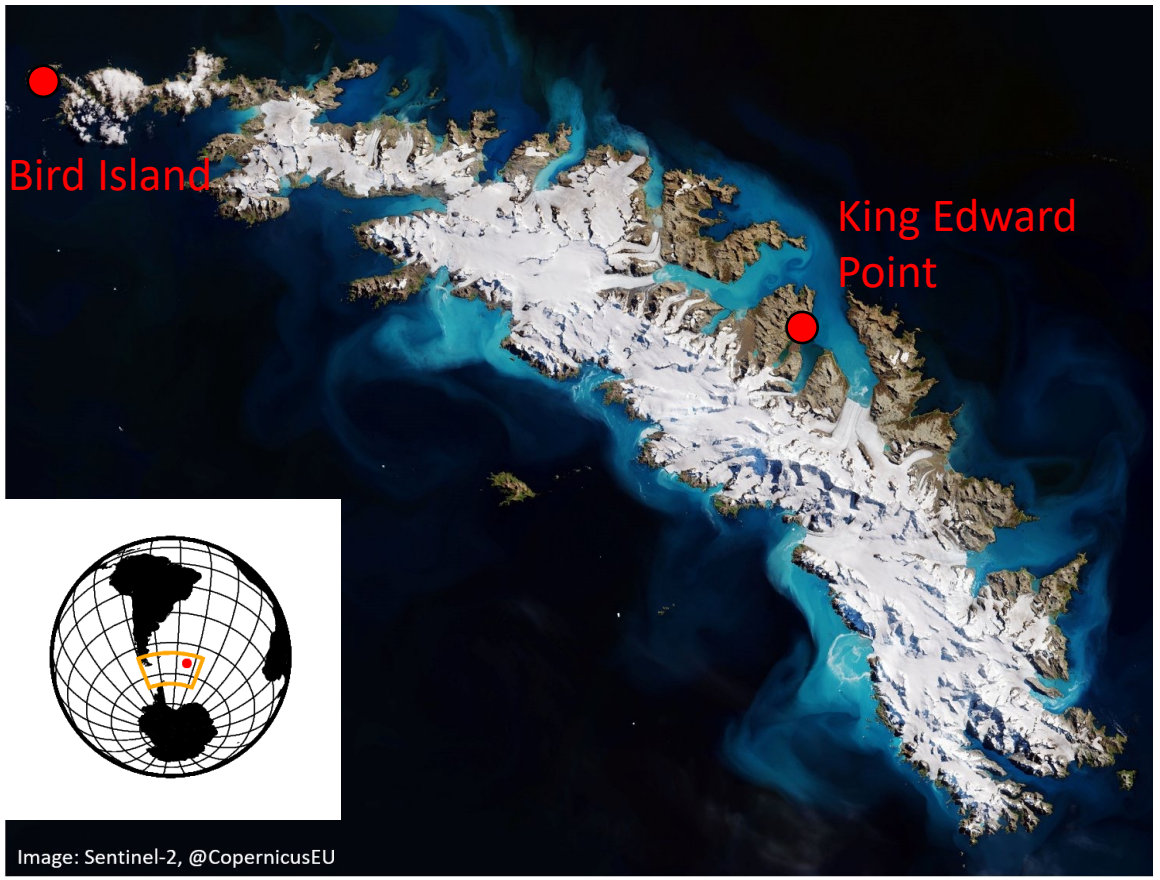

South Georgia provides an outpost in a largely under-sampled region of the globe that is of critical importance to the global climatic system.

- Zone of the **westerly winds**, which affect regional weather and climate (see poster presentation Erkihune et al., session G010-12)
- Barrier to the **Antarctic Circumpolar Current (ACC)**, which is a driver of the global thermohaline circulation and, thus, of the global climate
- Associated with the ACC is the **Antarctic Convergence**, where colder Antarctic and warmer sub-Antarctic water masses meet. This results in an upwelling of nutrients, which in turn, stimulates biodiversity

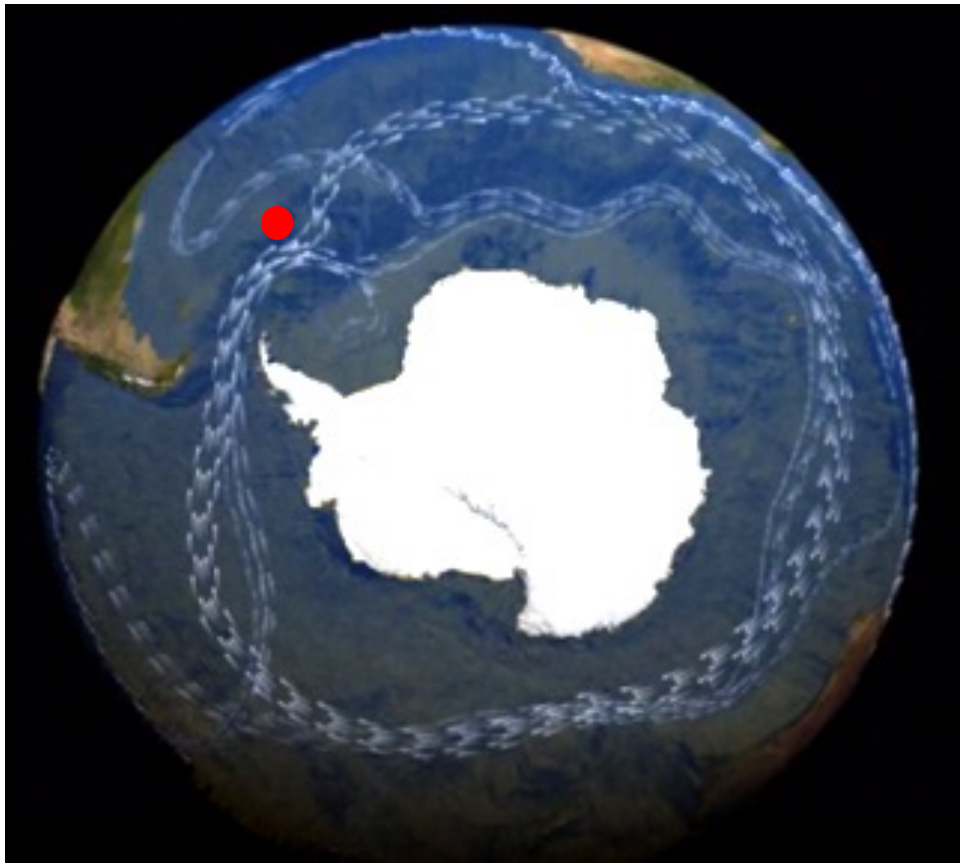

Wikipedia (2020)

The South Georgia Microcontinent lies between the South American Plate (SAM) and Scotia Plate (SCO) in a tectonically active region.

- The overall tectonic setting is well understood
- There is less agreement on the details
  - How did the SGM get to its location?
  - How does it move in between the SAM and SCO plates?
  - Why is it 3000 m in altitude?

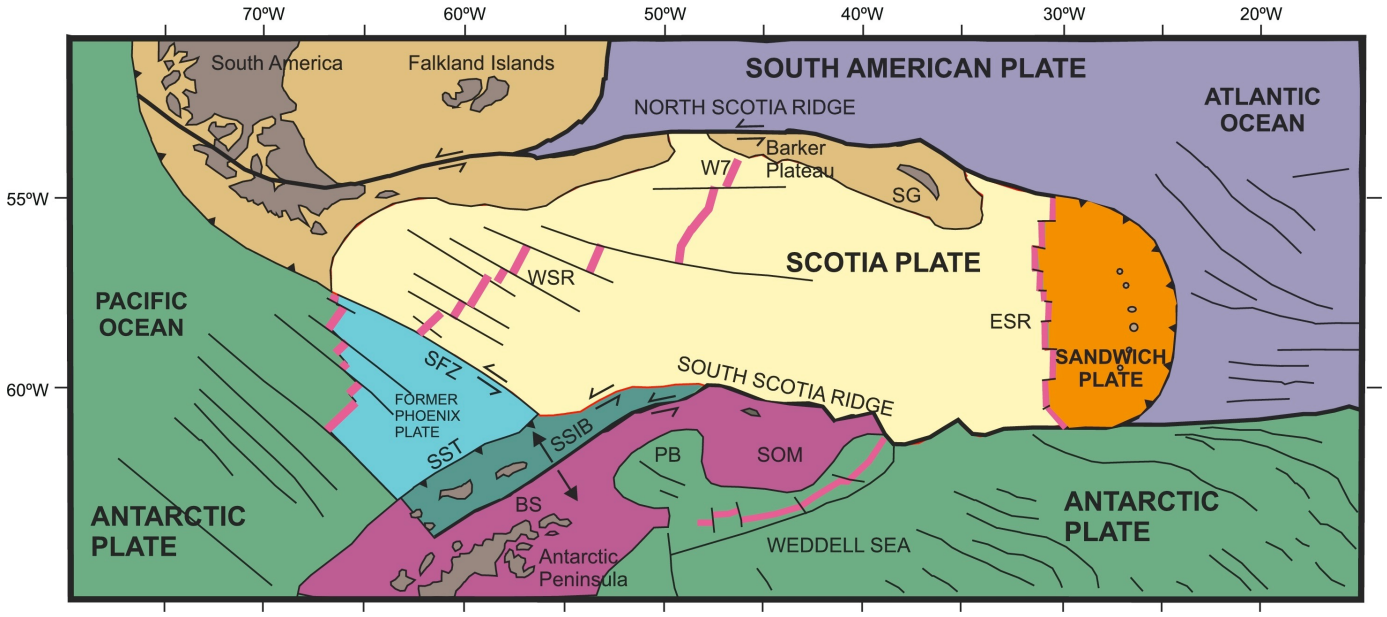

Tectonic setting of the Scotia Plate. WSR: West Scotia Ridge; ESR: East Scotia Ridge; SOM: South Orkney microcontinent; PB: Powell Basin; SST: South Shetland trough; BS: Bransfield Strait; SFZ: Shackleton fracture zone; SSIB: South Shetland Islands Block; SG: South Georgia. Adapted from Riley et. al. (2019).

Why monitor Vertical Land Movements at Tide Gauges ?

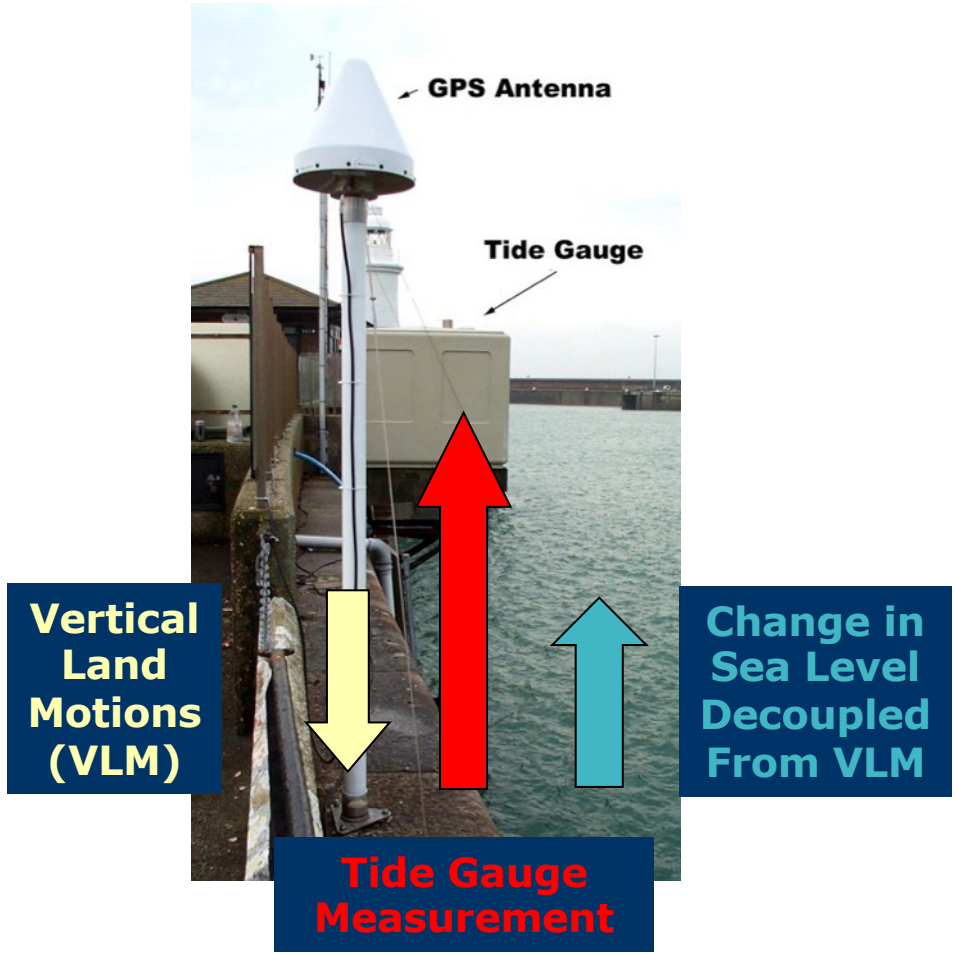

- Tide gauges (TG) measure local sea level
- Vertical land movements (VLM) are determined from GNSS at or close to the tide gauge
- The change in sea level de-coupled from VLM can be inferred:
  SLR = MSL + VLM

The continuous GNSS Stations KEPA and KRSA

GNSS antenna and mast with unobstructed sky view on top of Brown Mt. Solar power system, enclosures with batteries and electronics, structural frame, radio antenna and weather station in 30m distance to mast. Antenna location on bedrock but some multipath from reflective rock surface below antenna.

GNSS antenna and mast with obstructed sky due to Mt. Duse. Mains power and communications to KEP radio room in 120 m distance. Many problems since early 2017 with not all data having been recoverable. Antenna location on concrete monument in gravel beds.

Further GNSS Installations

- Consortium of the University of Texas at Austin and Memphis University
- NSF Project
- Installed 3 stations in late 2014
- At periphery of main island

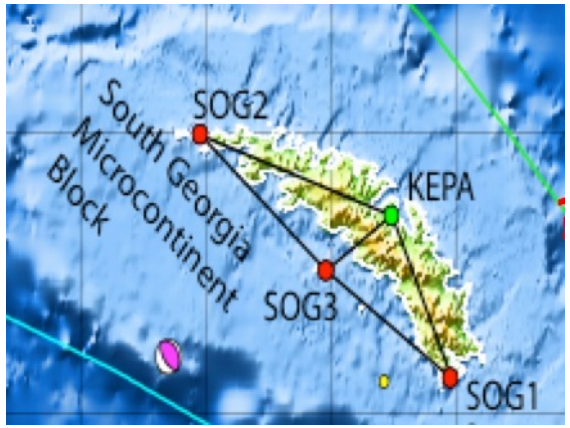

Benchmark networks geodetically link the sensors together for long-term monitoring, especially important for the tide gauge and GNSS.

- Two Benchmark networks were established: on Brown Mountain and at KEP
- At KEP to provide geodetic reference for the tide gauge and tie it to the GNSS station KRSA
- On Brown Mt. enable a tie if monument of KEPA gets destroyed by severe weather

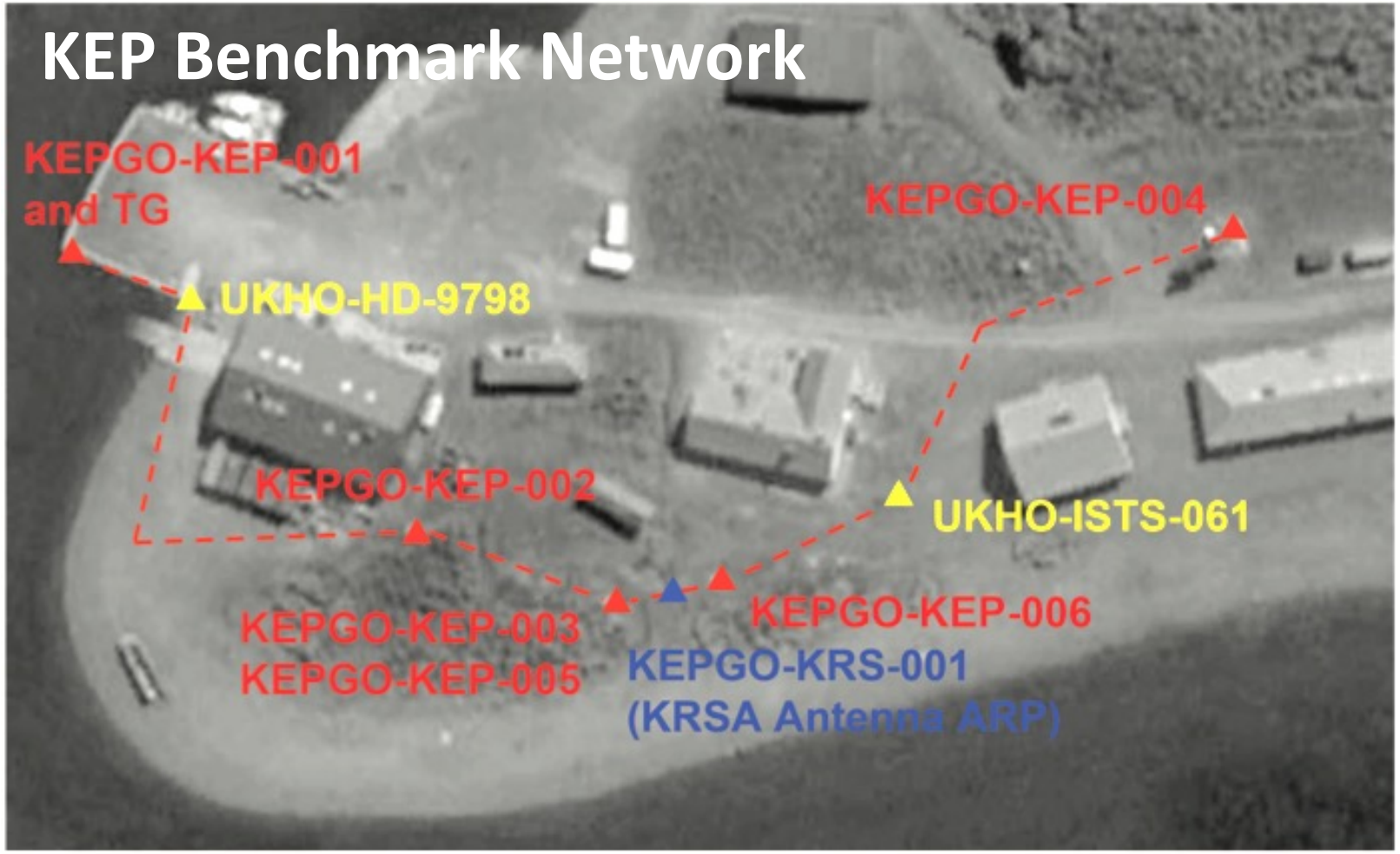

Our updated GPS solution (ULVLM2020) follows largely the 3rd IGS reprocessing campaign strategy.

- Based on Bernese GNSS Software v5.2 (Release Feb 2020)
- DD network processing strategy
- CODE satellite and ERP products
- IERS Conventions 2010
- ITRF2014
- …

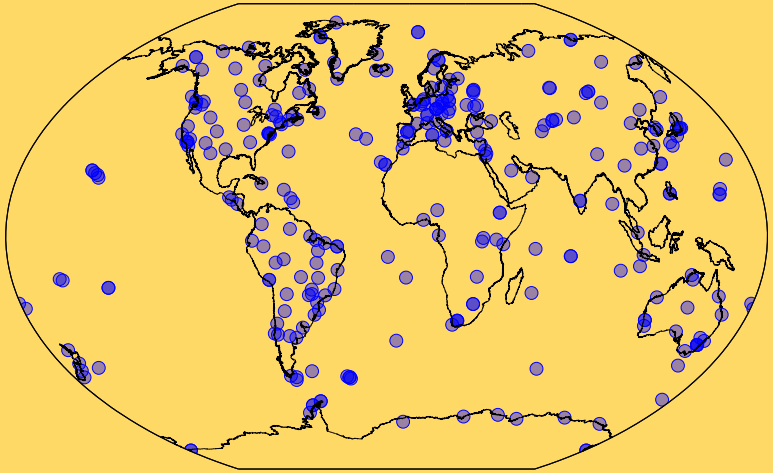

RF network, consisting of ~300 IGS stations

- Estimated parameters include
  - Coordinates and receiver clocks
  - Ambiguities
  - Troposphere
  - …

- Time series analysis using Hector software v1.6
- Stochastic characterization using white + power-law noise model

The GNSS time series are of varying quality and length due to instrument issues. All show uplift but KEPA provides the most complete data set, yet it has the largest WRMS.

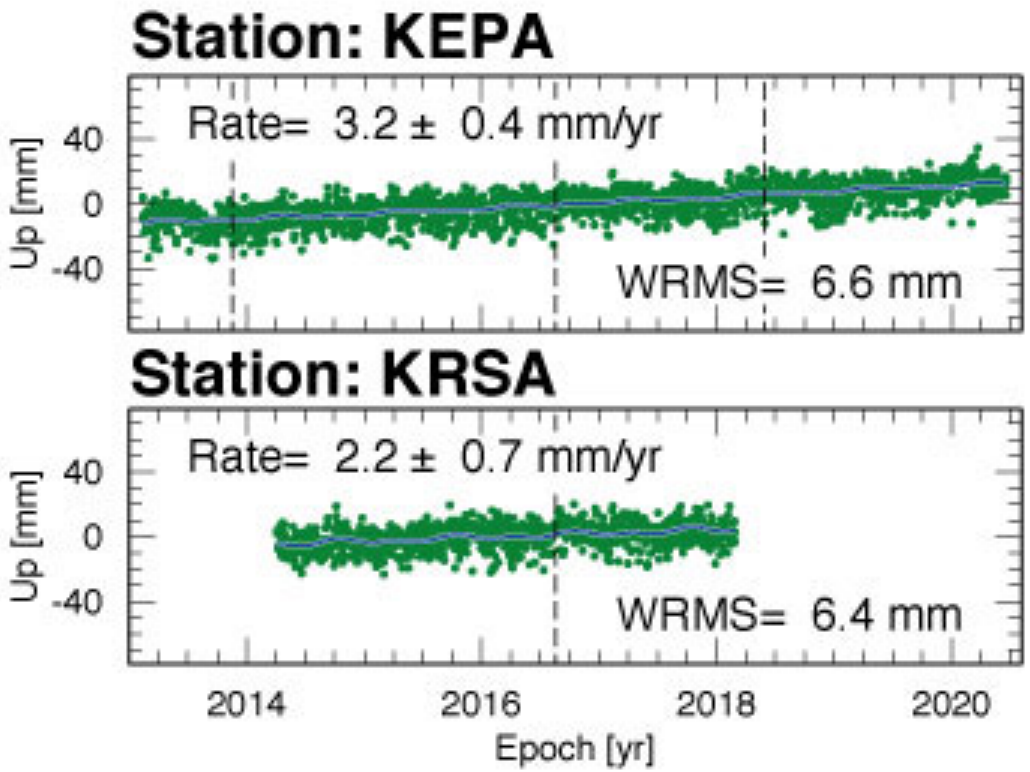

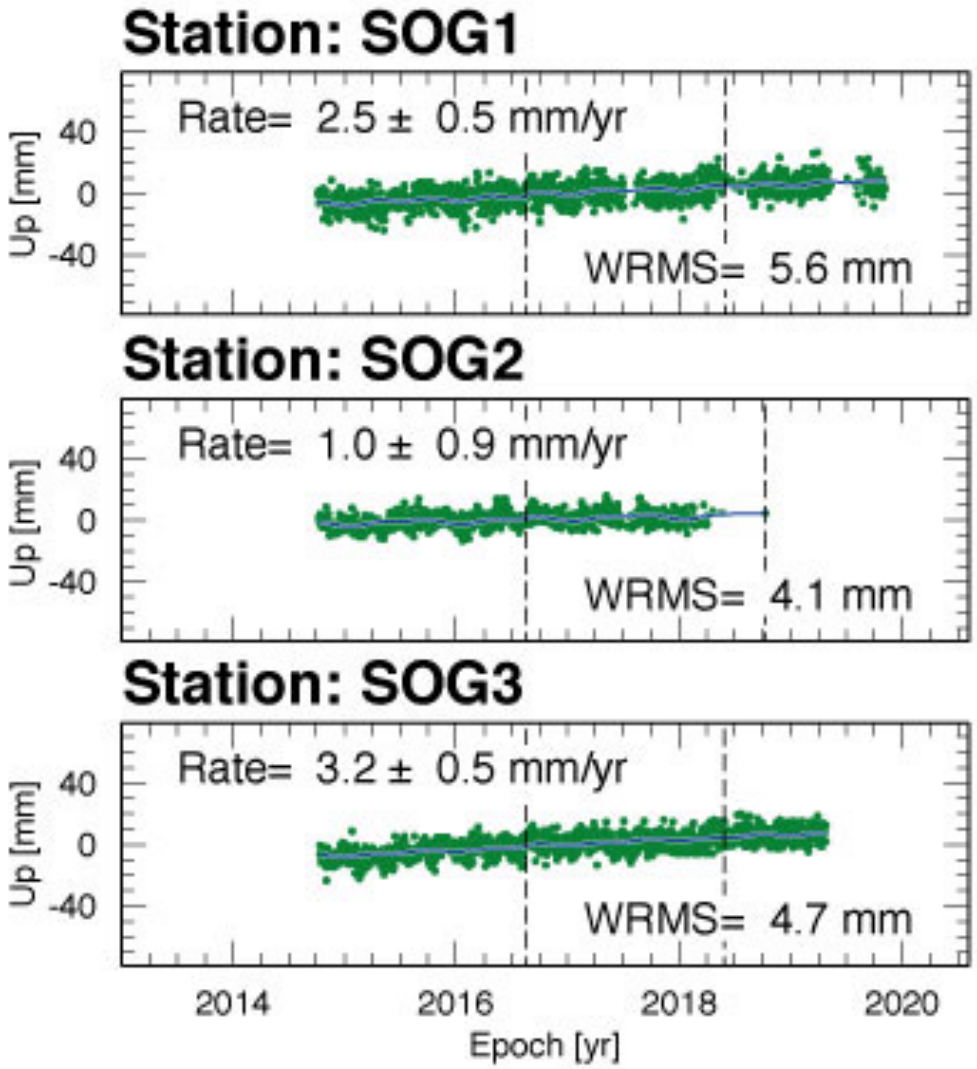

Offsets:
Nov 13, 2013: M7.7 Scotia Sea EQ, 60.274°S 46.401°W
Aug 19, 2016: M7.4 South Georgia Island Region EQ, 55.285°S 31.877°W
May 27, 2018: Reference Frame Change ITRF2008 to ITRF2014

The 5 levelling campaigns between the KEP BMs during 2013-2020 reveal continued subsidence of the KEP wharf and TG BM (KEPGO-KEP-001).

Benchmark	Distance [m] from Start	Campaigns 2013 Height [m]	2014 Height [m]	2017a Height [m]	2017b Height [m]	2020 Height [m]
KEPGO-KEP-004	0	3.7600	3.7600	3.7600	3.7600	3.7600
UKHO-ISTS-061	68	3.0757	3.0749	3.0753	3.0753	3.0754
KEPGO-KEP-006	97	3.4000	3.4008	3.4007	3.4007	3.4007
KEPGO-KEP-003	115	2.7704	2.7676	-	-	-
KEPGO-KEP-005	115	2.7693	2.7701	2.7700	2.7699	2.7696
KEPGO-KEP-002	174	2.8145	2.8125	2.8126	2.8128	2.8125
UKHO-HD-9798	205	1.3465	1.3396	1.3350	1.3349	1.3332
KEPGO-KEP-001	235	1.3229	1.3154	1.3089	1.3087	1.3062
Tide Board	236		1.1531	1.1469	1.1466	1.1447
Tide Gauge	236	0.6560	0.6469	-	-	-

Stable Ground

Subsidence

Between 2013-2020 the TG BM subsided in total by 1.67 cm at an average rate of 2.3 mm/yr.

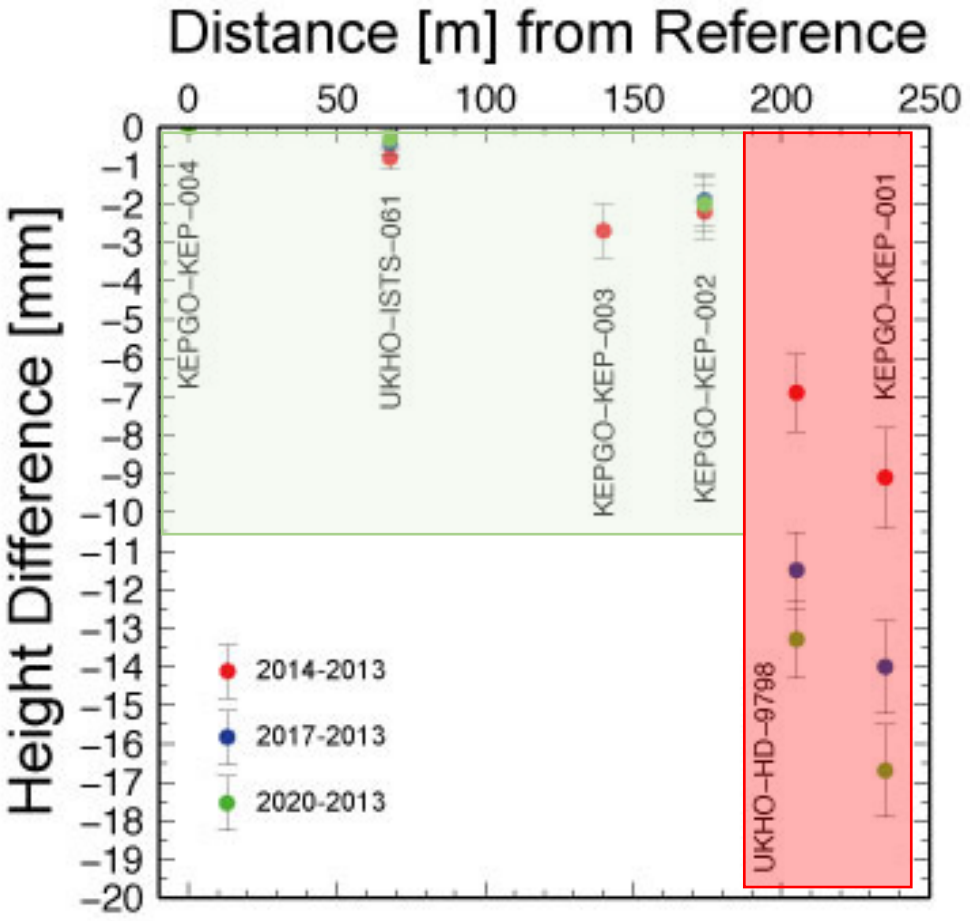

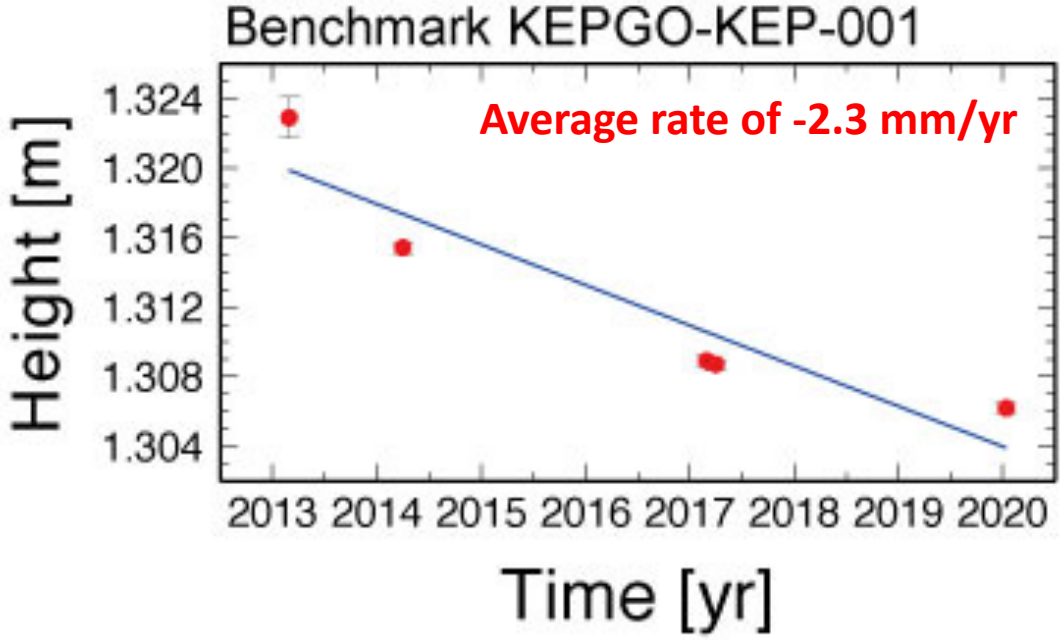

The TGBM (KEPGO-KEP-001) subsided by 1.67 cm over the past 7 years but we don't know when this started. We fitted a linear rate, but it could easily be approximated by an exponential decay.

The daily MSL record for the KEP TG shows no significant sea level trend for 2008-2020…

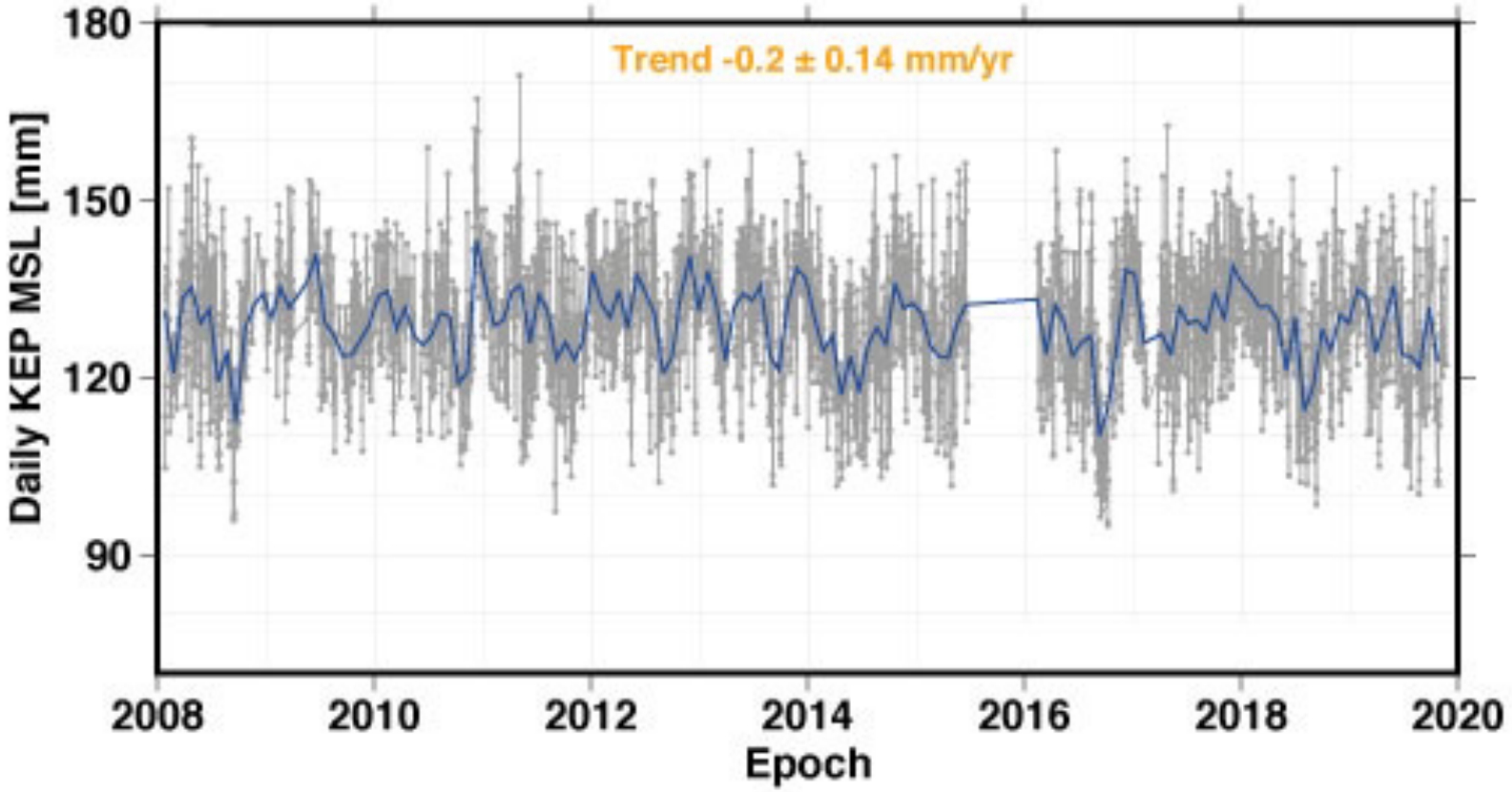

…but we know that the area at KEP is rising by 3.2 mm/yr and 3.0 mm/yr as indicated by KEPA and KRSA, respectively, while the KEP wharf and the TG are subsiding by on average 2.3 mm/yr.

We can use the sea level anomaly (SLA) product from NASA's sea level MEaSUREs Programme to compare to the KEP MSL record.

Monthly SLA from satellite altimetry around South Georgia for 10/1992 – 01/2019 show high consistency in their variations and trends.

NASA MEaSUREs v4.2 data set of merged TOPEX/ JASON-1, -2 and -3 satellite altimetry

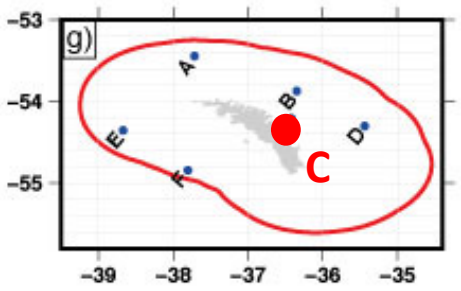

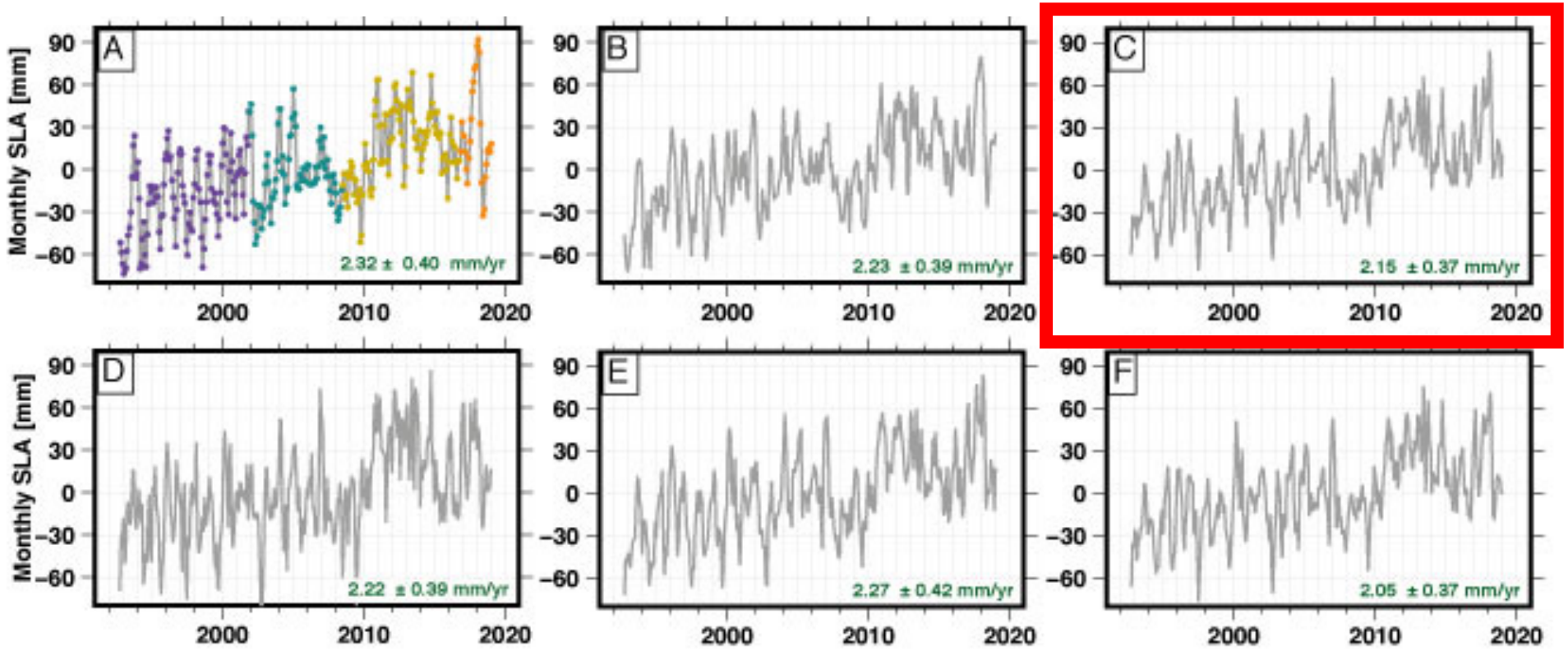

Monthly SLA for point C (off Cumberland Bay, 55.5°S, 36.5°W) shows good agreement with the other time series, i.e. it is representative of the satellite altimetry measurements from further offshore.

The sea level observations from satellite altimetry at location C and the KEP TG for 2008-2020 show high consistency with a correlation between the monthly averages of 0.83.

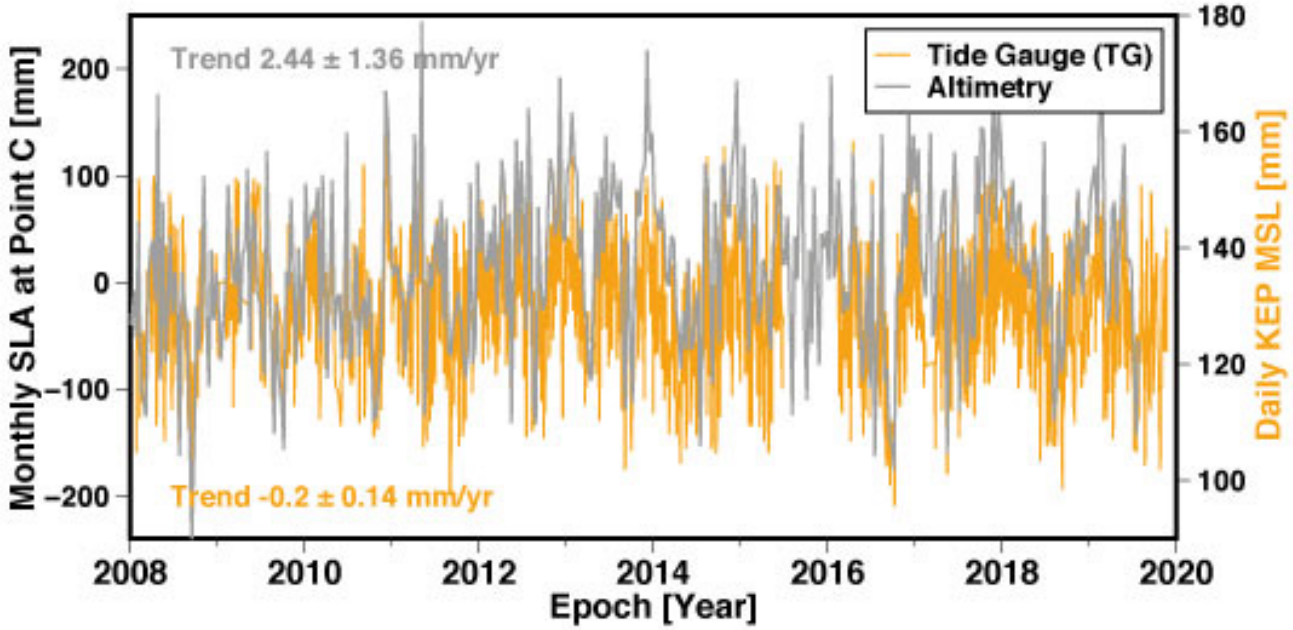

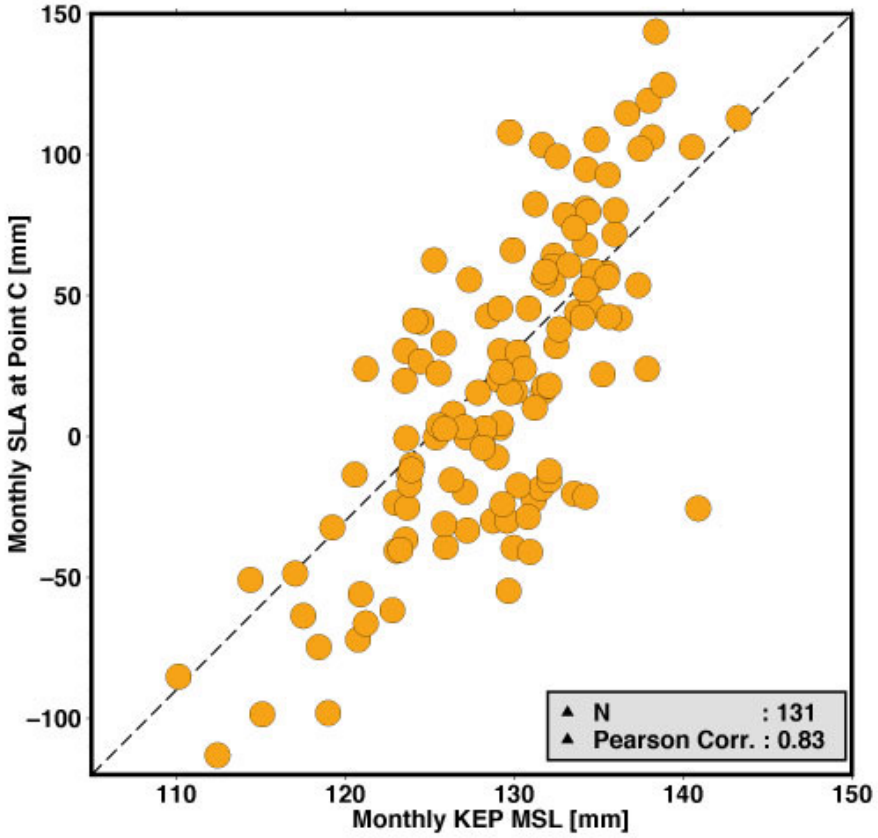

The comparison of the sea level change estimates from this analysis with those of July 2019 show an improvement in the agreement between TG and satellite altimetry results.

Technique	Time span	Interval	Modelling	Trend [mm/yr]
		July 2019		
SLA	2008-2018	10-day	linear, WN	4.3 ± 1.5
MSL	2008-2018	daily	linear, WN	-1.5 ± 0.8
		November 2020		
SLA	2008-2019	monthly	linear+periodics+noise	2.4 ± 1.4
MSL	2008-2020	daily	Linear+periodics+noise	-0.2 ± 0.1

... allow, while NOT statistically significant, following mind game:

$$SLC_{TG} = MSLTG + VLMGNSSS + VLM_{Level} = -0.2 + 3.0 + (-2.3) = 0.5\,\text{mm/yr}$$

(as compared to 2.4 mm/yr for SSH)

$$VLM_{ALT} = -SSHALT - MSLTG - VLM_{Level} = -2.4 - (-0.2) - (-2.3) = 0.1\,\text{mm/yr}$$

(as compared to 3.0 mm/yr for VLM_{GNSS})

Geodesy and Geospatial Engineering

INTERGEO 2022 OCT. 18 – 20 ESSEN

GNSS Reprocessing activities for an updated and quality controlled global data set of vertical land movement (VLM) estimates

Eshetu ERKIHUNE, Norman TEFERLE, Addisu HUNEGNAW

Geodesy and Geospatial Engineering
University of Luxembourg

INTERGEO Conference 18.10.22 - 20.10.22, Essen, Germany

UNIVERSITÉ DU LUXEMBOURG

Reprocessing of GNSS Observations

Table 1: Summary of IGS GNSS data reprocessing.

Description	1st Reprocessing	2nd Reprocessing	3rd Reprocessing
Data span	1994-2007	1994-2014	1994-2021
Reference Frame	IGS05 (ITRF2005)	IGS08(ITRF2008)	IGS20 ITRF2020 (Rebischung, 2021)
IERS Convention	IERS 2003	IERS 2010	IERS 2010
Geopotential Field	EGM96	EGM08	EGM08
Antenna calibration	IGS05 ANTEX	IGS08 ANTEX	IGS20 ANTEX (absolute calibration)
Tropospheric delay model	GPT/GMF	GPT2/VMF1	GPT2/VMF1
Higher order Ionosphere	Not applied	IERS 2010 (2nd order)	IERS 2010 (2nd order)
Orbit Dynamics	No Earth Albedo model	Earth Albedo model	Earth Albedo model

The University of Luxembourg (UL) is currently reprocessing a global GNSS data set following the most recent effort of the International GNSS Service (IGS).

New features in UL reprocessing:

- Modern ocean tide loading model, FES2014b (Carrere et al., 2016).
- New multi-GNSS absolute calibrations for a range of ground antennas (Rebischung et al., 2019)
- Improved solar radiation pressure models (Prange et al., 2020).
- New mean pole tide, adopting a new linear mean pole to compute rotational deformation (Ries et al., 2017).

UL repro3 GNSS Work

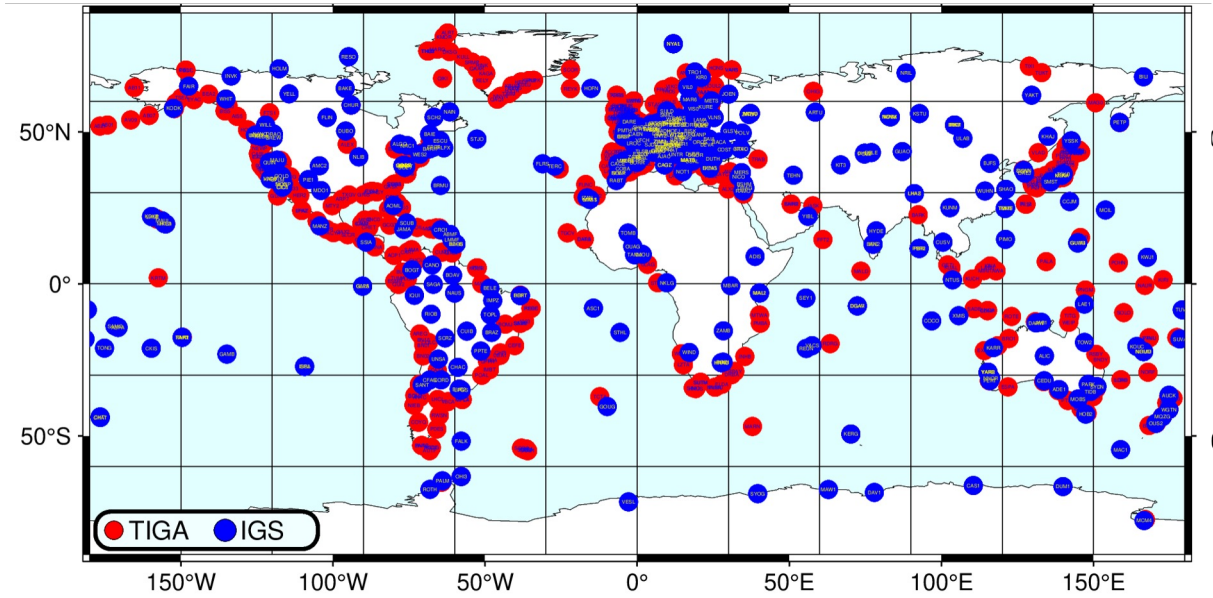

Figure 4: GNSS Network

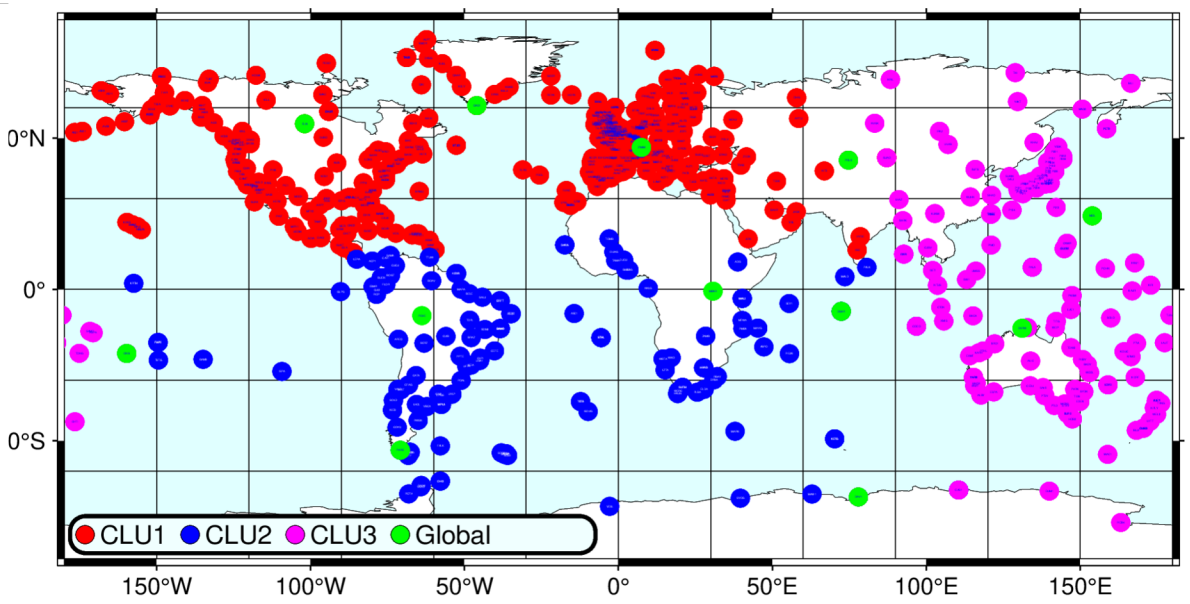

Figure 5: GNSS Network

- The GNSS data (RINEX format) were retrieved from the IGS and SONEL archive (www.sonel.org) amongst others.

- Distribution of GNSS stations in clusters for the GNSS processing strategy.

Geodetic time series analysis workflow

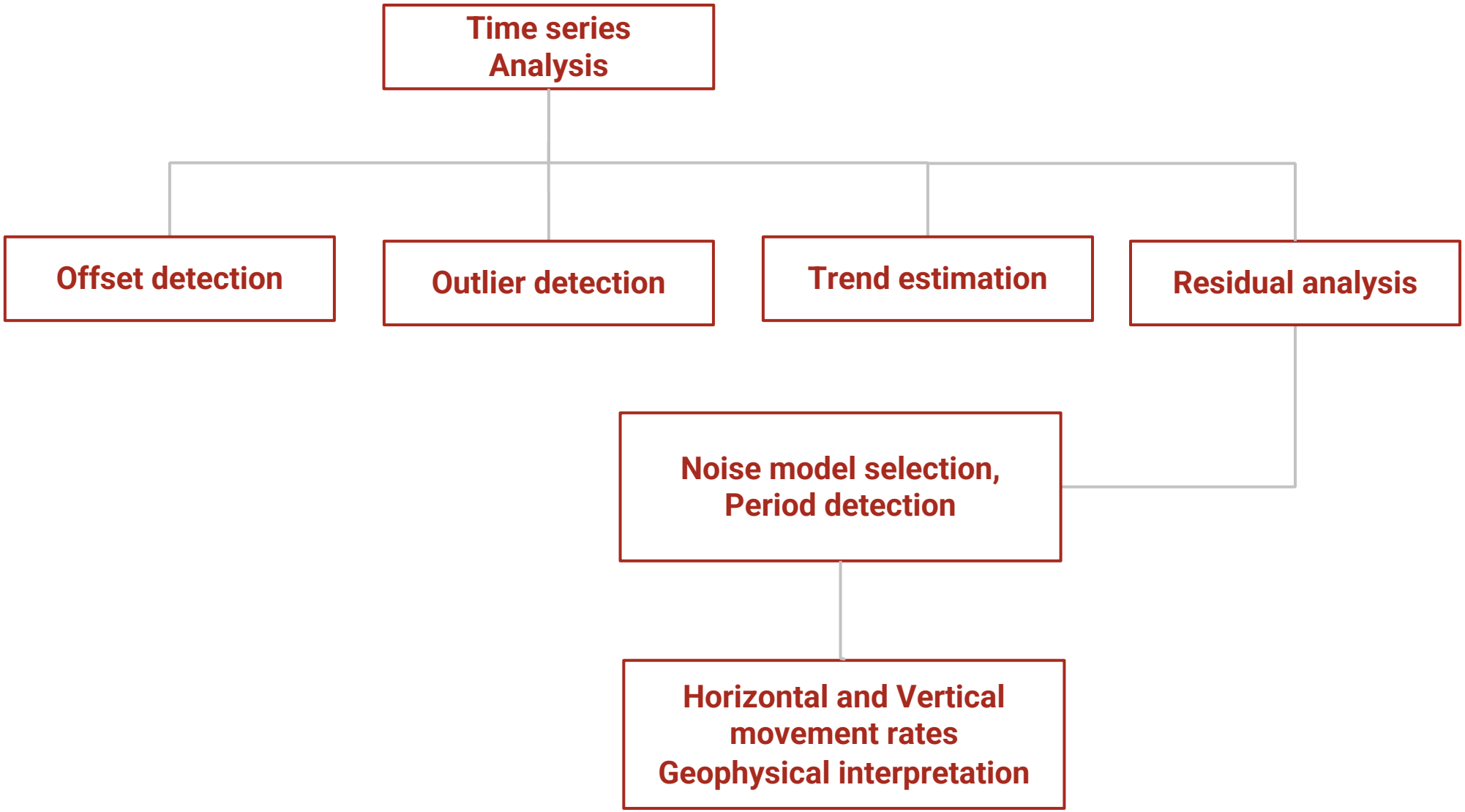

Figure 6: The diagram shows the steps taken in the analysis of the time series.

Selected Tide gauge stations (PSMSL)

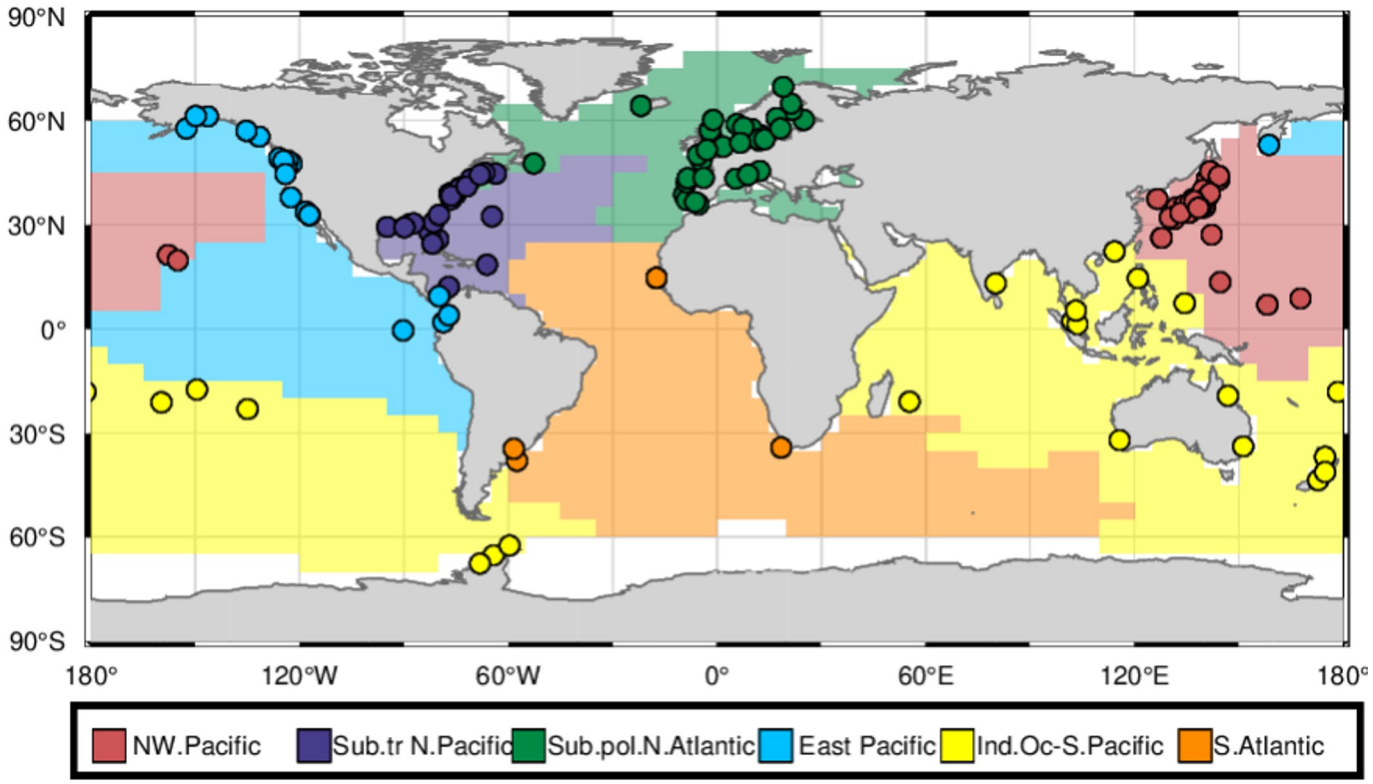

Figure 7: Tide gauge station locations and the corresponding ocean basins coded in different colors.

Record length for selected PSMSL sites

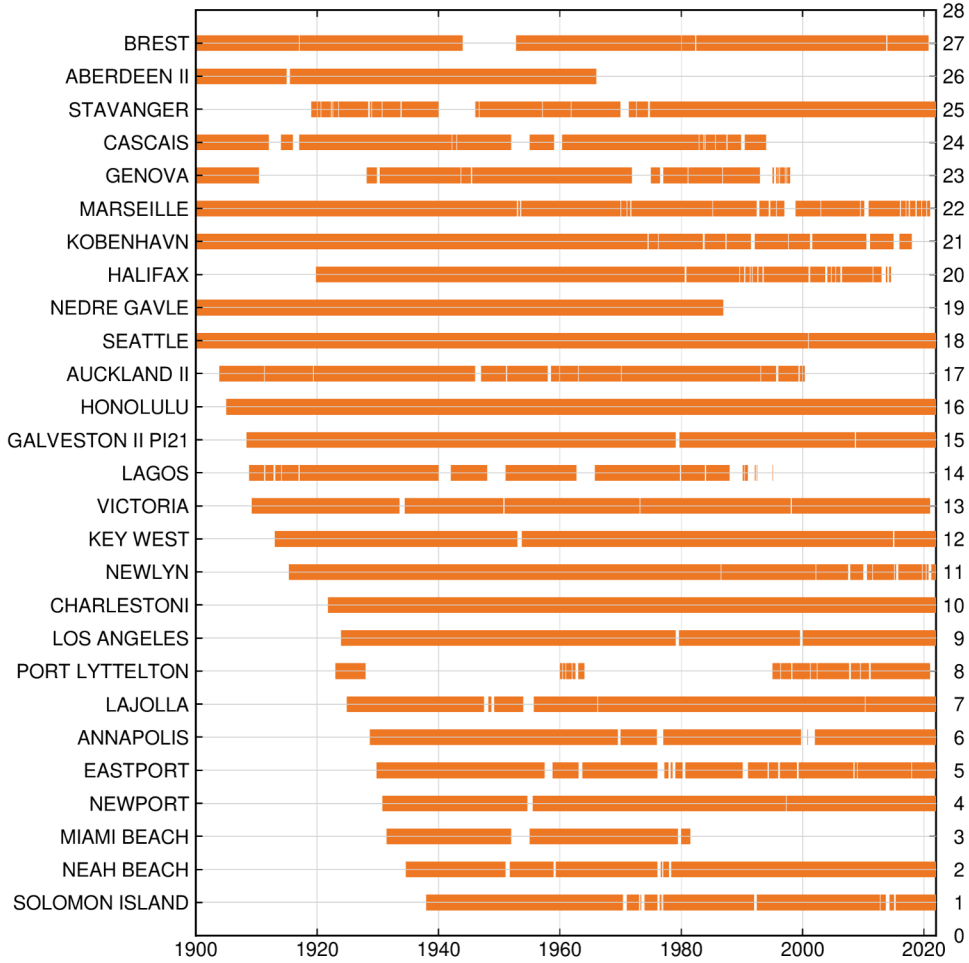

Figure 8: PSMSL tide-gauge stations and availability of tide-gauge records over the period 1900-2022.

Table 5: Trend estimates from GNSS and GIA and corrections for TG

	TG rate	GIA rate	GNSS rate	TG GNSS Corr.	TG GIA Corr.
Stations	**Trend** [mm/yr]	**Trend** [mm/yr]	**Trend** [mm/yr]	**Trend** [mm/yr]	**Trend** [mm/yr]
STAS	0.43 ± 0.14	0.60	0.86 ± 0.35	1.29 ± 0.26	1.03
BUDP	0.61 ± 0.12	0.07	0.91 ± 0.37	1.52 ± 0.26	0.68
MAR6	-6.03 ± 0.25	7.05	7.82 ± 0.36	1.79 ± 0.38	1.02
ABER	0.45 ± 0.22	1.01	0.84 ± 0.33	1.29 ± 0.33	1.46
NEWL	1.91 ± 0.12	-0.74	-1.01 ± 0.24	0.90 ± 0.18	1.17
BRST	1.01 ± 0.12	-0.62	-0.86 ± 0.26	0.15 ± 0.19	0.39
CASC	1.31 ± 0.2	-0.35	-0.48 ± 0.17	0.83 ± 0.23	0.96
LAGO	1.61 ± 0.26	-0.41	-0.21 ± 0.19	1.40 ± 0.04	1.20
MARS	1.35 ± 0.12	-0.33	-0.98 ± 0.40	0.37 ± 0.28	1.02
GENO	1.18 ± 0.07	-0.17	-0.43 ± 0.31	0.75 ± 0.17	1.01
EPRT	2.25 ± 0.24	-1.38	-0.23 ± 0.59	2.02 ± 0.59	0.87
NPRI	2.83 ± 0.16	-1.47	-0.85 ± 0.41	1.98 ± 0.33	1.36
USNA	3.79 ± 0.22	-1.59	-0.13 ± 0.23	3.66 ± 0.27	2.20
HLFX	3.07 ± 0.16	-1.88	-1.21 ± 0.25	1.86 ± 0.22	1.19
SOL1	3.91 ± 0.22	-1.74	-2.92 ± 0.50	0.99 ± 0.47	2.17
ALBH	0.74 ± 0.14	-0.55	0.34 ± 0.27	1.08 ± 0.21	0.19
SEAT	2.06 ± 0.11	-0.86	-1.44 ± 0.27	0.62 ± 0.18	1.20
NEAH	-1.75 ± 0.19	-1.19	2.83 ± 0.54	1.08 ± 0.48	-2.94
SCCC	3.47 ± 0.24	-1.16	-2.17 ± 0.64	1.30 ± 0.65	2.31
GAL1	6.57 ± 0.16	-0.94	-2.52 ± 1.77	4.05 ± 3.29	5.63
VTIS	1.04 ± 0.15	-0.85	-0.46 ± 0.22	0.58 ± 0.20	0.19
SIO3	2.05 ± 0.15	-0.84	-0.01 ± 0.34	2.04 ± 0.27	1.21
TAKL	1.26 ± 0.17	-0.76	0.96 ± 1.35	2.22 ± 1.99	0.50
LYTT	6.95 ± 1.78	-0.74	-1.72 ± 0.48	5.23 ± 2.01	6.21
HNLC	1.56 ± 0.13	0.08	-0.53 ± 0.30	1.03 ± 0.22	1.64

GNSS VLM versus GIA VLM rate corrections

Table 6: Mean and standard deviations of individual sea level change estimates

	No Corrections	VLM Corrections	
	TG Trend [mm/yr]	TG+GNSS Trend [mm/yr]	TG+GIA Trend [mm/yr]
GMSL	1.75 ± 0.233	1.60 ± 0.55	1.35
RMS	2.47	1.18	1.69

- There is a large spread of GIA estimates relative to GNSS (see Figure 9).
- There is improved agreement between the sea level rise estimates after correction with the observed rather than modelled VLM.
- The 27 tide gauges shown are exposed to VLM due to different processes, not just GIA.

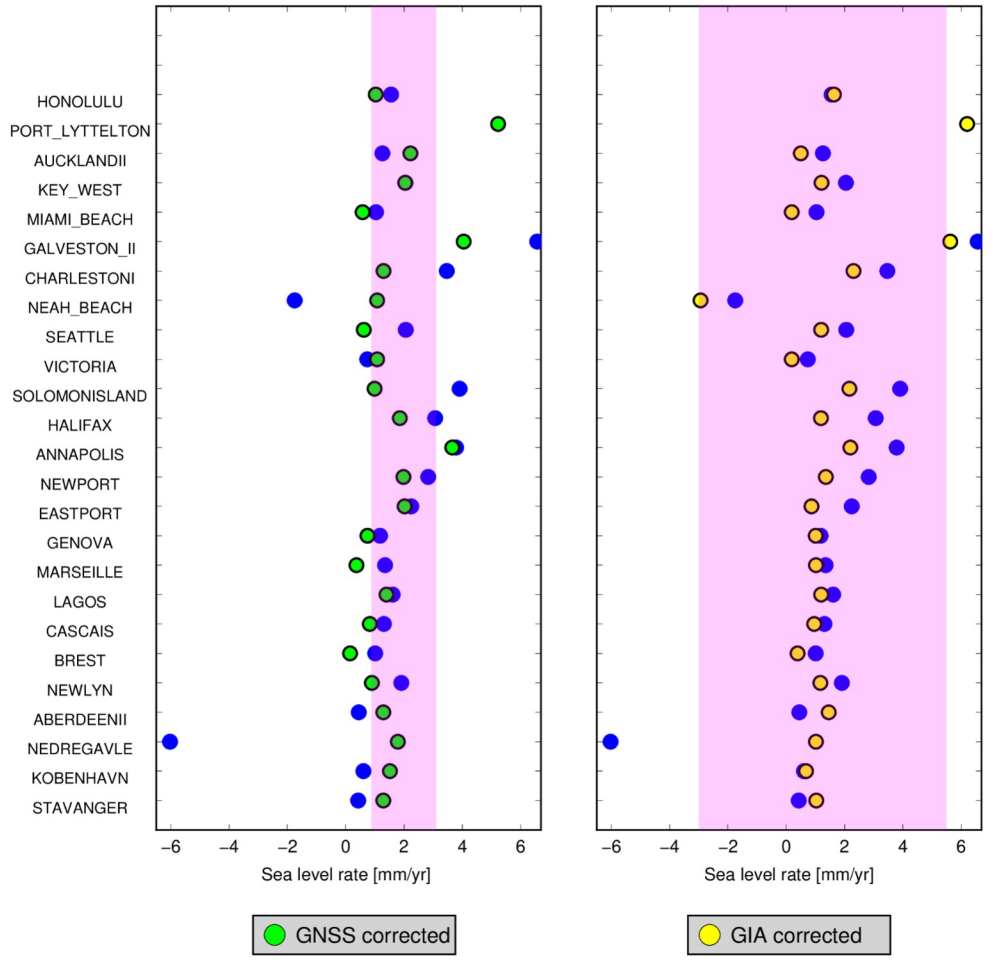

Figure 9: GNSS corrected (a) and GIA model corrected (b) GMSL. The pink bands indicate the spread of the sea level rise estimates after correction.

GNSS meteorology for severe weather and climate change monitoring

GNSS Meteorology and Climatology

- Near-real-time contributions to EUMETNET GNSS Water Vapour Programme
- Improved weather forecasts for Europe
- Showed potential to improve forecasts even on regional scales, e.g. Luxembourg

- Long-term GNSS processing for GNSS climatology
- Investigations of stochastic properties of atmospheric water vapour estimates

Near-Real Time (hourly) networks

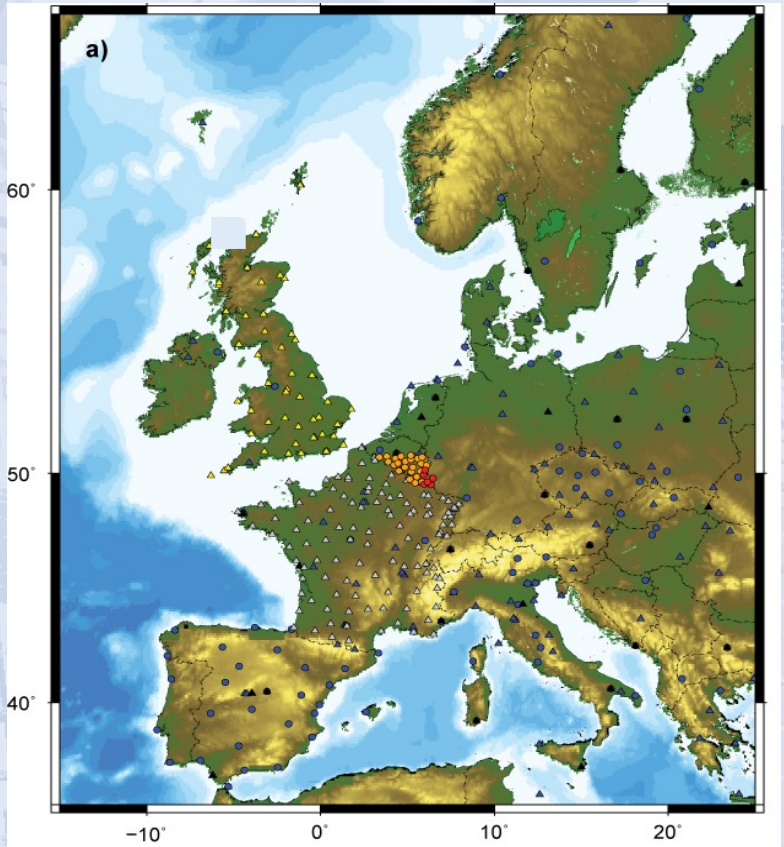

Red: *SPSLux*, orange: *WALCORS*
gray: *RGP*, yellow: *OSGB+Geonet*
blue: *EPN*, black: *IGS*

Real-Time GNSS for Storm Tracking

- Real-Time GNSS can provide atmospheric water vapour every few seconds
- It is possible to track were the water is and were it is likely to rain – central storm area
- Example of Hurricane Harvey Gulf of Mexico, August 2017

- Collaborations with MétéoLux, MétéoFrance, Danish Meteorological Institute and the UK MetOffice

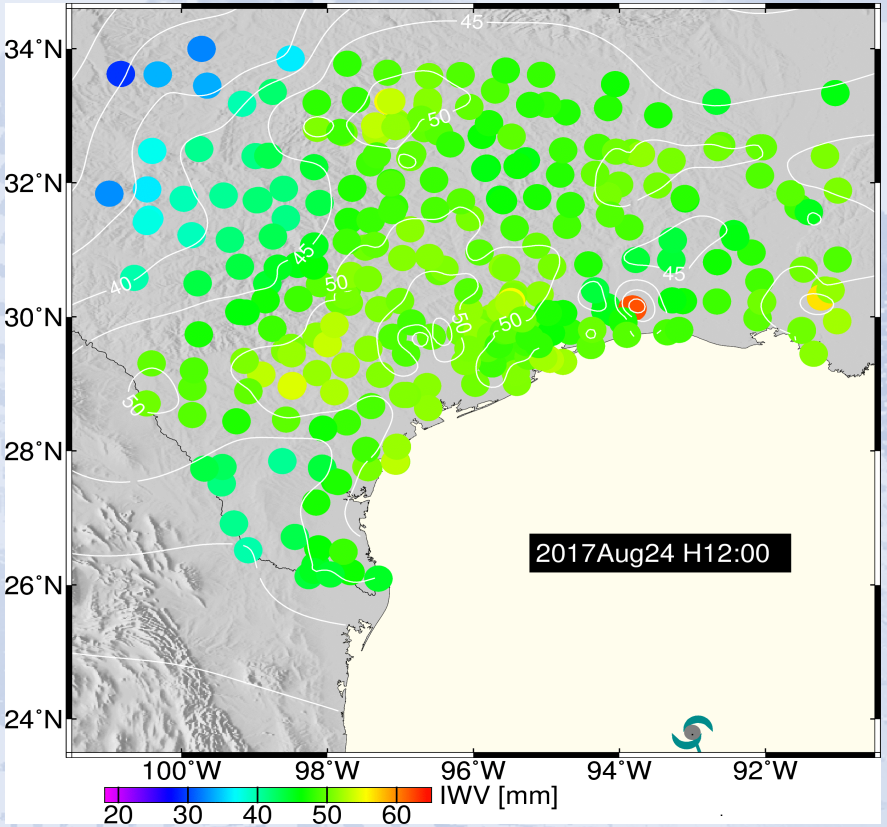

Integrated Water vapour field (Precipitation WV) variations estimated from dense ground network of GPS during Hurricane Harvey in 2017. Gulf of Mexico

Geodesy and Geospatial Engineering

Advanced Asymmetry Tropospheric Products for Meteorology from GNSS and SAR observations (VAPOUR)

- FNR-funded under the OPEN Call 2018
- 3 years (02.2019 – 10.2022)
- PI: Felix Norman Teferle
- Co-PI: Addisu Hunegnaw

Website: www.vapour.lu

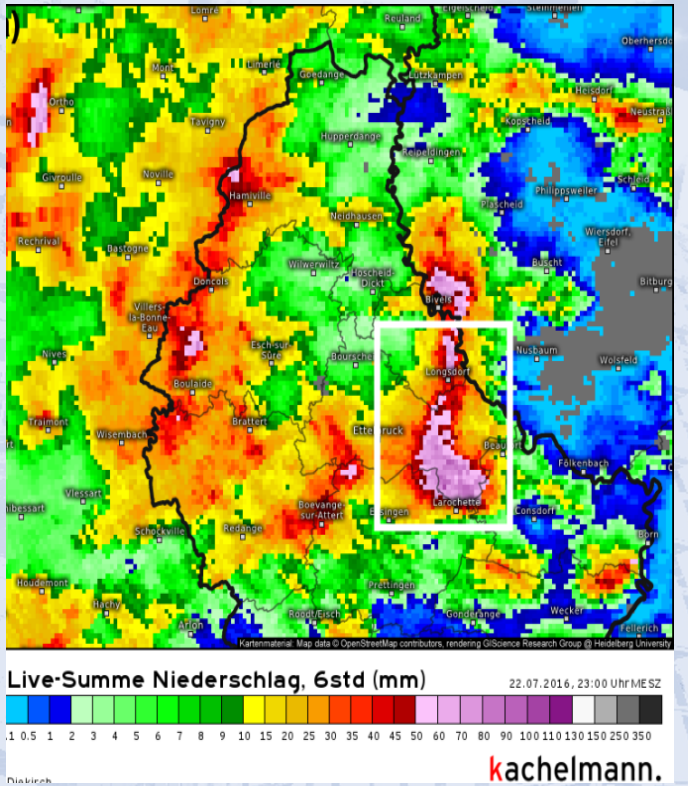

a)

b)

a) A 6-hourly precipitation (in mm) from C-band radar image. b)The resulting flash floods in Larochette, Luxembourg, 22 July 2016.

Objectives of VAPOUR

Flooding events are considered amongst the most serious natural hazards in Europe

- VAPOUR aims to better quantify and understand atmospheric water vapour by improving processing of GNSS and SAR techniques
- To provide next generation of advanced spatiotemporal atmospheric GNSS meteorology products
- To better account for the distribution of atmospheric water vapour within the troposphere
- To enhance numerical weather prediction (NWP) models for forecasting (e.g. Aladdin - MétéoFrance)
- This will improve the prediction of severe weather, such as the potential for flash floods in Luxembourg and elsewhere

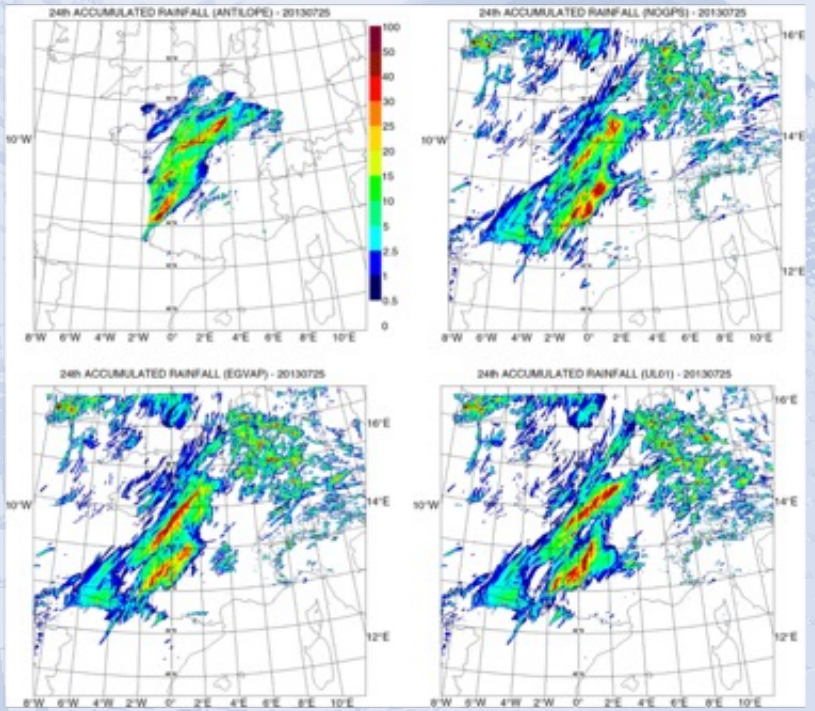

(Mahfouf et al, 2015)

Geodesy and Geospatial Engineering

VAPOUR

UNIVERSITÉ DU LUXEMBOURG

Luxembourg National Research Fund

On the Application of Multipath Stacking Maps for Improved Severe Weather Tracking and Low-cost Antenna Calibration

Felix Norman Teferle, Addisu Hunegnaw, Hüseyin Duman, Hakki Baltaci, Yohannes G. Ejigu, and Jan Dousa

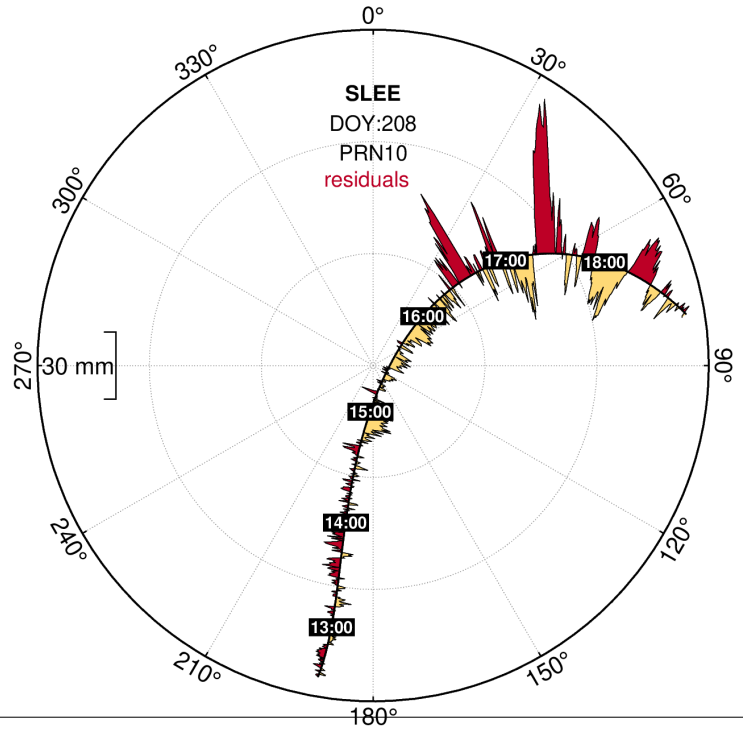

Post-fit residuals during the severe weather

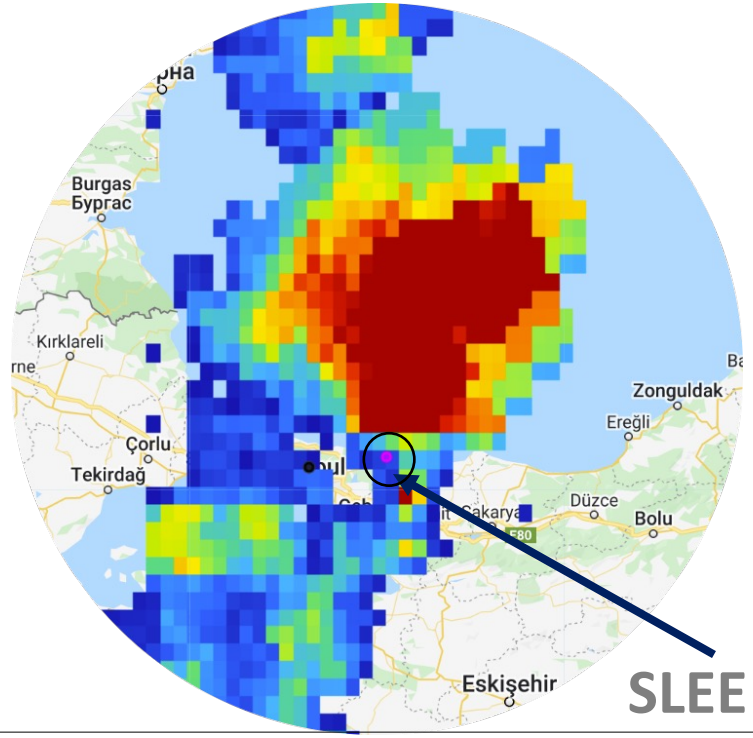

Precipitation 27 July 2017, 17:00 UTC, Turkey

Severe weather events are predicted to increase in intensity and frequency due to climate change and a better understanding and prediction of these is necessary.

- Slant Wet Delay (SWD) would provide more spatial information on such events than commonly used Zenith Wet Delay (ZWD) and horizontal gradient estimates, but SWD are not operationally assimilated in numerical weather prediction (NWP) models.
- There are at least two reasons for this:
  - SWD estimates require an extra processing step and are estimated as a parametrized form of Zenith Total Delay (ZTD) and the horizontal gradients.
  - **Slant Total Delay (STD) and hence SWD is sensitive to site-specific multipath (MP).**
- Using **Fuhrmann et al. (2015)'s "congruent cells"**, we developed a MP stacking map from a running average of 21 days of past observations (see **AGU FM 2020,** EGU21 and EGU22 presentations).
- However, the resulting maps contain the combined effects of MP **and** insufficiently modelled errors**, e.g. antenna phase centres**.

Synoptic scale circulation that contributed to a severe weather event on 27 July 2017 in Istanbul, Turkey

- During the afternoon hours of July 27, 2017, extreme flash flooding struck Istanbul, Turkey.
- Numerous people were injured, there were several fatalities and severe damage to property and infrastructure.
- Surface temperature of Istanbul reached $34°C$ ($5°C$ above the average)
- A significant amount of moisture was carried by strong southwesterly winds, which resulted from excessive warming of Marmara Sea surface temperatures ($24.9°C$), increasing the convergence of low-level moisture.
- This led to thunderstorms, stormy and gale-force winds (120 km/h) with extreme lightning activity

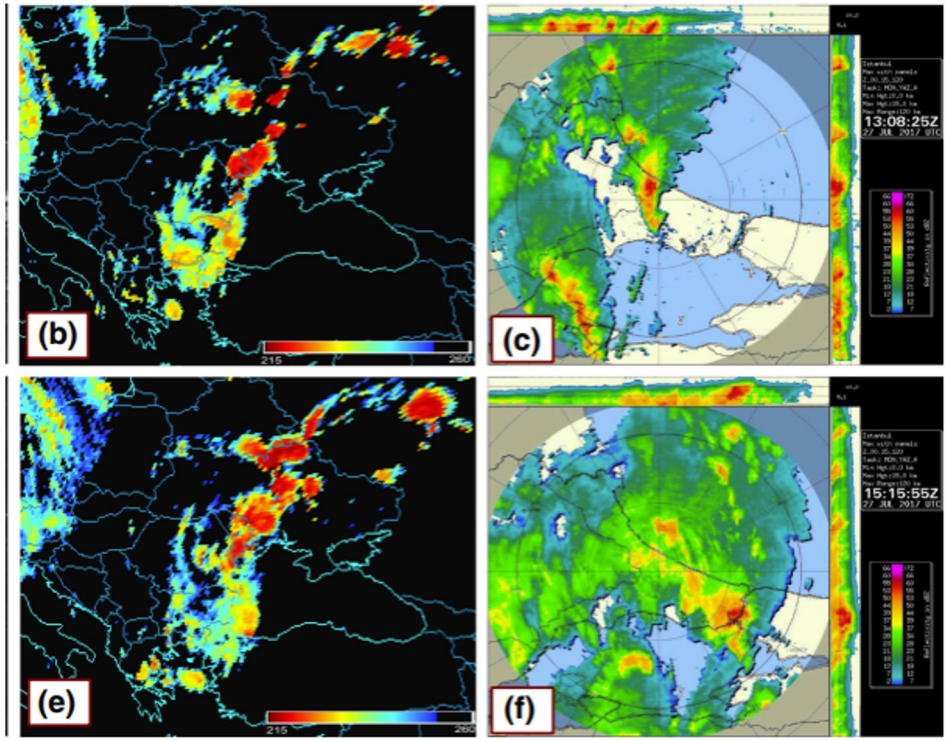

Fig. **b)** 10.8 μm channel of brightness temperature (K) imagery from 13:00 UTC on 27 July 2017. Pixels with brightness temperature K are shown. **c)** Radar MAX product of 13:08 UTC. **e)** and **f)** for 15:15 UTC on 27 July 2017.

The 54 GPS stations that were processed from and around Turkey, with a particular focus on the severe weather event on July 27, 2017.

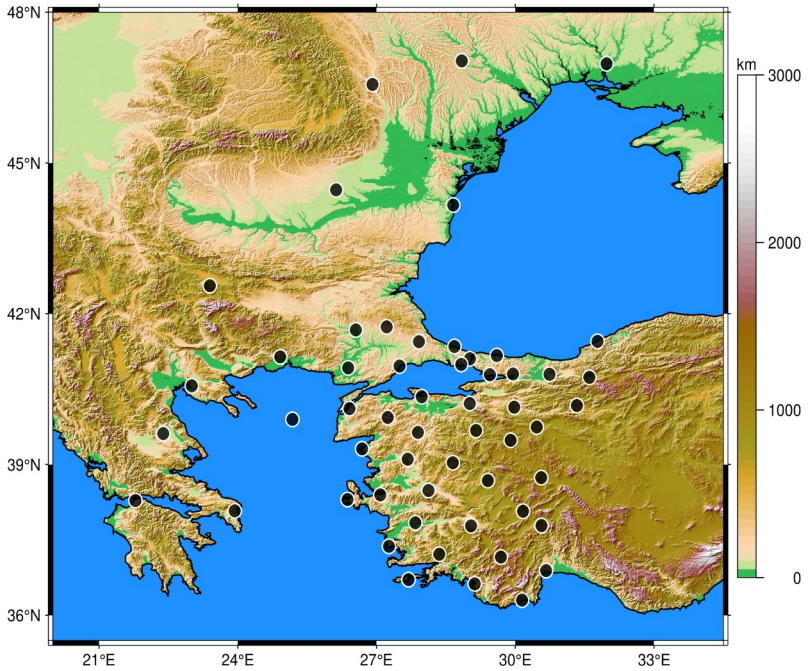

Daily RINEX GPS-only data were processed over a period of 3 months

Processing method:

- PPP by Kalman filtering using JPL-GipsyX GNSS engine
- Estimated parameters:
  - positions (1 XYZ per station) using ITRF14
  - Zenith Tropospheric Delay (epoch-wise)
  - Zenith Wet Delay (ZWD) (epoch-wise)
  - Linear gradients (East, North, epoch-wise)
  - Ambiguity
  - Constraints on ZWD and gradients using RW processes at $10\ \mathrm{mm} \cdot \mathrm{h}^{-1/2}$ & $1.0\ \mathrm{mm} \cdot \mathrm{h}^{-1/2}$

Products:

- Satellite orbit and clock products from JPL
- Ionosphere-free linear combination at 30s intervall and 5-degree elevation cut-off
- Satellite and receiver type-mean PCV/PCOs
- VMF1GRID for tropospheric delay modelling
- High-order ionosphere corrections applied

Construction of STD from ZTD and gradients with additional corrections for residuals and MP.

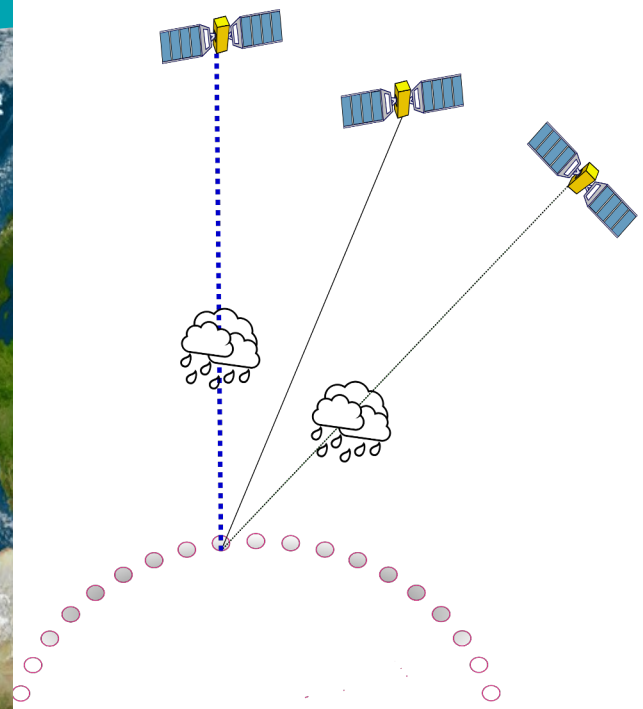

$$STD = T_{atm}(e,\alpha) = ZTD \cdot mf(e) + \xi(e,\alpha) \cdot mf_{grd}(e,\alpha)$$

$$STD = T_{atm}(e,\alpha) = ZTD \cdot mf(e) + \xi(e,\alpha) \cdot mf_{grd}(e,\alpha) + residuals(e,\alpha)$$

$$STD = T_{atm}(e,\alpha) = ZTD \cdot mf(e) + \xi(e,\alpha) \cdot mf_{grd}(e,\alpha) + residuals(e,\alpha) - \mathbf{MPS}\ (e,\alpha)$$

The isotropic and non-isotropic components of slant precipitible water vapour (SPWV)

- Neglecting the dry component between station $\boldsymbol{i}$ and satellite $\boldsymbol{m}$, the slant precipitable water vapour (SPWV) can be written as:

$$SPWV_i^m = \frac{1}{\Pi}\left[PWV \cdot mf(e_i^m) + S_i^m\right]$$

- We measure S_i^m by accurately modelling and correcting for clock delays, satellite orbits, hydrostatic delays, the isotropic part and site-specific MP

- Isotropic component of slant water computed from PWV
- S_i^m, represents the non-isotropic component
- S_i^m is zero for a perfectly isotropic atmosphere
- S_i^m is negative when the GNSS signals pass through areas of low water vapour relative to PWV
- S_i^m positive when the GNSS signal passes through areas of high water vapour relative to PWV

Post-fit residuals and MPS maps for SARY. Clear site-specific MP is affecting the station. To supress the error, the residuals were averaged for 21 days and the resulting map incorporated to produce non-isotropic slant delay.

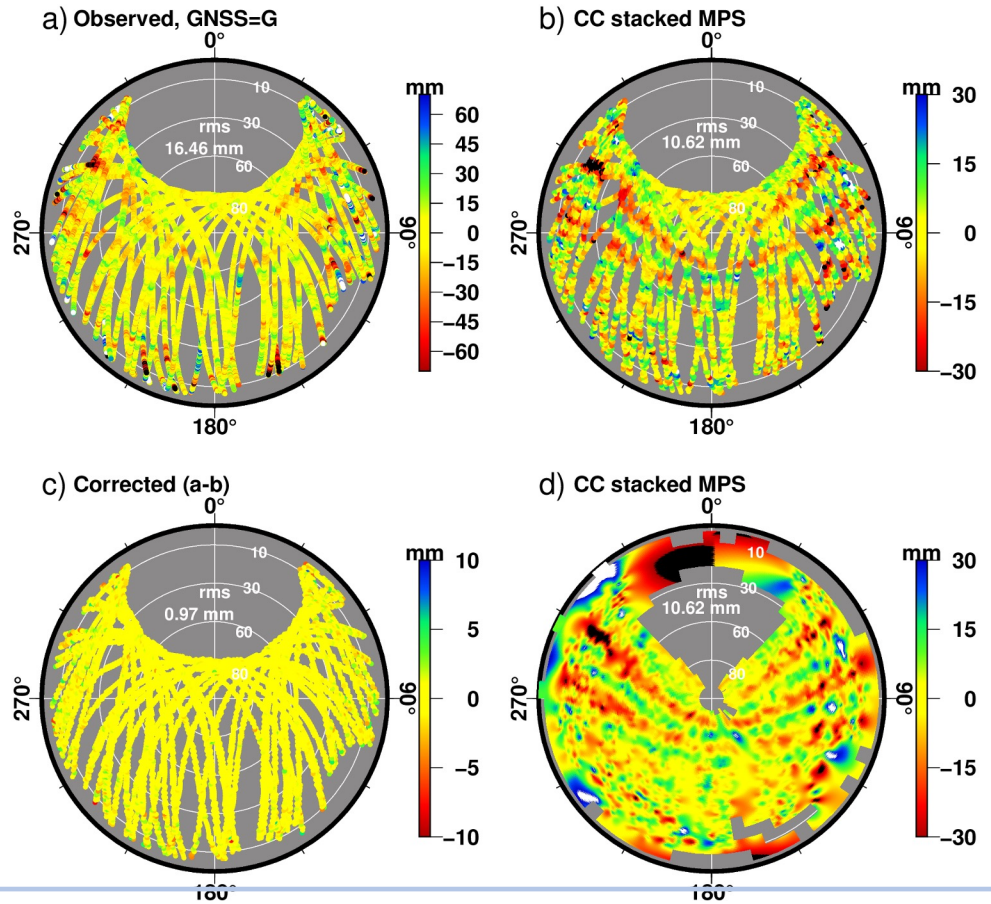

a) GPS raw post-fit residuals above the local horizon (gaps due to GPS satellite tracks) **b)** Multipath stacked map **c)** Ccorrected post-fit residuals **d)** interpolated MPS

The station is located on the roof of the white building. Power lines cross along the east-west direction with respect to the station.

Stacking of the post-fit residuals provide corrections to remove errors due to mainly MP effects as a function of elevation/azimuth

Skyplots of the post-fit residuals at ISTA and SLEE for DOY 208 during the storm for satellite PRN21 and PRN10, respectively. Note the difference in scale.

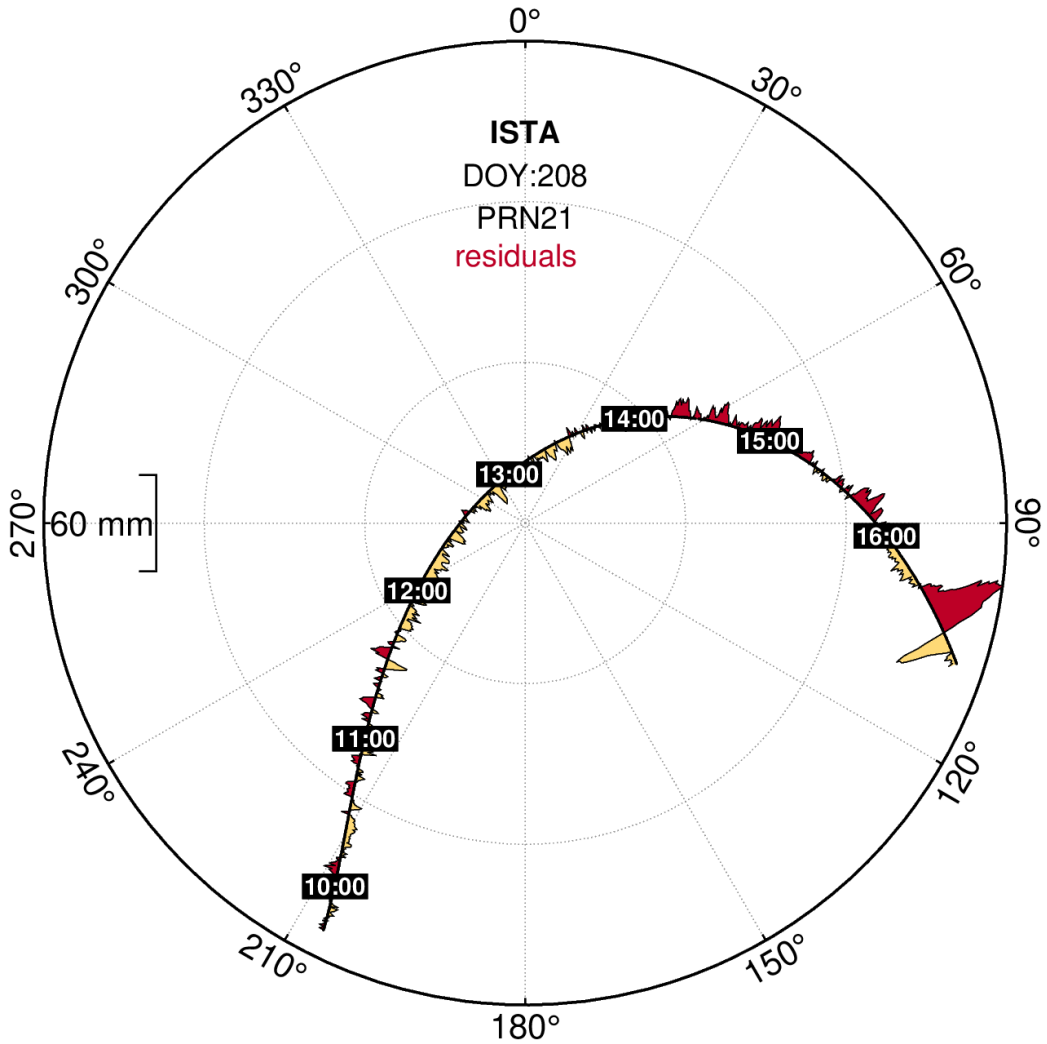

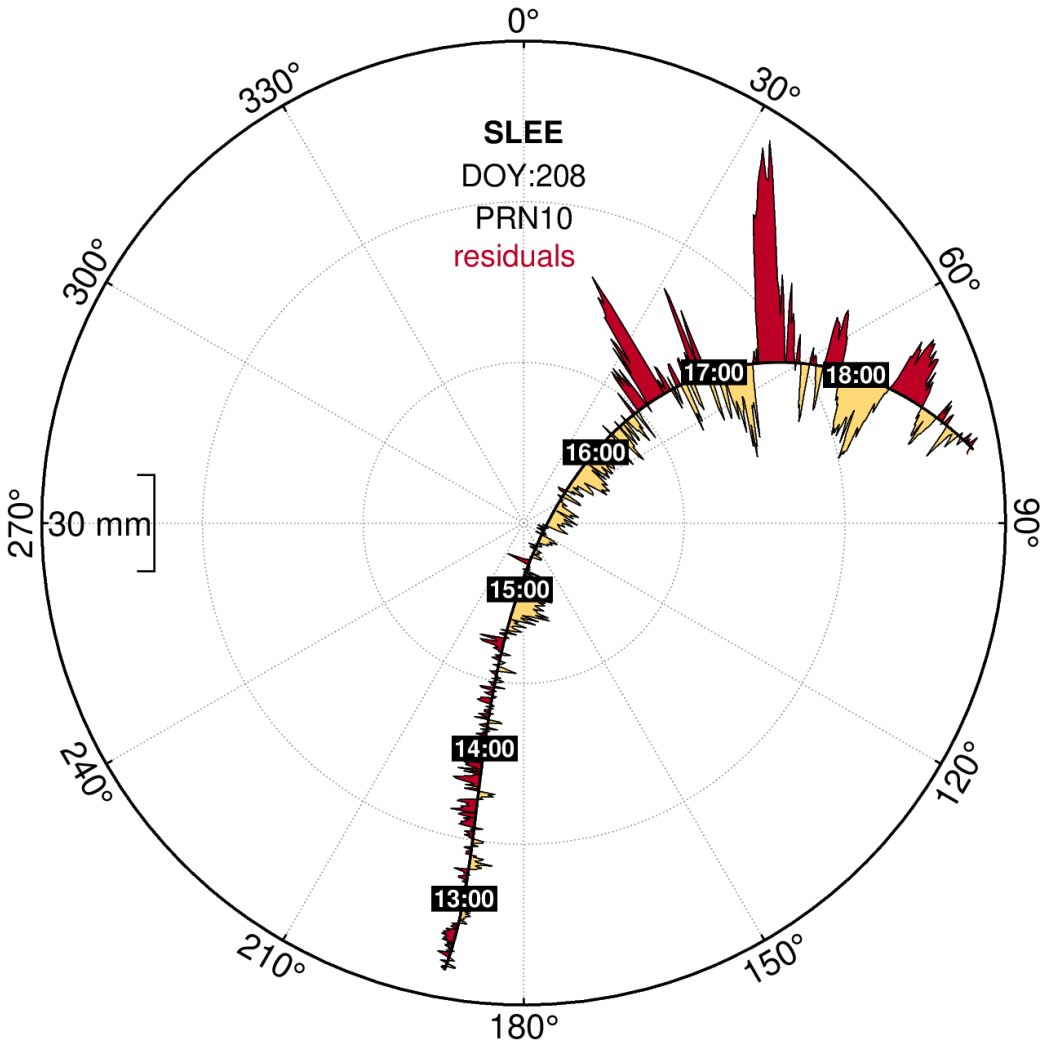

Investigation of the isotropic and non-isotropic SPWV variations for PRN10 and PRN21 at SLEE and ISTA vs time.

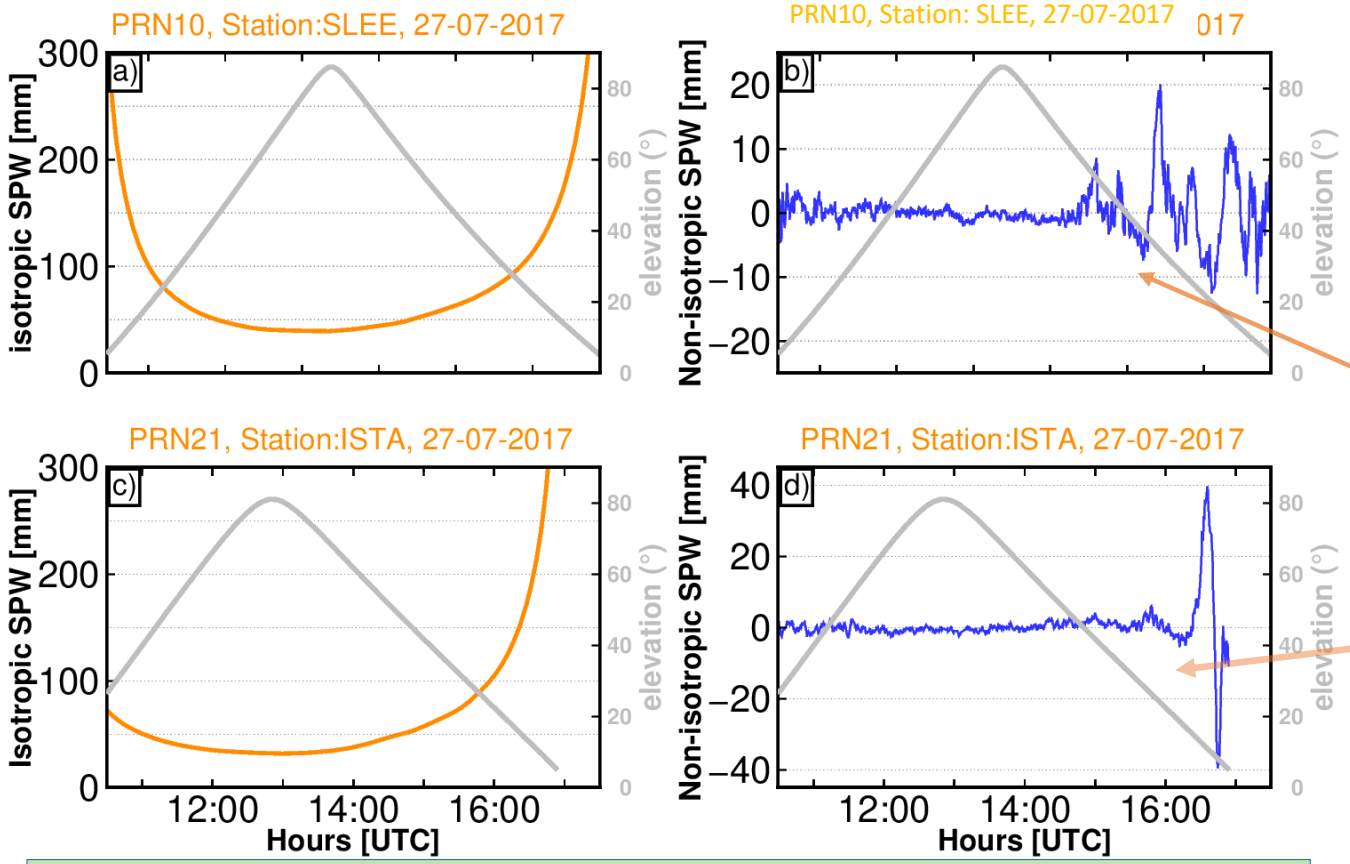

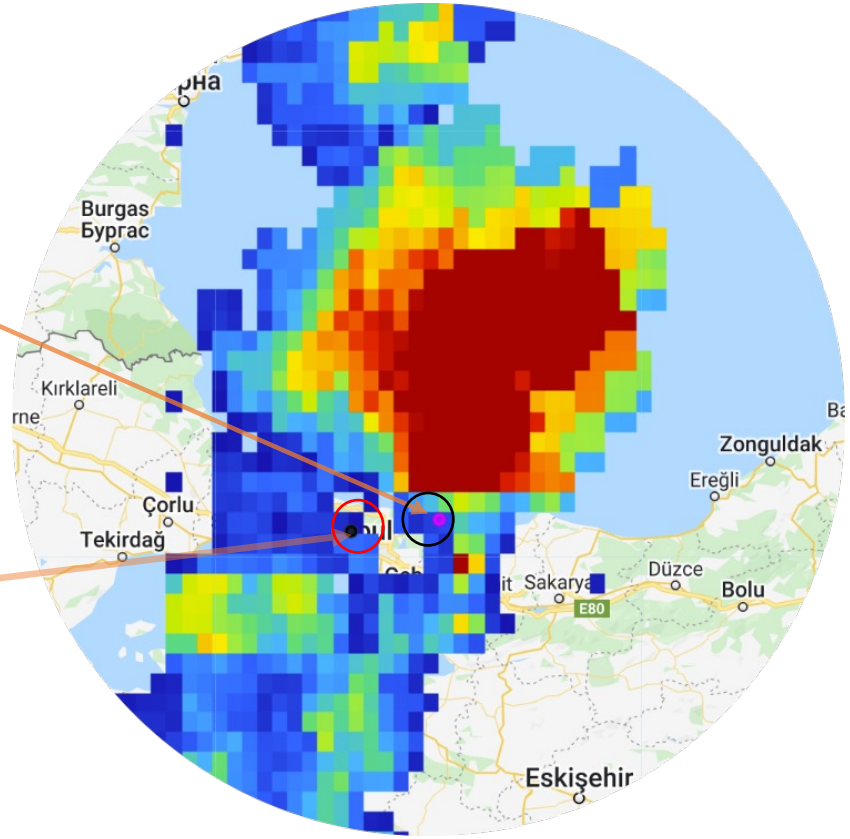

The isotropic (left) and non-isotropic (right) SPWD. For SLEE the non-isotropic contribution reaches **20**% of the isotropic component.

GPM precipitation at 17:00 UTC:

The effect of MPS on the estimate of the non-isotropic SPWV for ISTA and SARY for different satellites.

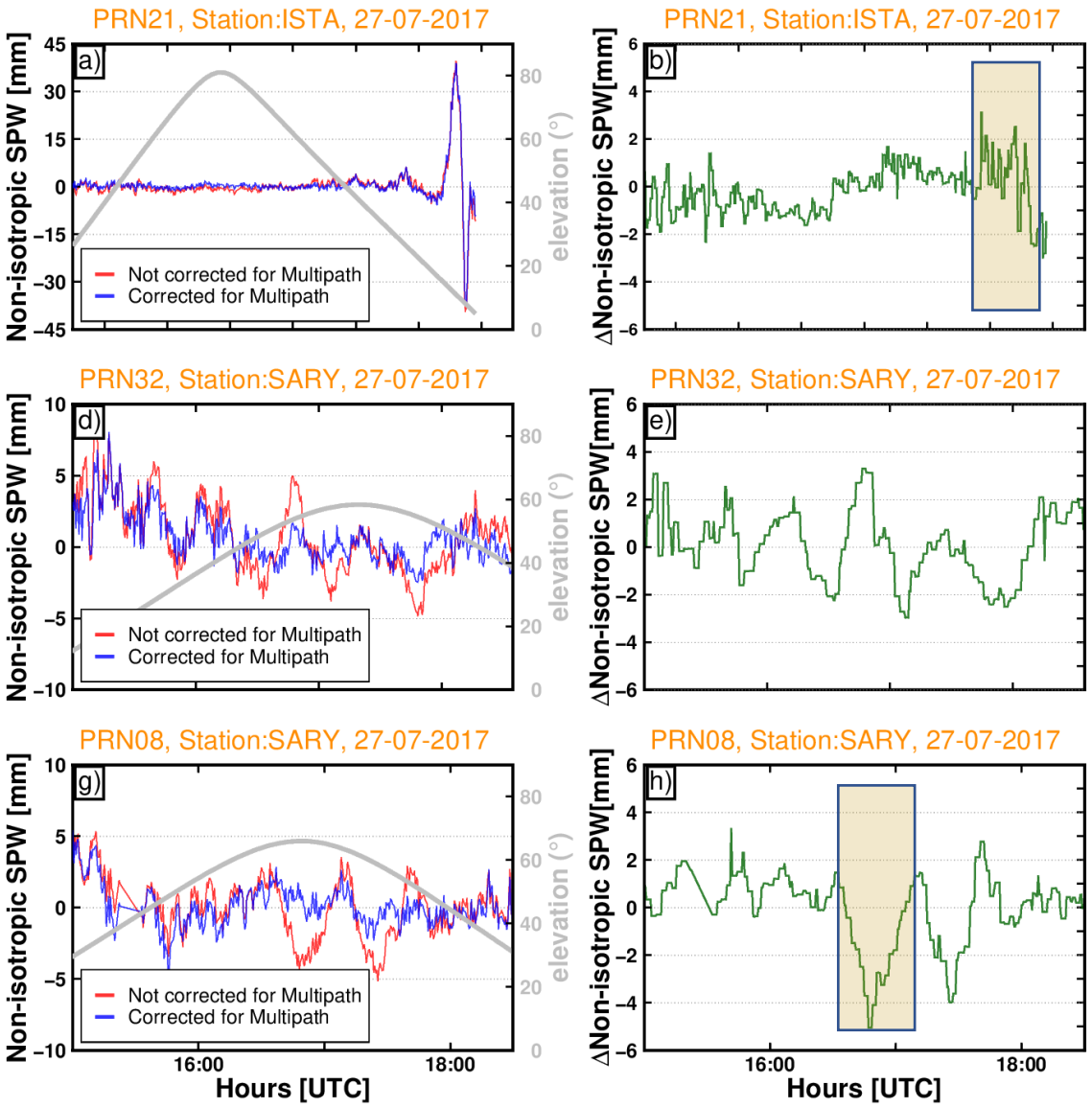

Non-isotropic (left) SPWV with MP correction (blue colour) and without MP correction (red colour) and their differences (right panels) for ISTA and SARY.

For SARY, which is adversely affected by MP, the peak variability difference can reach $5\ mm$.

Not correcting for MP at ISTA, the 3 mm variations in SPWV can be as large as 0.8 mm of equivalent PWV at 10°. For SARY, the 5 mm variations in SPWV can be as large as 4.3 mm in equivalent PWV at 60° elevation angle.

The SWD biases, RMS and standard deviations between ERA5 and GPS solutions (same epoch, elevation and azimuth) for 54 stations and corrected and not corrected cases.

SWD difference statstics [All] [mm]			
With post-fit residuals and MPS			
Comparison	Bias	RMS	SD
ERA5-GPS	1.7	55.5	55.5
With post-fit residuals			
ERA5-GPS	1.7	56.0	55.9
Without post-fit residuals and MPS			
ERA5-GPS	1.8	53.9	53.9

Comparison **for all satellites** for 24 hours during the severe weather event

SWD difference statstics [PRN10] [mm]			
With post-fit residuals and MPS			
Comparison	Bias	RMS	SD
ERA5-GPS	5.1	40.4	40.1
With post-fit residuals			
ERA5-GPS	5.8	40.6	40.3
Without post-fit residuals and MPS			
ERA5-GPS	6.7	41.3	40.9

Comparison **for one satellite (PRN10)** for 24 hours during the severe weather event

BIM and information model exchange in civil engineering, architecture and cultural heritage

Scanning the Past: A 3D Model of Trausch's Library

Norman Teferle[1], Lars Wieneke[2], Shahoriar Parvaz[1], Quentin Bebon[1], and Dietmar Backes[1]

[1]*Geodesy and Geospatial Engineering, Department of Engineering, FSTM, University of Luxembourg*

[2]*Luxembourg Center for Contemporary and Digital History (C²DH), University of Luxembourg*

Presented at: *"Producing Historiography in a Changing World - Practices of Historians in Analog and Digital Contexts", Bibliotheque Nationale du Luxembourg, 5-6 May 2022, Luxembourg*

What are the objectives of this study?

- At the start of the project the objective was
  - To capture and and generate a 3D model of Trausch's Library containing the building and bookshelves which clearly show the book spines of each book to allow identification
- As the project progressed the idea for the creation of a subsequent "virtual experience" of Trausch's Library arose. This required us
  - To carry out a study to investigate pathways from the 3D model of Trausch's Library to a public virtual experience
    - Linking of books (via spines) to scans of the pages
    - …

Geospatial Capturing Technologies and Building Information Modelling for Digital Cultural Heritage

- Geospatial capturing technologies allow to
  - collect highly detailed information about Cultural Heritage objects
  - complete accurate 3D models
  - safeguard and preserve many Cultural Heritage sites

- Building Information Modelling (BIM)
  - provides an information system at architectural scale
  - facilitates the management of semantically enriched 3D models
  - unique database for all data of the building
  - support for Augmented Reality (AR) or VR applications
  - web sharing
  - …

What is Historic Building Information Modelling (HBIM) and what is it used for?

- Application of BIM principles to cultural heritage objects
- Focusses on a comparison between existing buildings and well-known architectural grammar
- HBIM applications are manifold: e.g. conservation, restoration planning, construction simulation, disaster preparedness

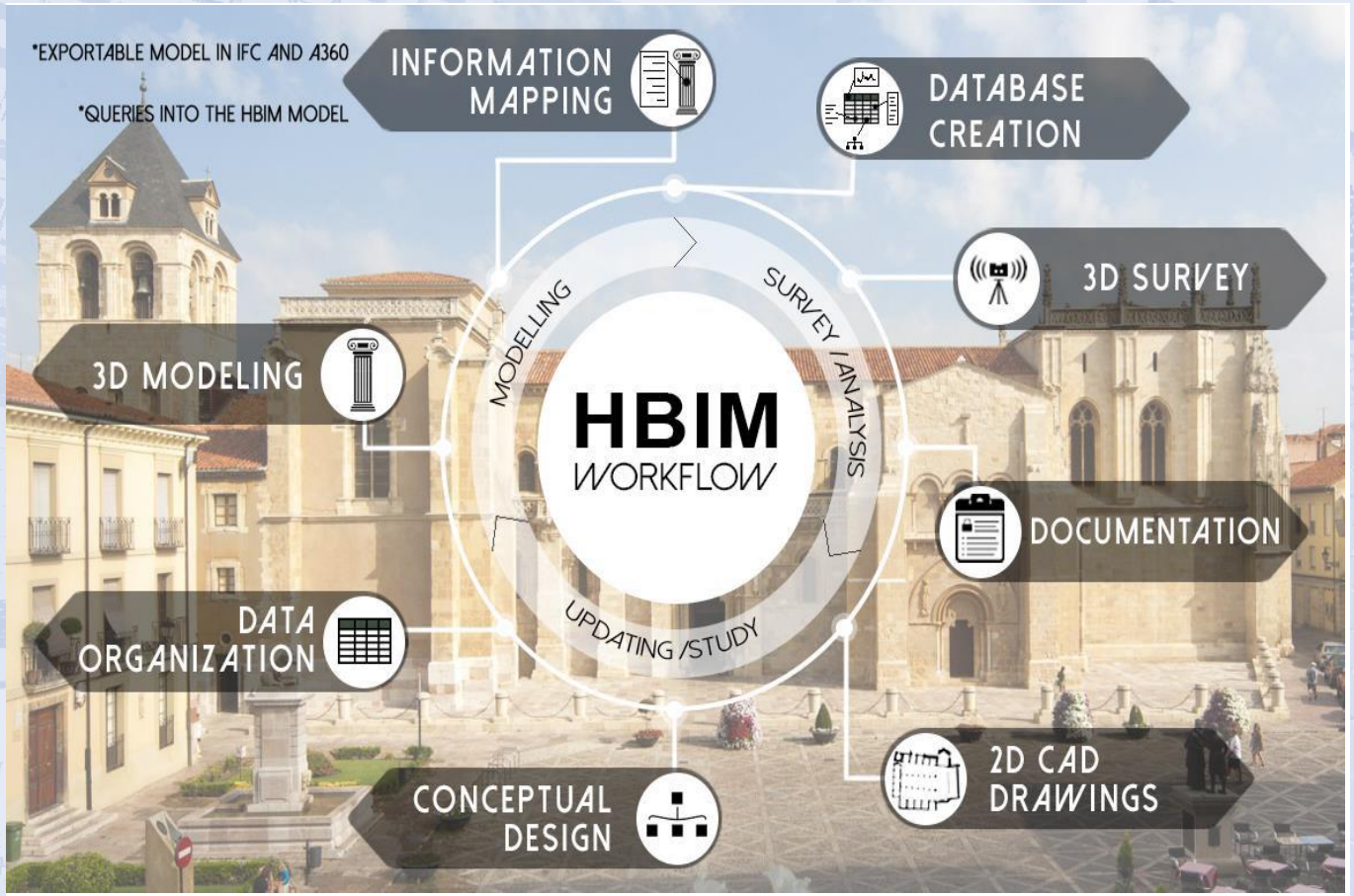

3D Survey

Establishing a coordinate reference and capturing the building and bookshelves

What are the main 3D reality capturing technologies for cultural heritage objects?

- Digital close-range photogrammetry
- Laser scanning
- and combinations of these in mobile mapping systems

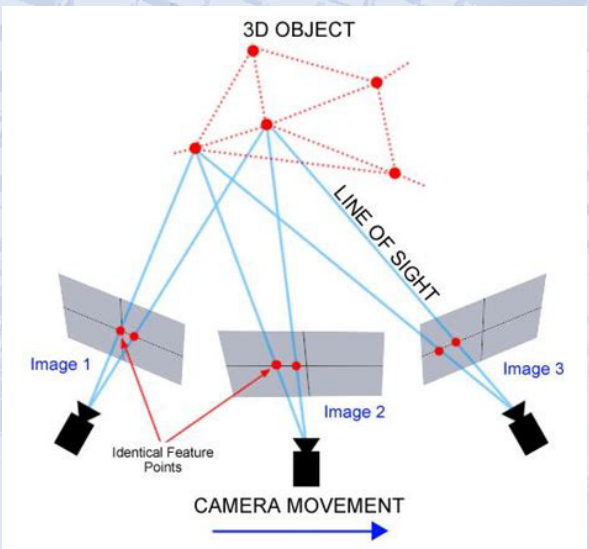

- Both technologies have pros/cons but have complementary features
- But, they need external information to merge their coordinate results

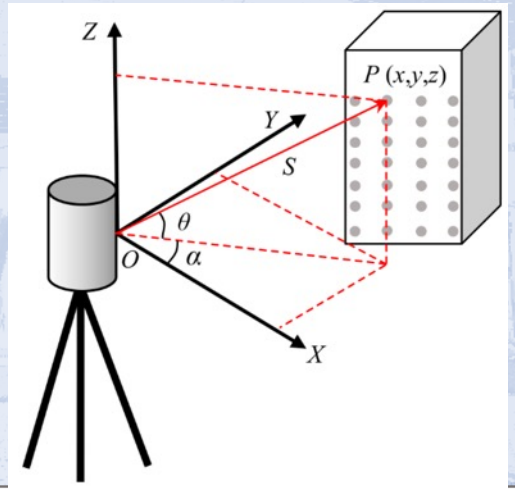

Geodetic framework for providing a coordinate reference for the Villa Trausch

- Real-Time Kinematik (RTK) GNSS Measurements
- Total station measurements

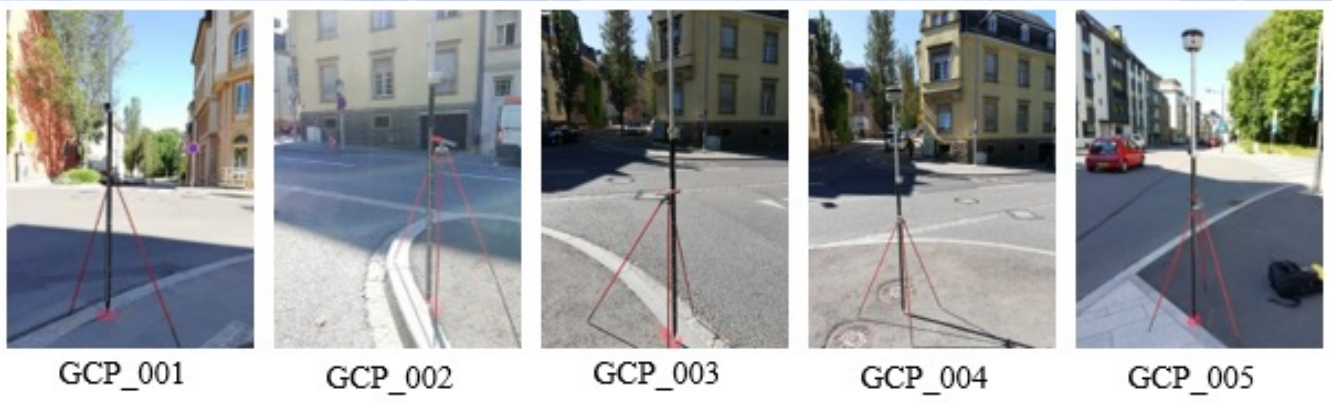

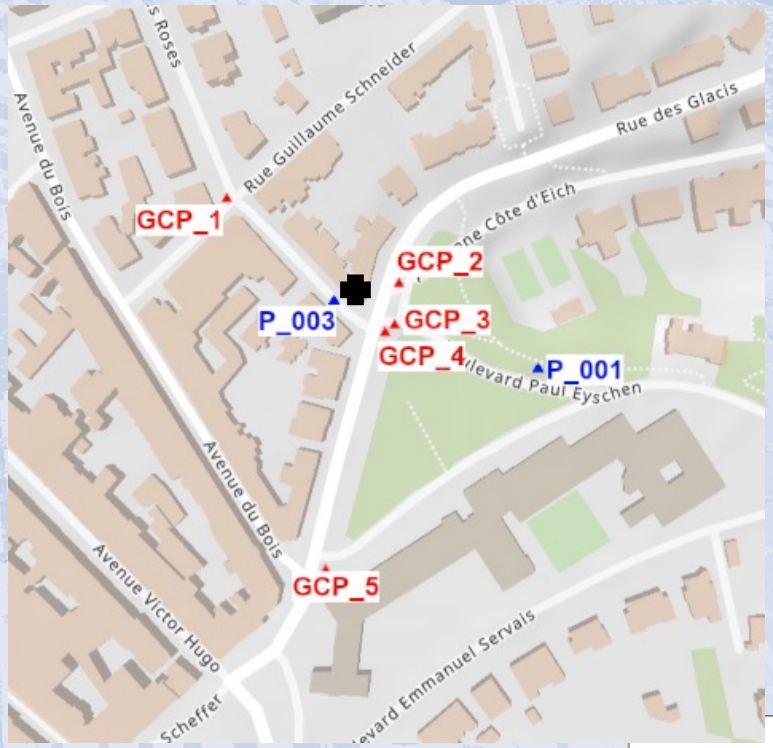

The coordinate frame inside the building in support of the reality capturing technologies

- Topographic survey inside the building using a total station
- Creation of a rigid coordinate frame as reference system for all measurements
  - Use of temporary targets
- Observations were adjusted with the least square adjustment method to estimate coordinates and quantify errors (LisCAD software)

The surveying campaign inside the building was an overdetermined control network

Basement

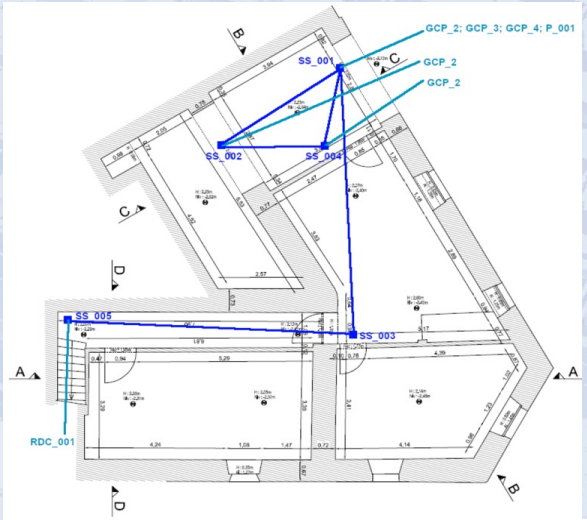

Ground Floor

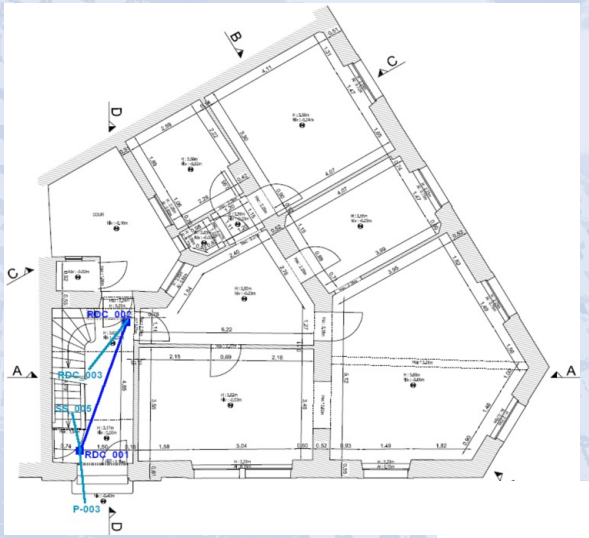

1st Floor

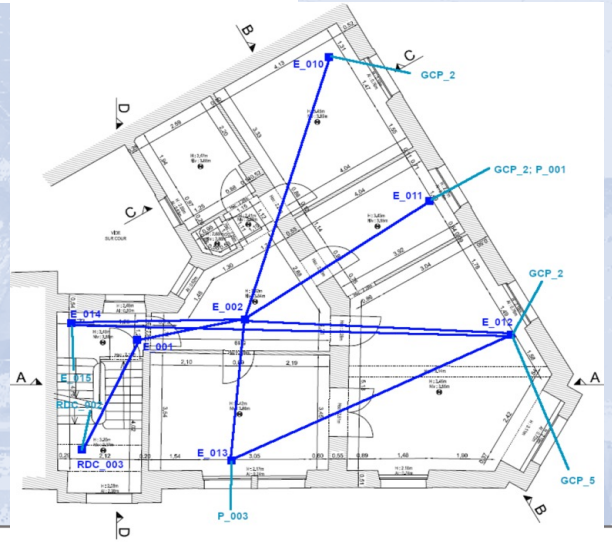

2nd Floor

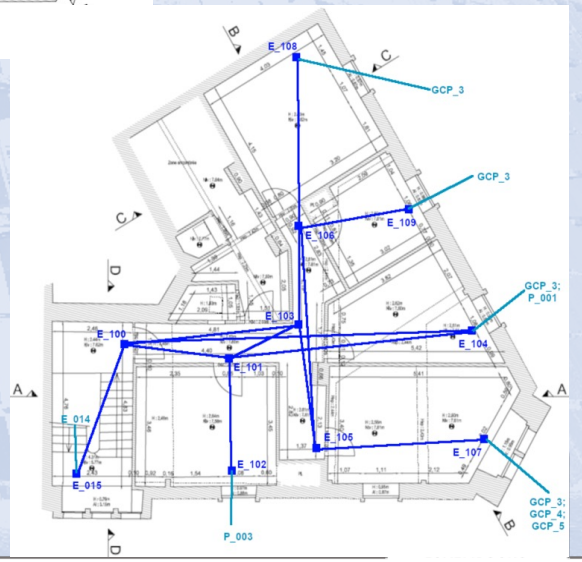

We used a laser scanner and a mobile mapping system to capture the outside and inside of the Villa

- Faro Focus S350
  - room scans with 1/5 resolution and 3x quality
  - bookshelves with 1/4 resolution and 4x quality parameters
- Zeb Horizon handheld mobile mapping system

The results of the laser scanner capture were more than adequate for the application

- Approx 7,000,000,000 points (billion)
- Mean point error of 1.5 mm
- A minimum overlap ratio of 12.9%
- Maximum point error of 48.9 mm

Co-registered point cloud of the building exterior

Cross-evaluation between laser scanner and mobile mapping results shows cloud-to-cloud distances of less than 15mm

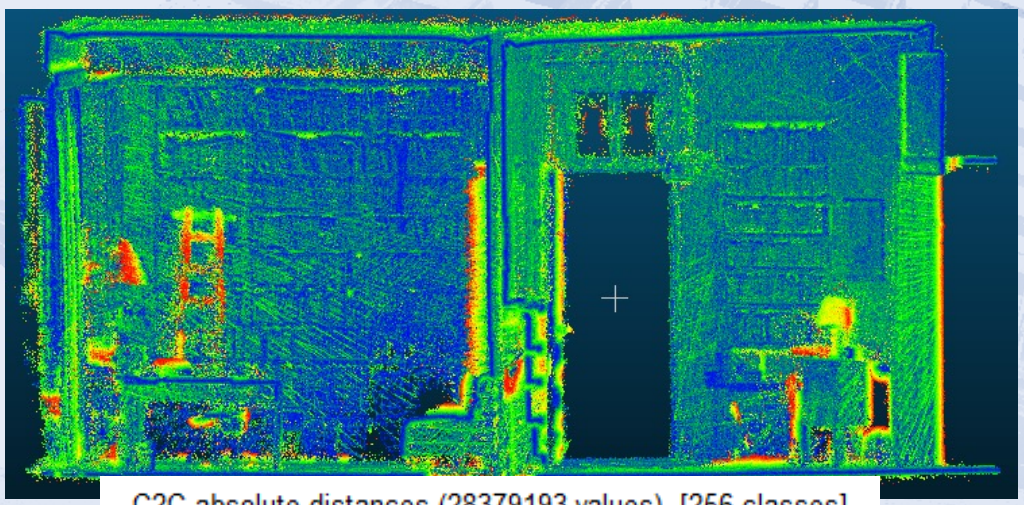

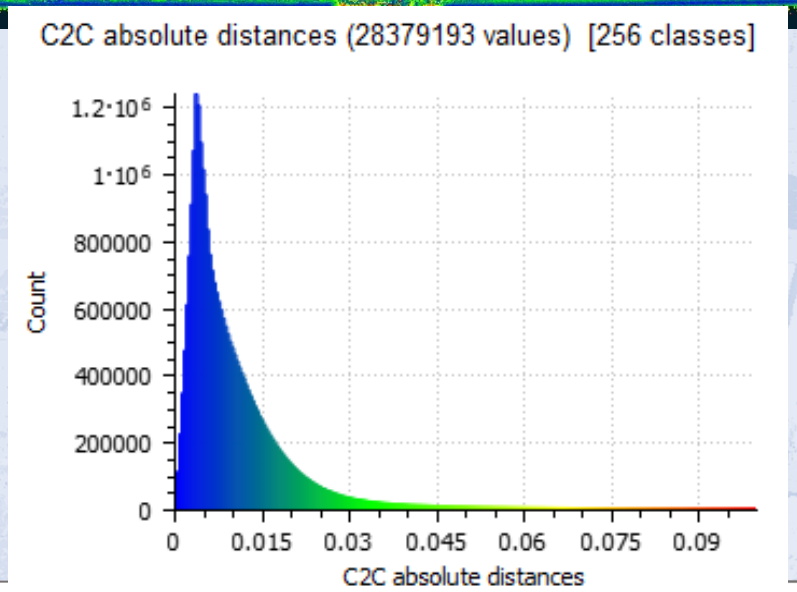

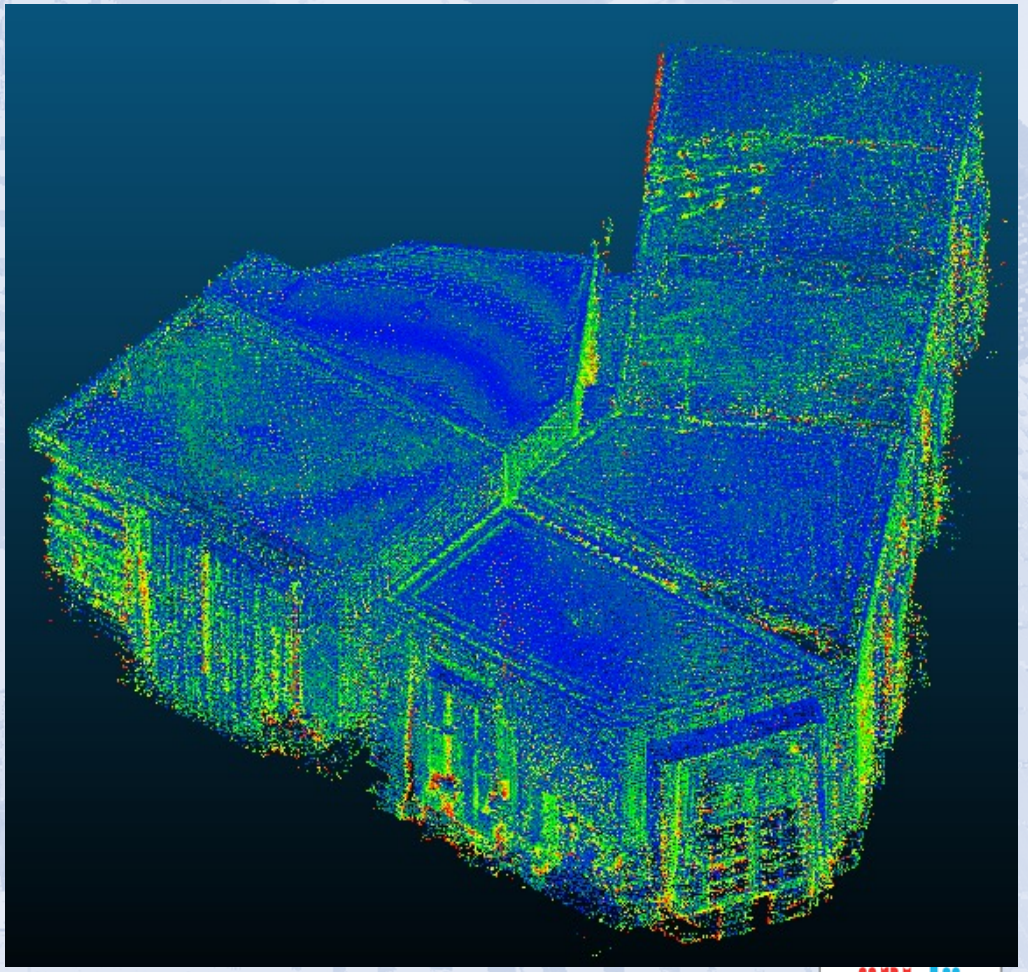

The photogrammetric survey of the bookshelves

- Nikon D800 (36.8 Mega-Pixel)
- Fixed focus around 60 centimetres. Parameters: ISO400 and F16

The 33 bookshelves on 3 floors of Trausch's Library

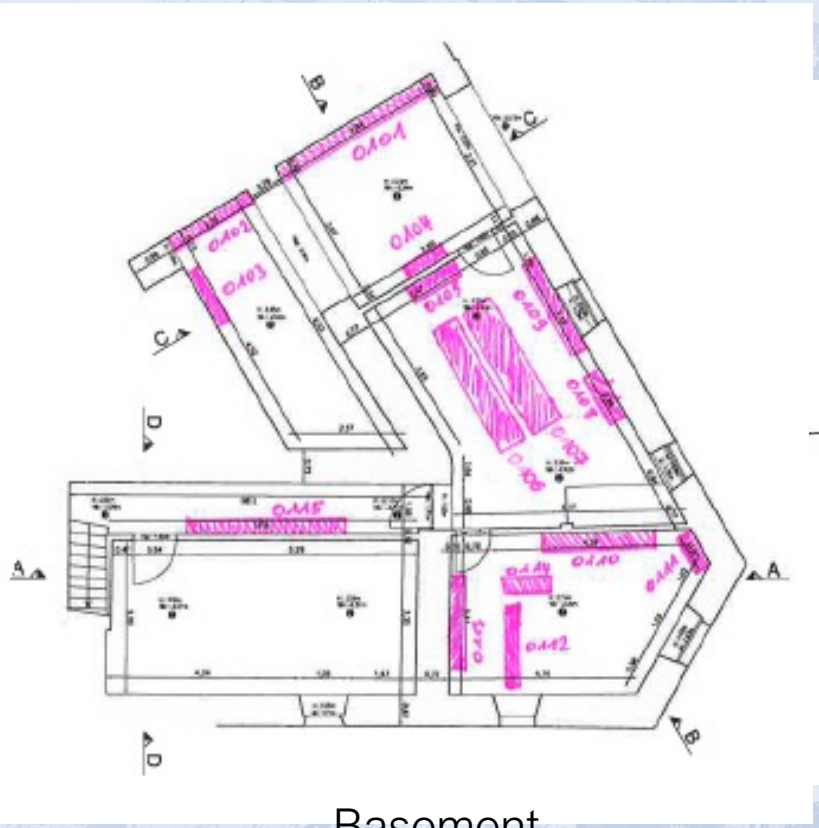

Basement

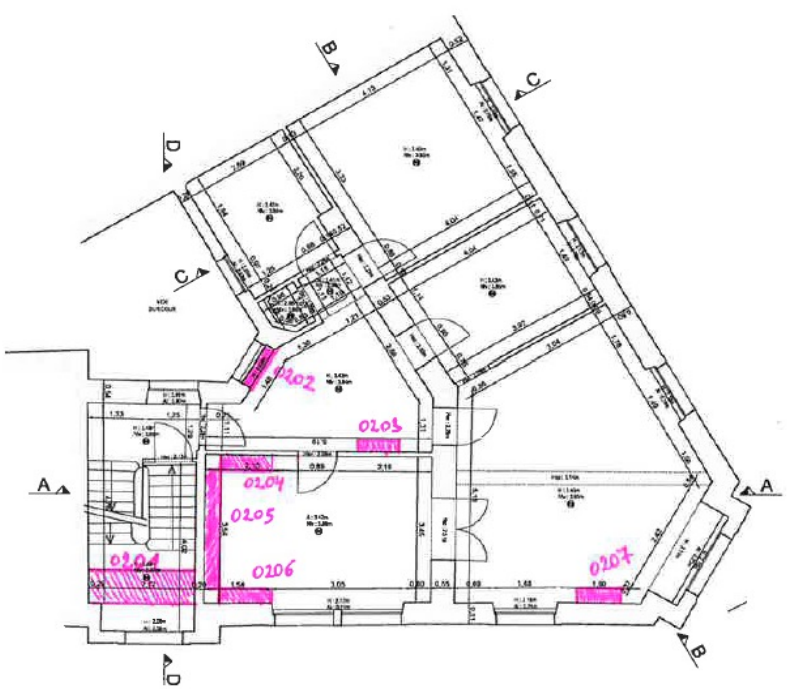

1st Floor

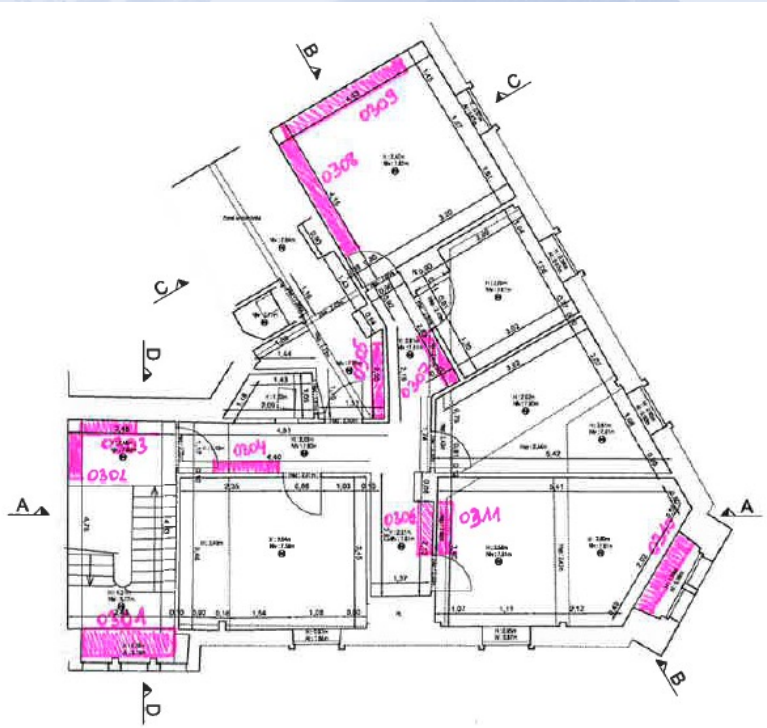

2nd Floor

An orthophoto was generated for each of the 33 bookshelves

- Employ the Agisoft Metashape software
- An image enhancement step was introduced in order to reduce voids (mainly edge areas) in initial orthophotos
- However, only incremental improvements were achieved, many voids remain, probably due to coverage/quality issues

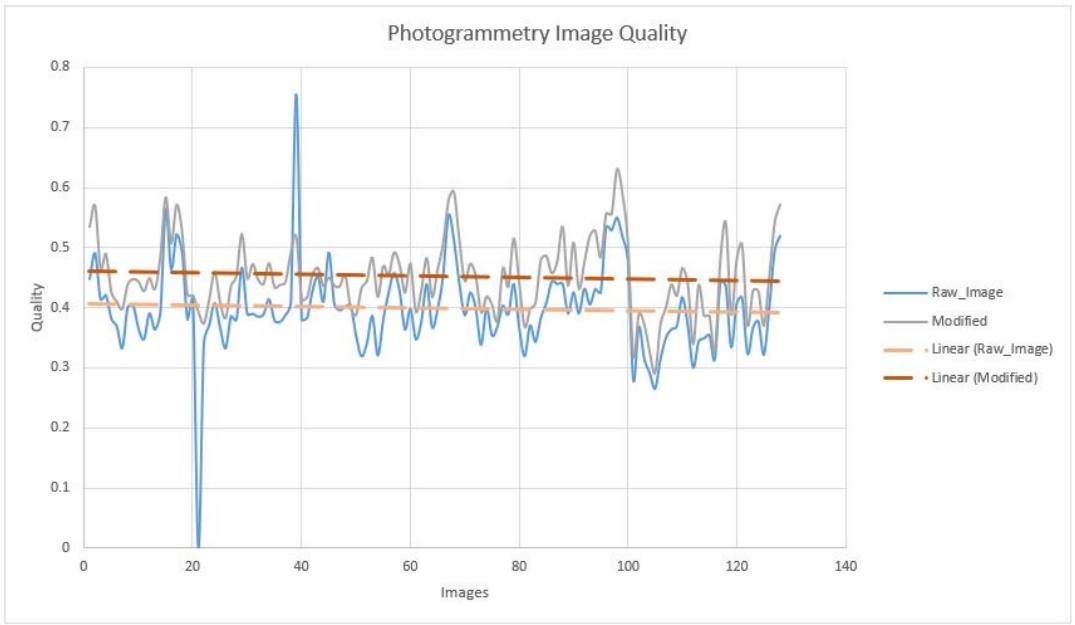

Using the generated orthophotos of the bookshelves a coordinate system for the location of books was derived

- i.e. $Book_{ID} = \mathbf{02\ 05\ 02\ 04\ 047}$
- **Alternative:** $Book_{ID} = \mathbf{02\ 05\ 02\ 06\ 047}$ **(matrix in database)**

The cross-evaluation between laser scanner survey and photogrammetry shows cloud-to-cloud distances with standard deviation of 1 cm

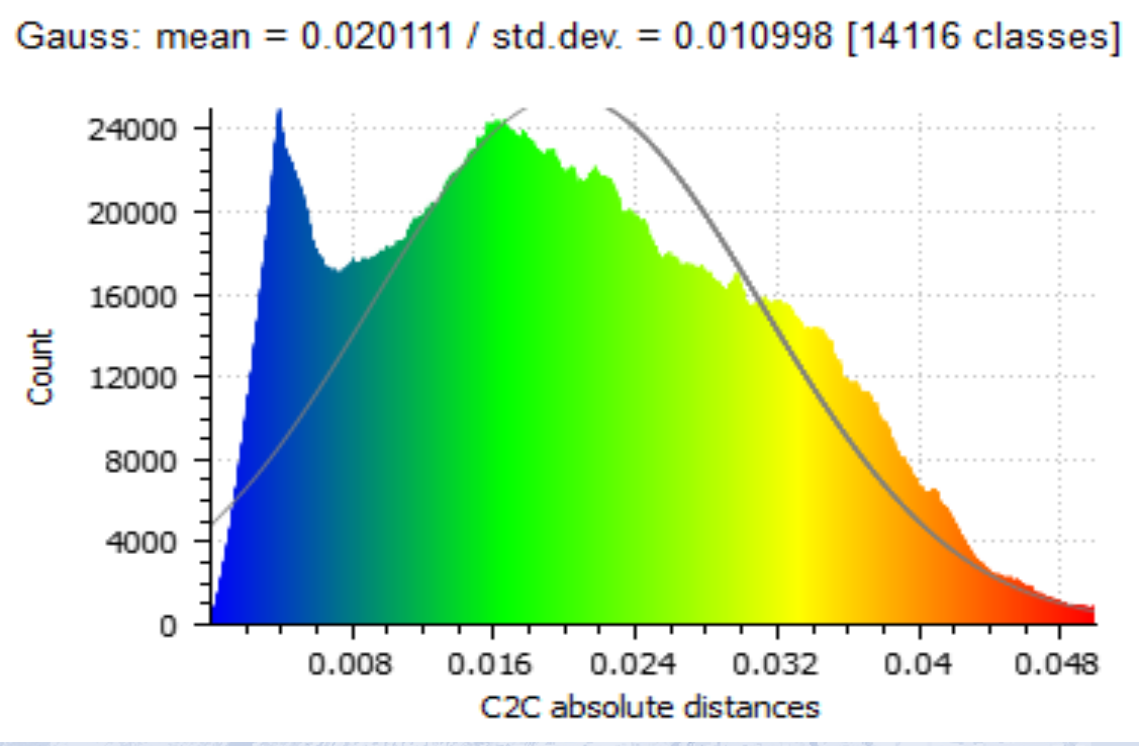

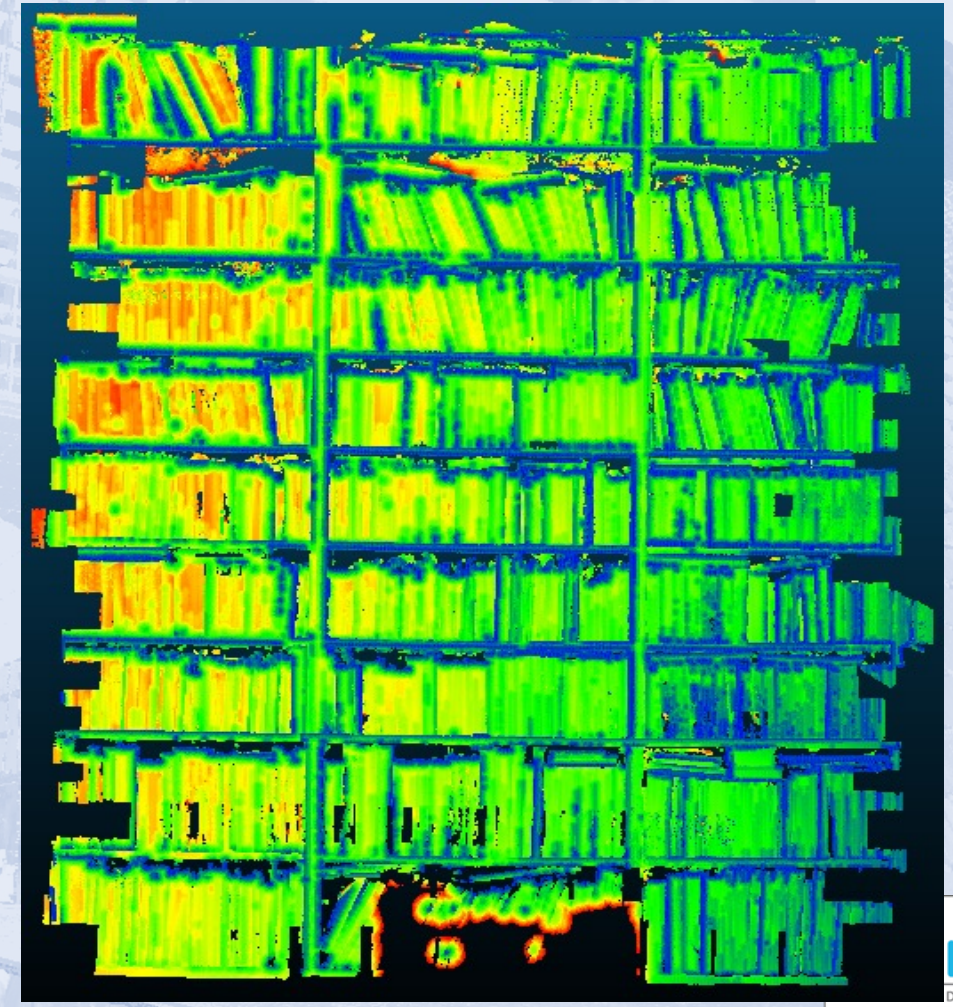

3D modelling

using the Autodesk Revit BIM software

The modelling phase required a hybrid solution including parametric and direct modelling

- Parametric modelling: for repetitive and geometrizable elements (some instance parameters for local editing)
- Direct modelling: extracting 2D profiles from the point cloud and modelling through functions such as extrusion, void and sweep

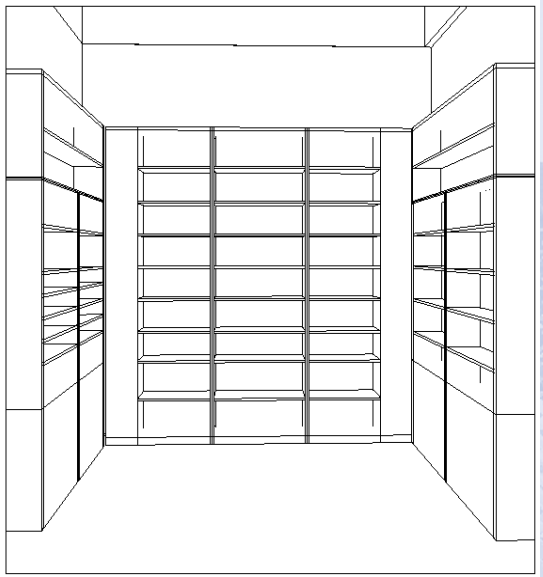

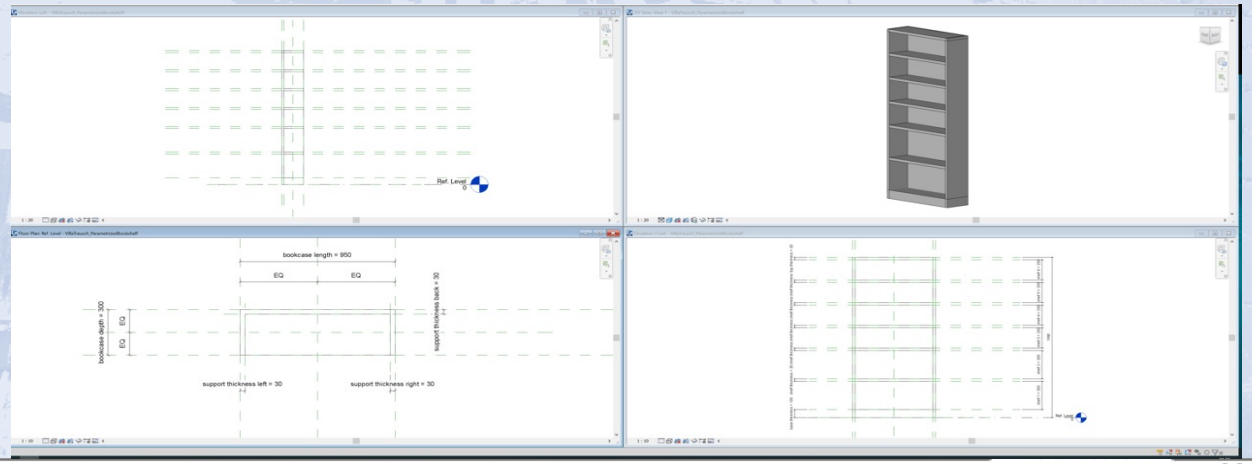

Interior Modelling was carried out using parametric and direct modeling within the BIM environment

- The building structure would be based on direct modelling
- Bookshelves and furniture on parametric modelling

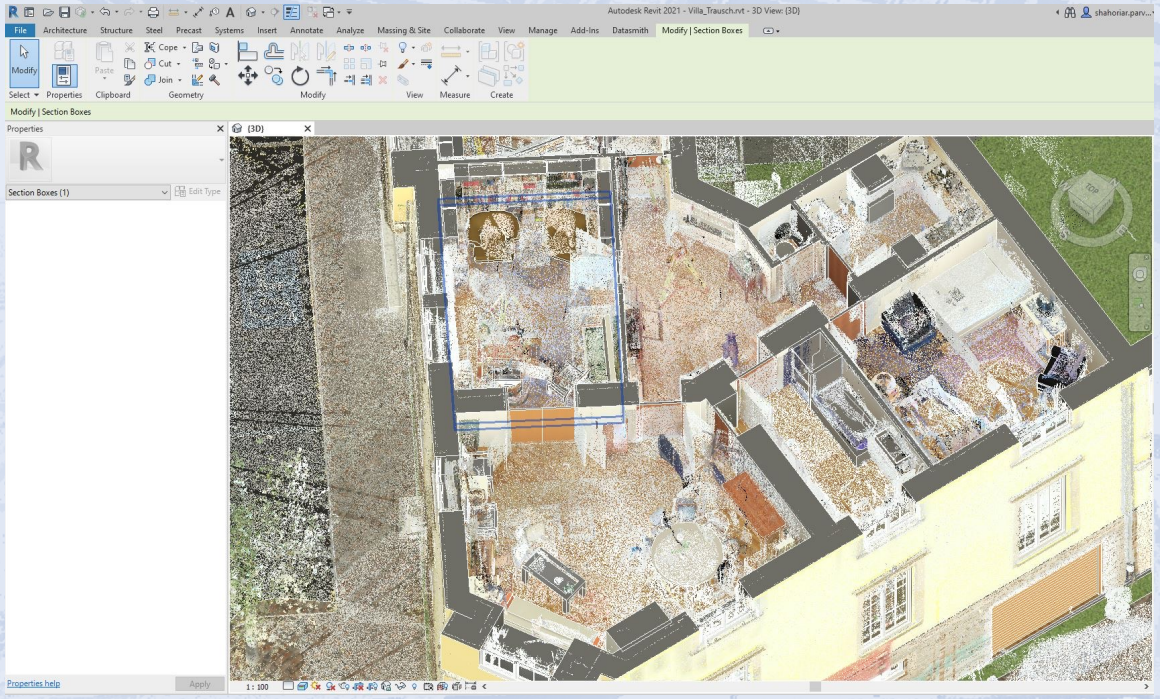

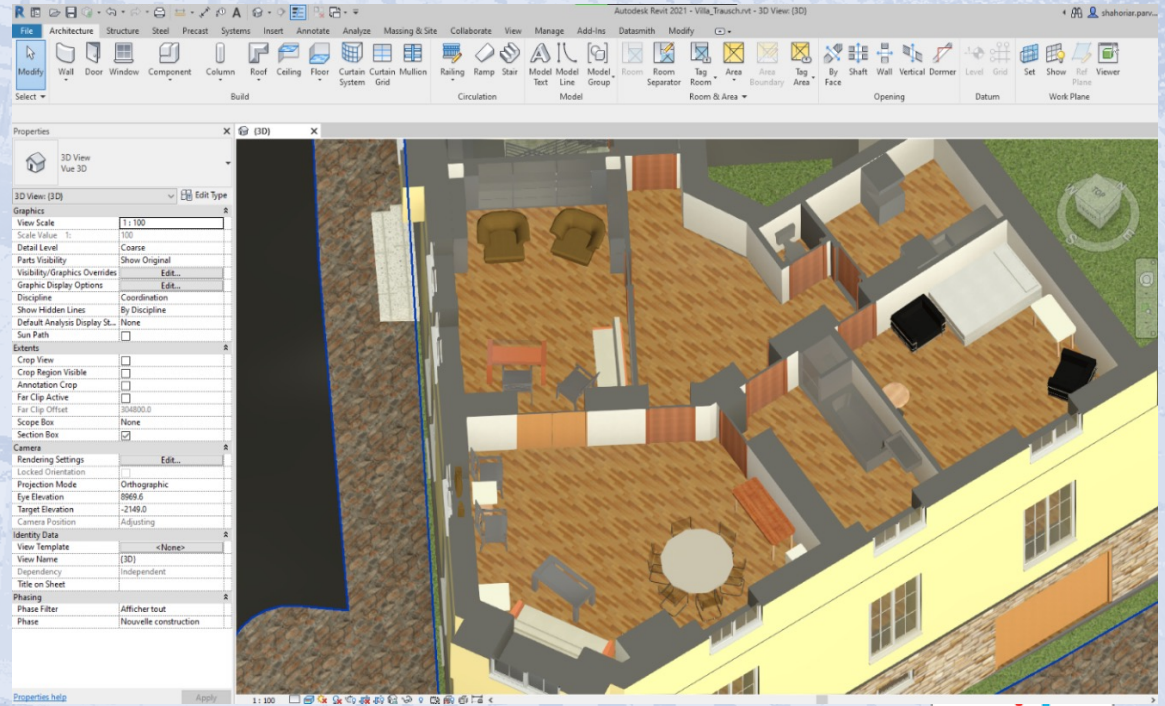

Example Model Views of Floors and Bookshelf Locations (1)

Basement

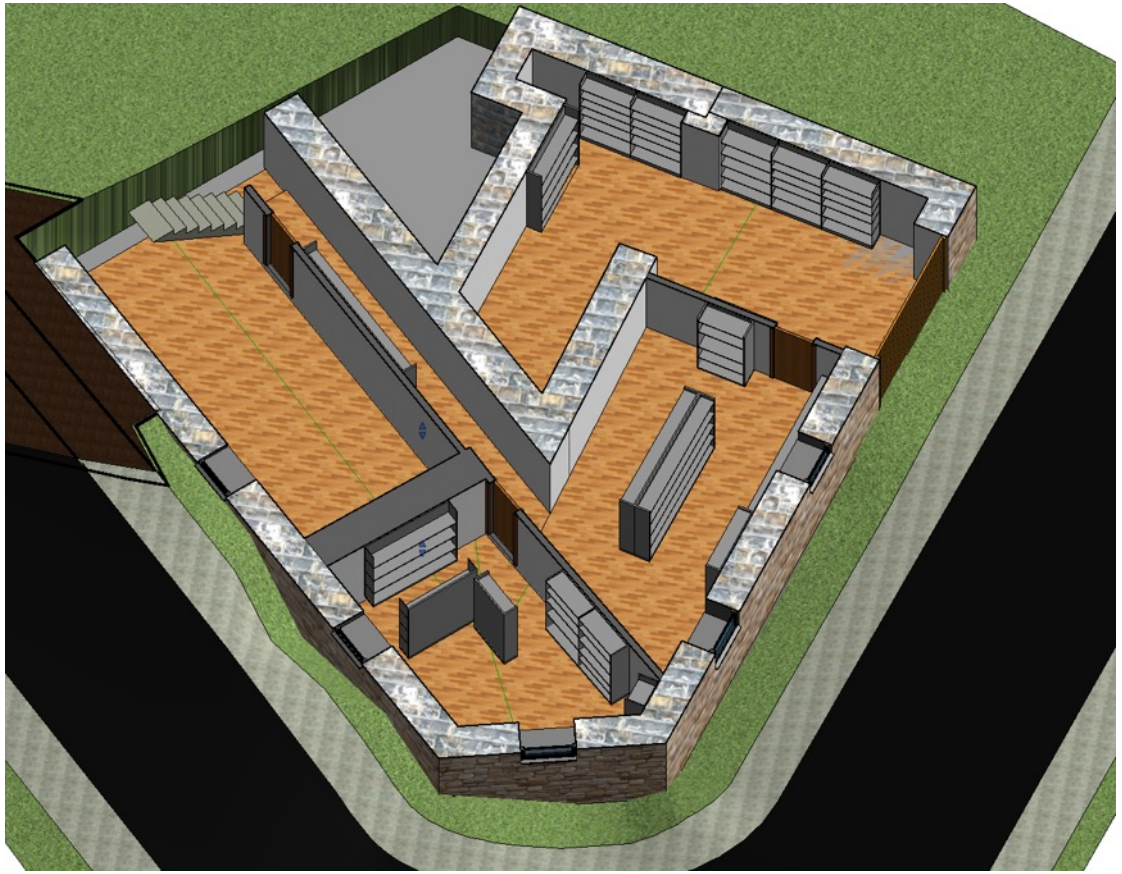

First Floor

Example Model Views of Floors and Bookshelf Locations (2)

Second Floor

Third Floor

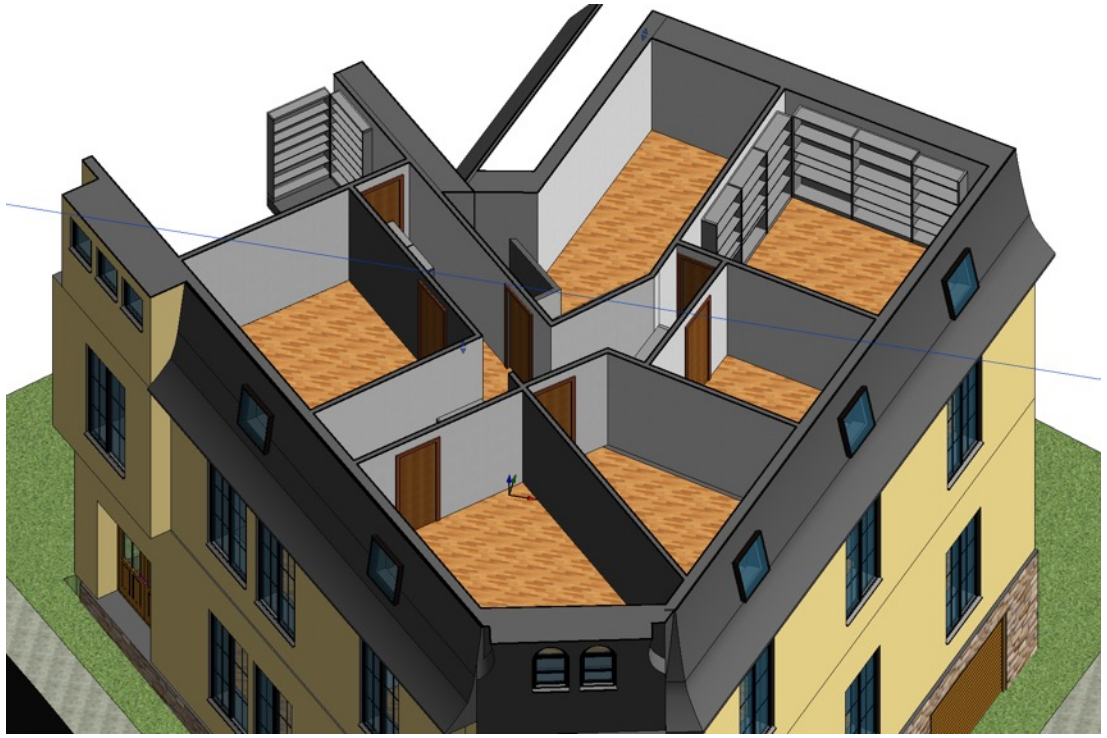

Linking the 3D model with the point cloud allows an assessment of the accuracy of the model

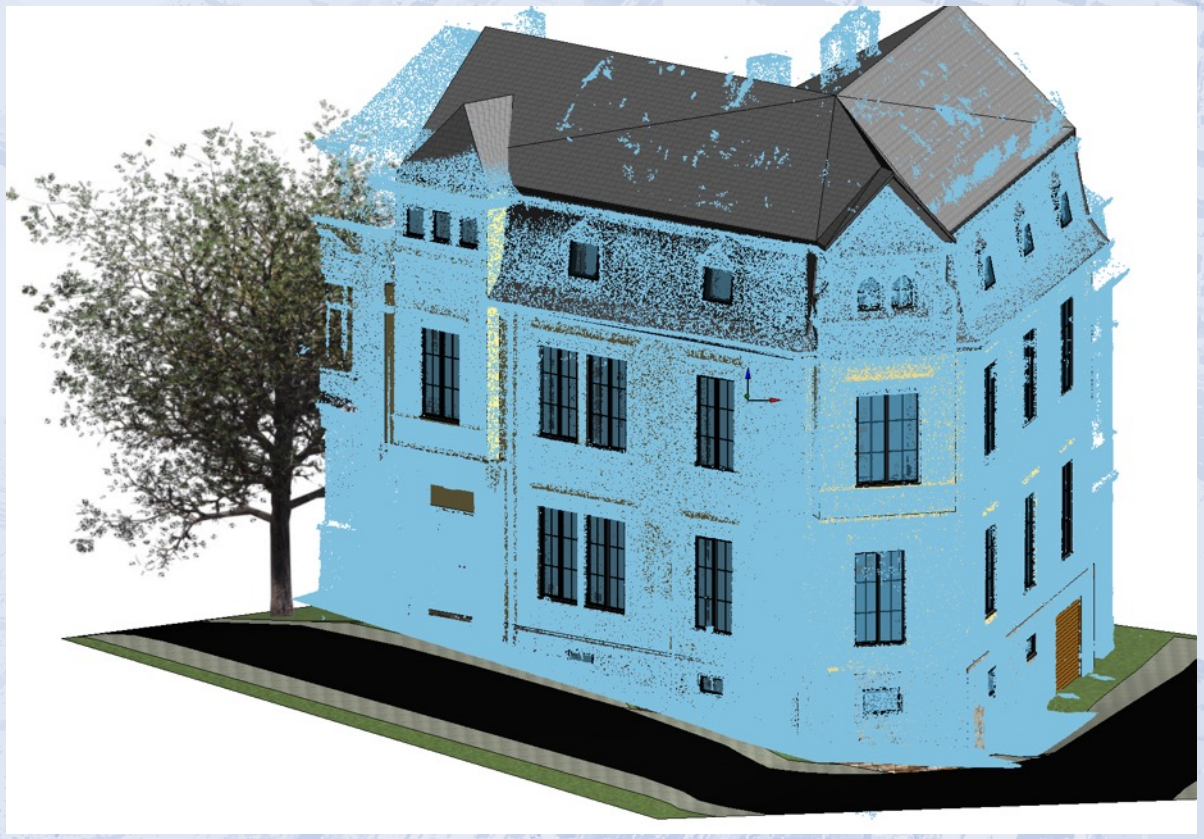

Highlights differences between reality and model

How accurate is the 3D building model?

A metric comparison between the 3D virtual model and point cloud was designed within Point Layout to evaluate the geometric model reliability.

- For facades the differences range from 0 – 1 cm
- For roof areas the differences range form 10 - 15 cm

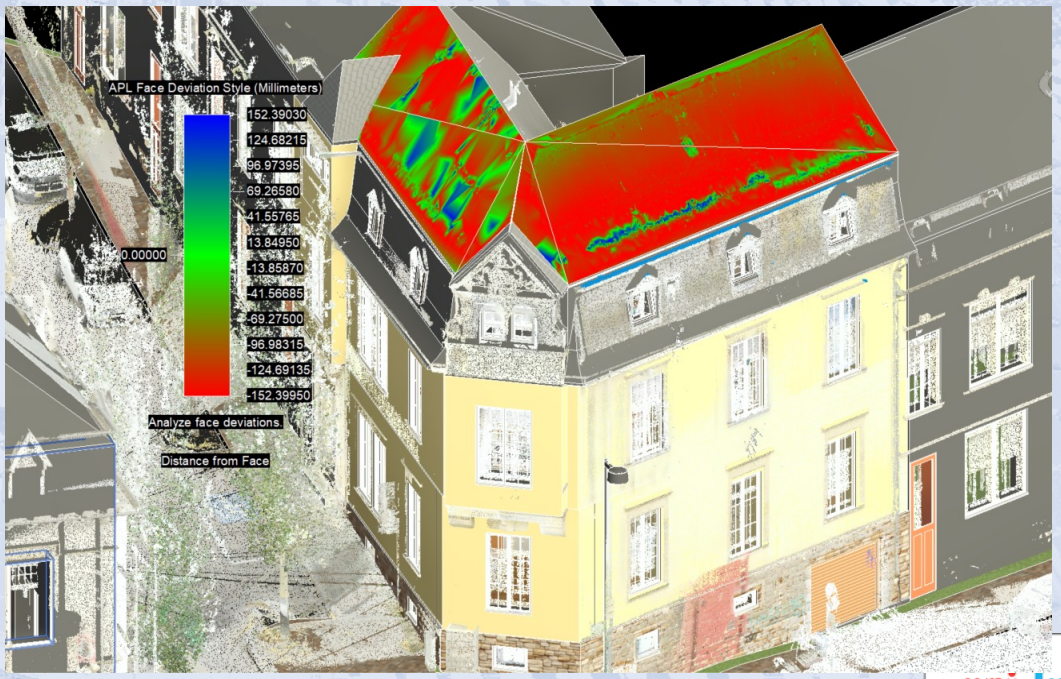

The VR Experience

Investigating pathways to move from the 3D building model to a VR experience

Investigating the software Twinmotion and the Datasmith plugin for generating a photorealistic representation

- Twinmotion is an incredibly simple-to-use real-time visualization tool built on the Unreal Engine from Epic Games, this platform enables users to create, modify, and apply materials to objects in a scene
- Datasmith is designed to solve the specific challenges faced by people outside of the game industry who want to use the Unreal Engine for real-time rendering and visualizations.

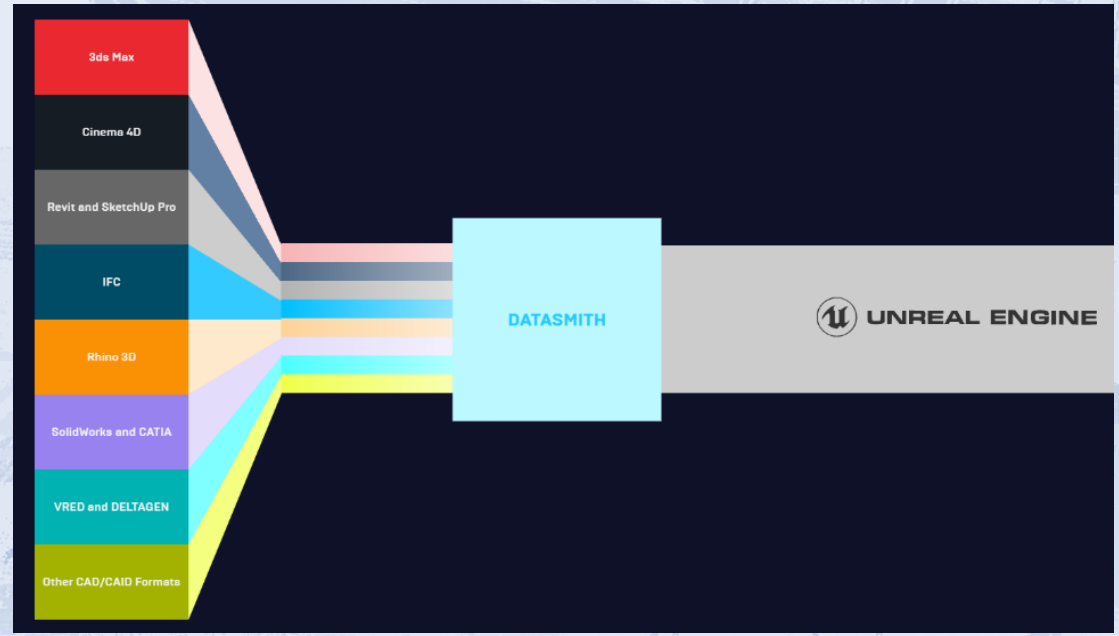

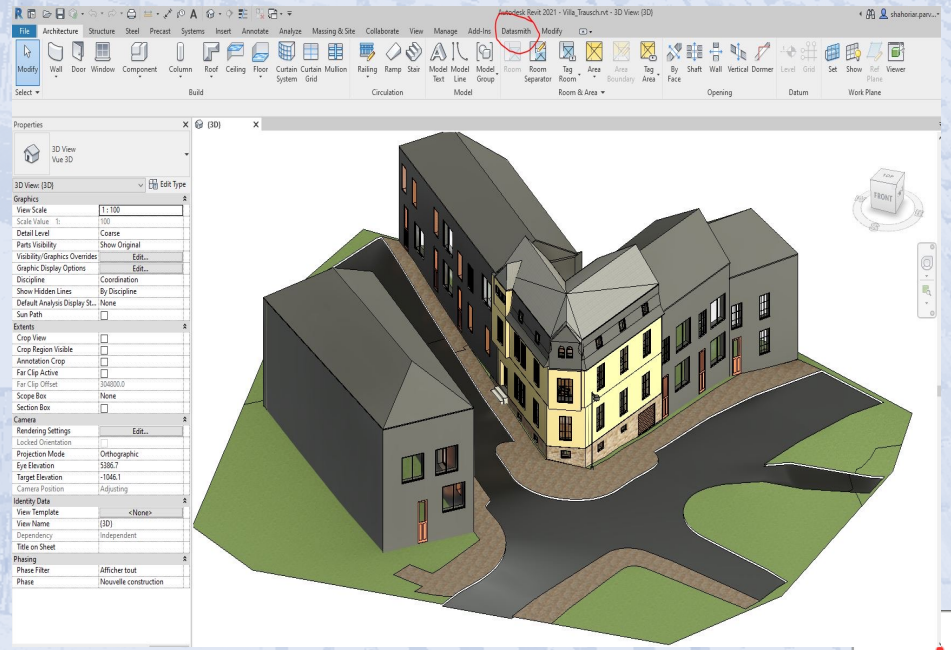

Investigating panoramic images for generating a VR experience

- The 3DVista VR software allows users to input panoramas from various 360° and DSLR cameras
- During the laser scanning also images were collected that are used to provide colour for the scan points
- Using the scanner software full-colour resolution panoramic images were exported
- The VR experience had to be based on reduced size images (from 96dpi to 25dpi) to run smoothly

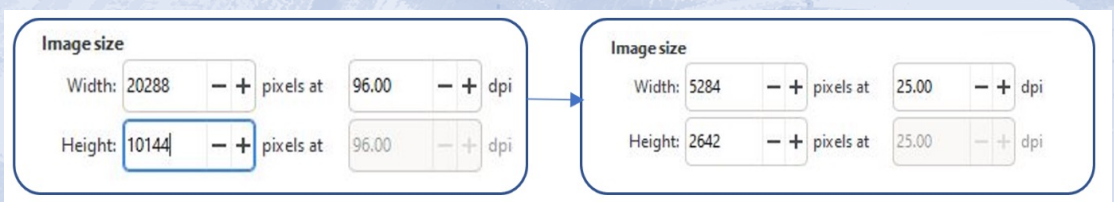

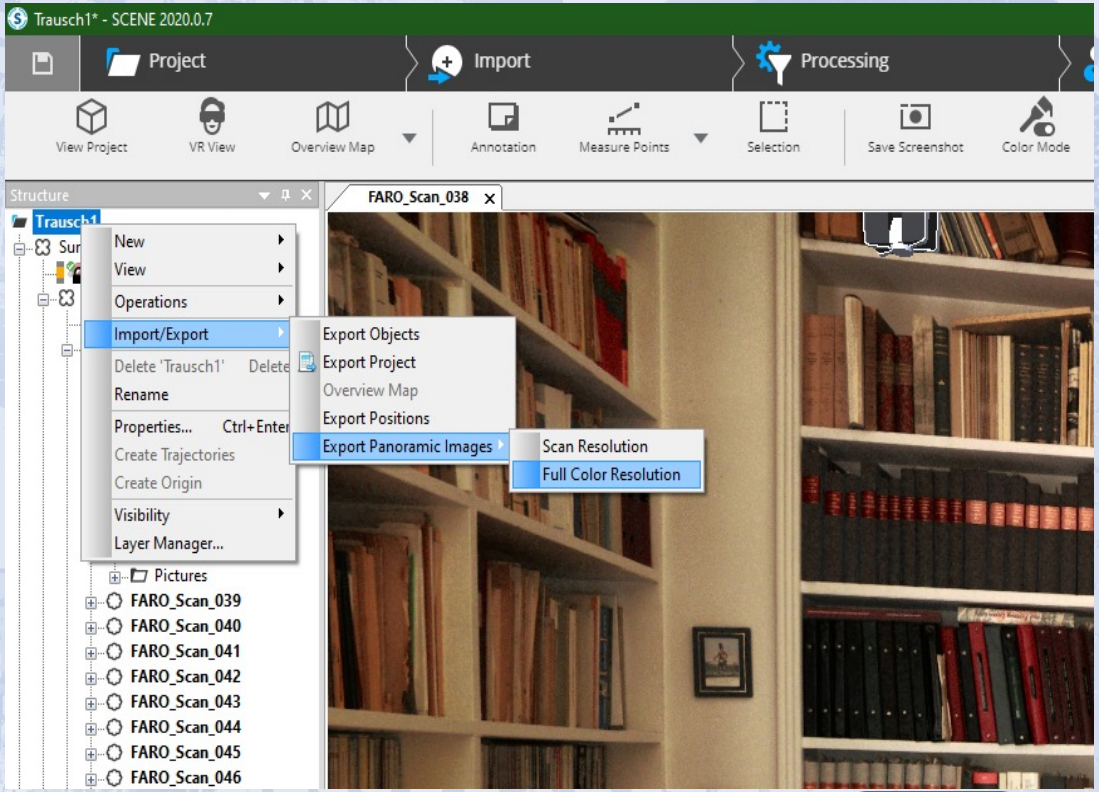

Investigating a polygonal hotspot to link book scans to the VR experience

Book spines can be divided into two polygonal hotspots; the upper one is linked with a high-resolution image; lower hotspot is linked with the scan (PDF) of this book.

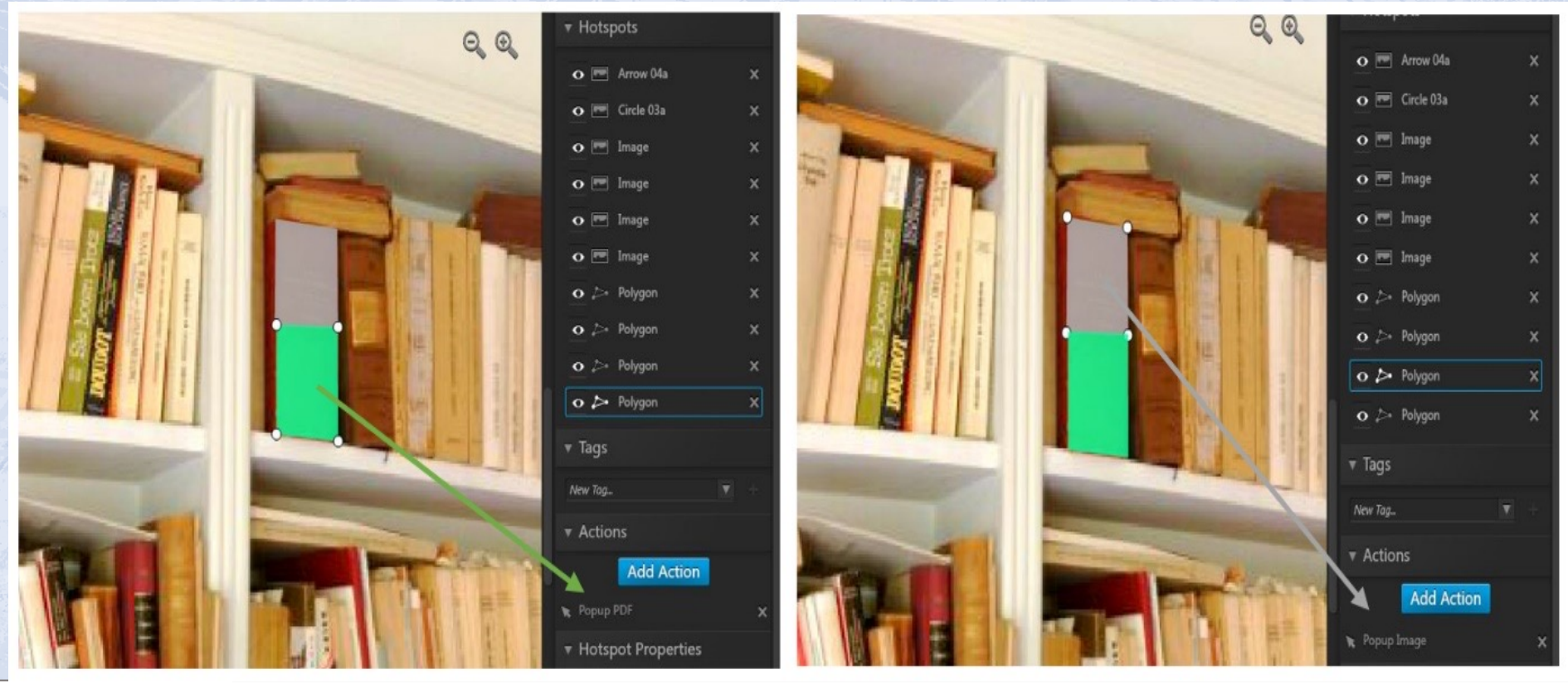

The 3D model and VR experience of the Villa Trausch are hosted on GitHub for test purposes (https://shahoriar3254.github.io/villa_trausch/)

Virtual tour of Villa Trausch

3D models of Villa Trausch

Next steps

1. Creation of a full high-fidelity model ready for web and VR consumption
2. Exploitation of this model for
    1. A general public outreach application to engage audiences with the life and work of Gilbert Trausch
    2. A facility to interlink the spatial configuration of Trausch's library with his thinking and oeuvre

Faculty of Science, Technology and Communication

ECON4SD Workshop

03 June 2022

PhD candidate : Arghavan Akbarieh

Supervisor: Prof. Norman Teferle

Work Package 6

Digital Technologies and Information Models for the End-of-Life Cycle of Built Assets

UNION EUROPÉENNE
Fonds européen de développement régional

UNIVERSITÉ DU LUXEMBOURG

Digital technologies and Information Models for the End-of-Life Cycle (EoL) Built Assets

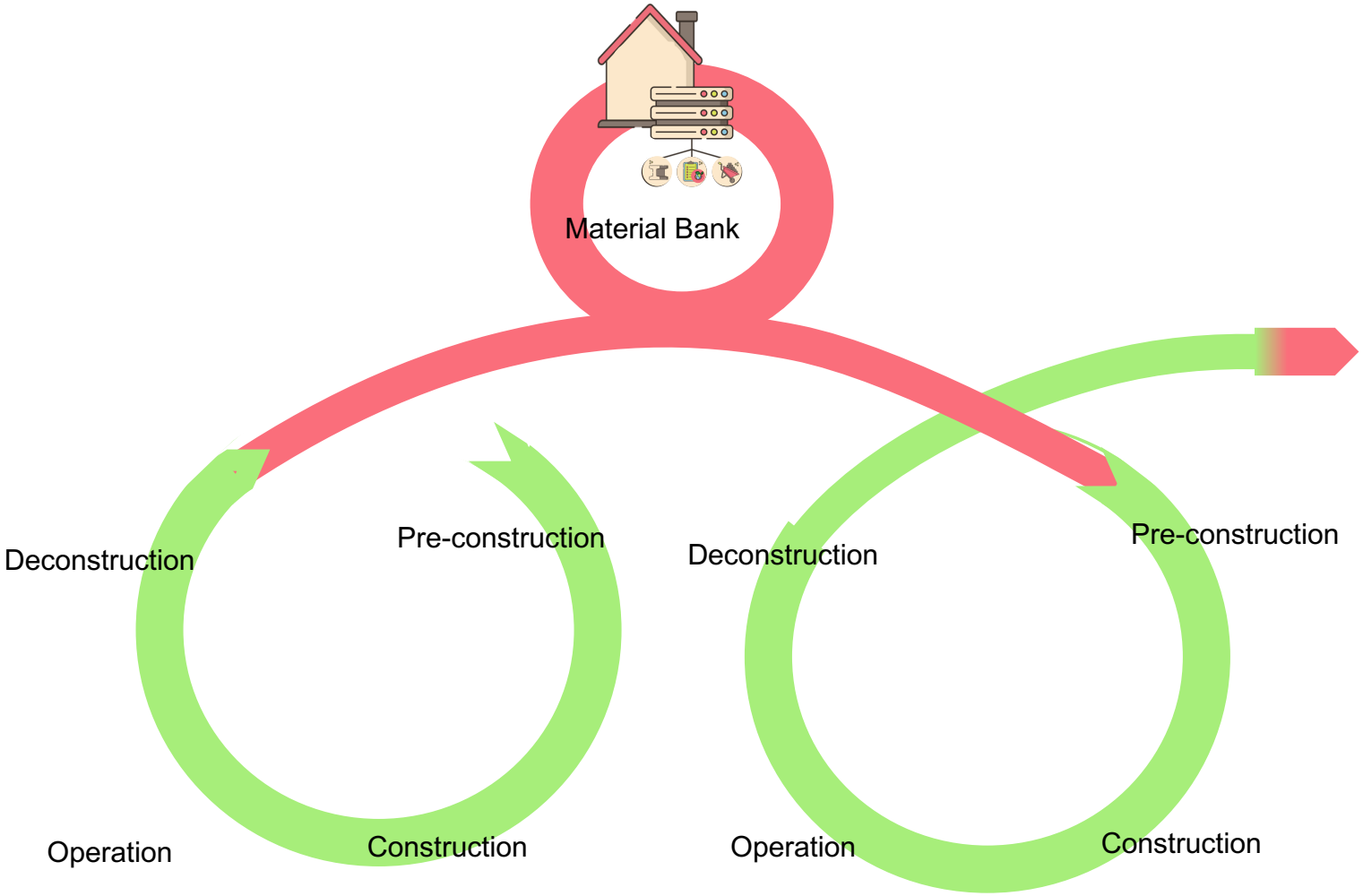

What is a Material Bank and how does it operate?

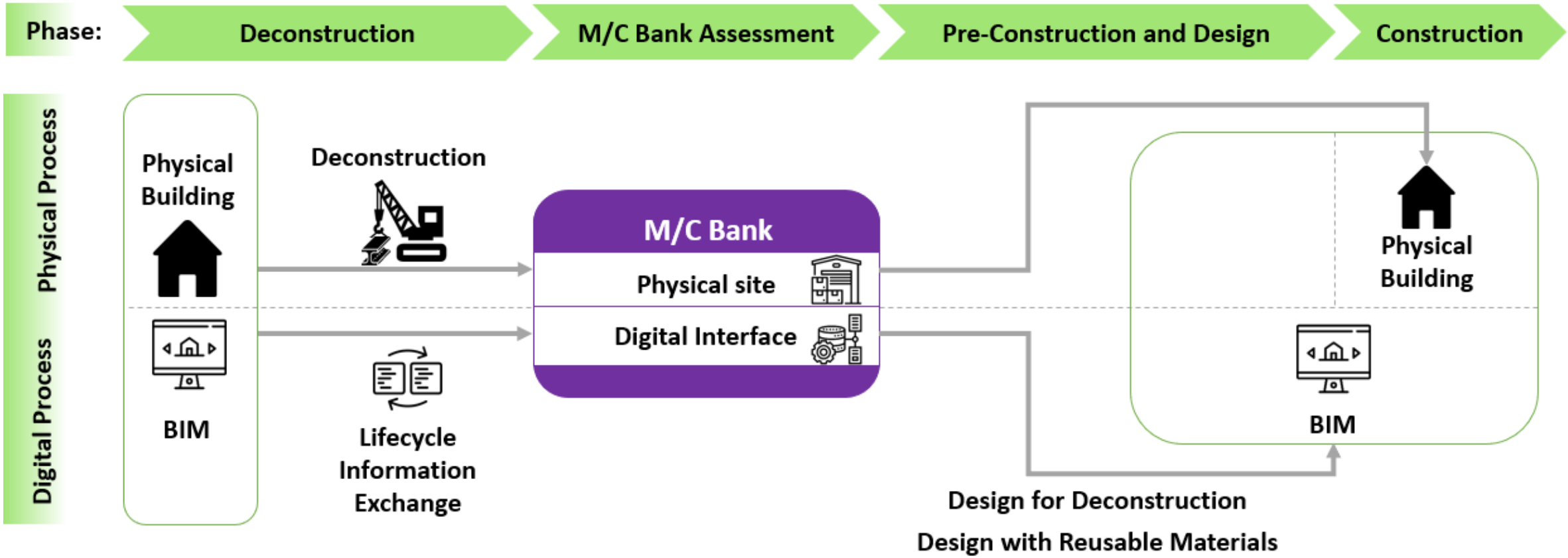

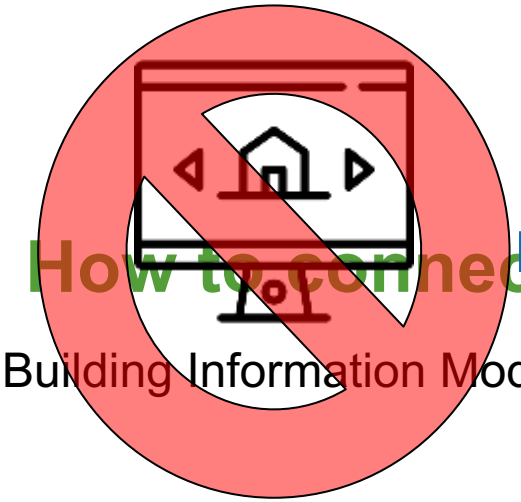

Building Information Model

What (Circular) Information?

How to connect a Building Information Model to a Material Bank?

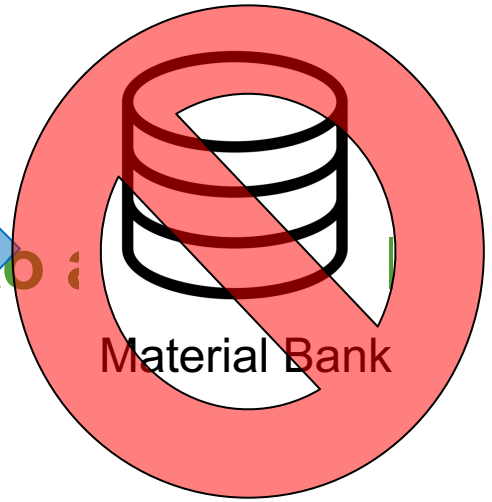

Material Bank

Why using OpenBIM approaches?

- Aim: To establish or improve interoperability between:
  - BIM Authoring Software
  - Databases
- Benefits:
  - Seamless exchange of data
  - No information loss
  - No dependency on proprietary software vendors
  - Open Data and Open source tools

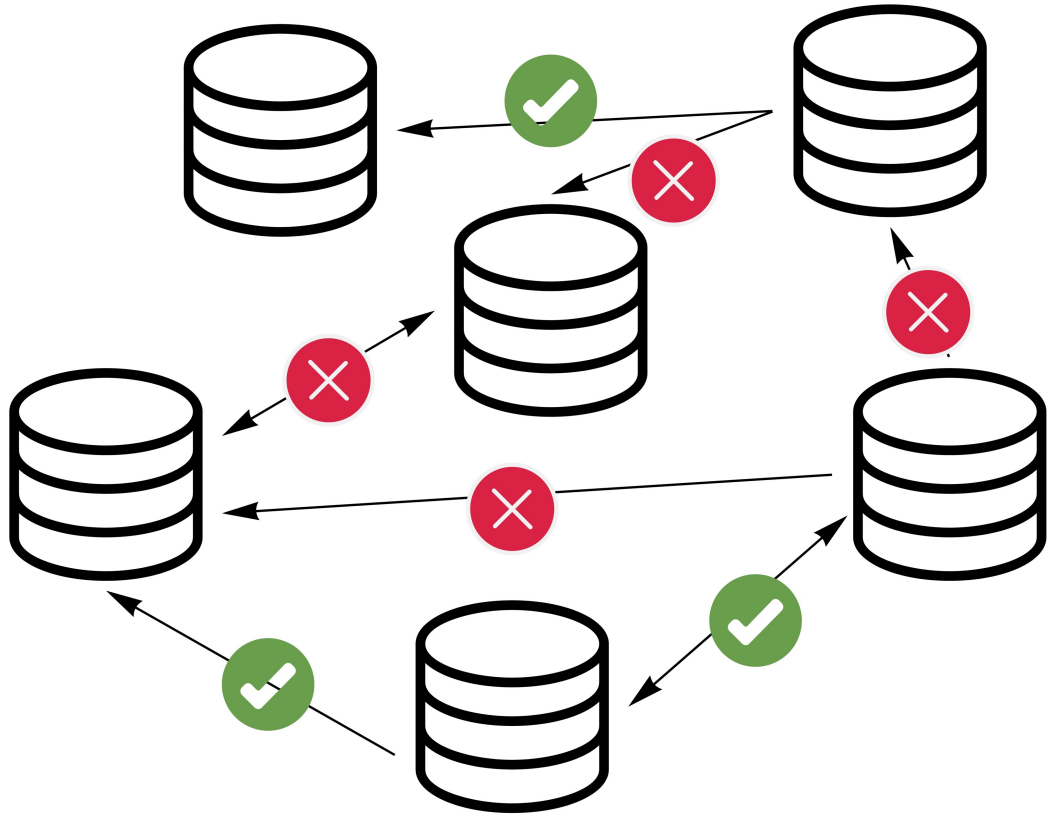

Information Exchange Solutions to support OpenBIM

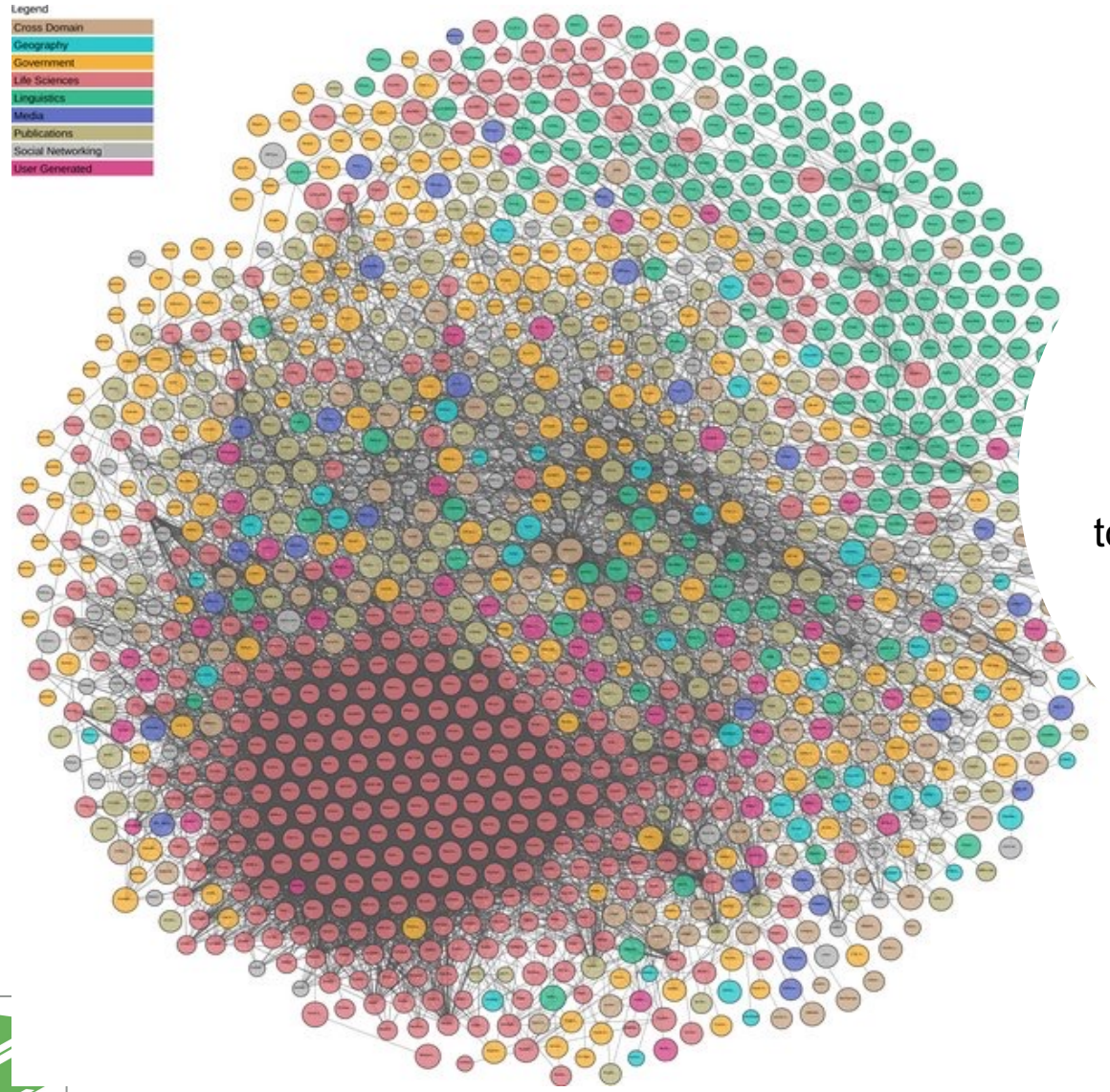

Human-readable data
should be presented in a machine-processable form
to be exchanged (in the present time)
and preserved (for future).

What is a formal Ontology?

- An “ontology” is a formal, machine-understandable, shareable and reusable set of vocabularies to transfer knowledge across a domain.
- It helps to create structured data using that can be further connected to other open data and be interpreted by machines.
- It enables open linked data querying from different sources.

- How?
  - By constructing ontological classes and relationships between classes.

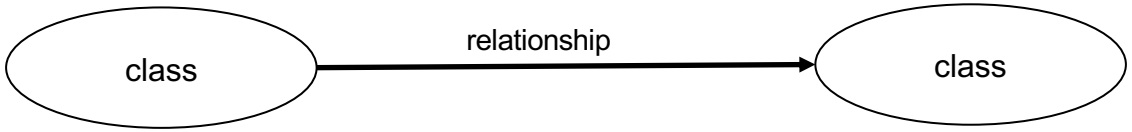

- What for?
  - To create a common language to connect to the linked open data and the plethora of material and lifecycle data there.

Proposal for Deconstruction and Reuse Ontology (DOR)

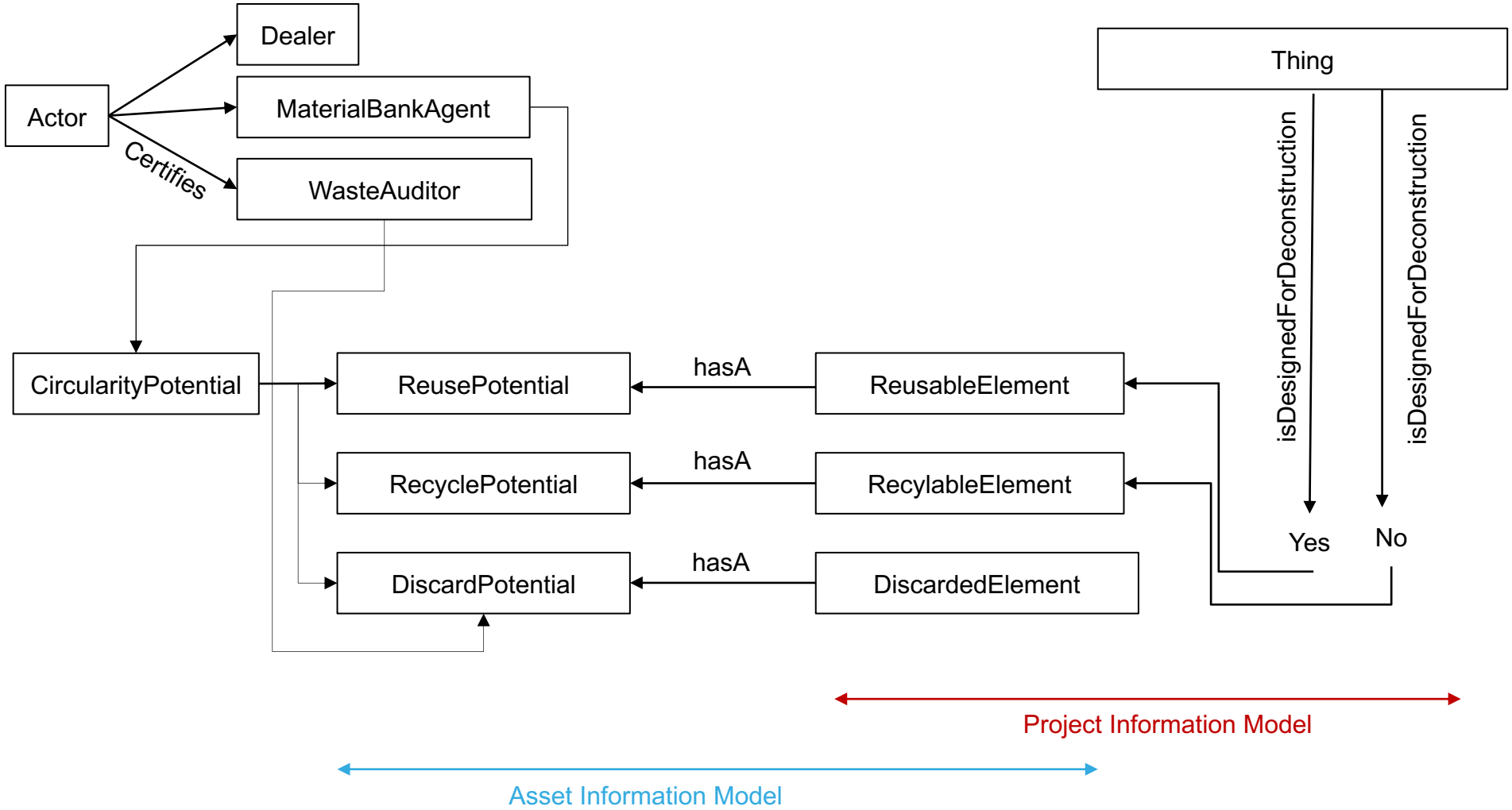

Proposal for The Ontology for Environmental Product Declaration (OEPD)

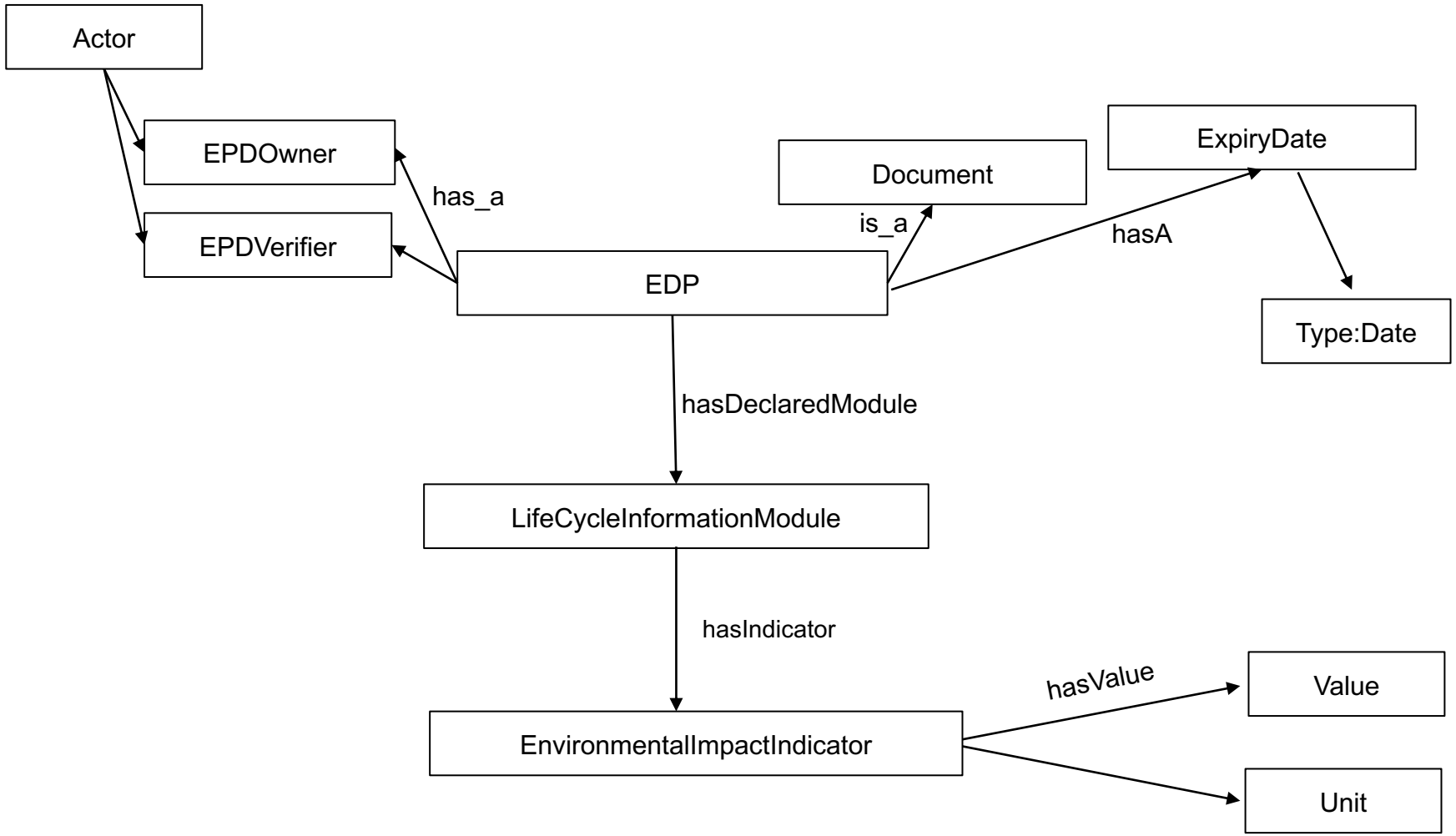

Deep Learning for classification, segmentation and modelling in geospatial data analyses

Automated Crater Detection

Using Deep Learning

NASA FDL Lunar Volatiles Team

D. Backes, E. Bohacek, A. Dobrovolskis, T. Seabrook

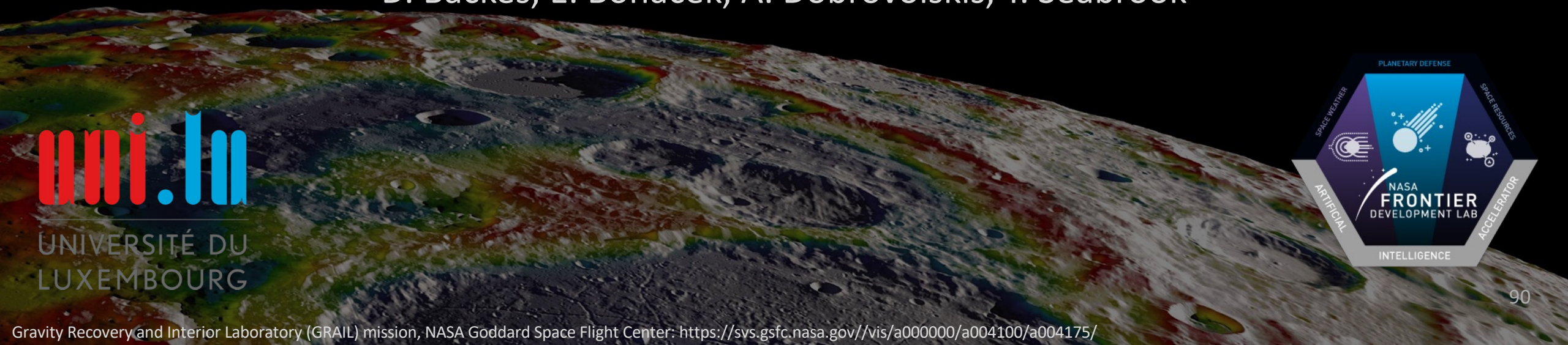

Gravity Recovery and Interior Laboratory (GRAIL) mission, NASA Goddard Space Flight Center: https://svs.gsfc.nasa.gov//vis/a000000/a004100/a004175/

Where is water on the moon?

- Craters near the poles
- Some floors of these craters never see the sun
- Permanently Shadowed Regions (PSRs)
- Extremely difficult to map with photogrammetric methods

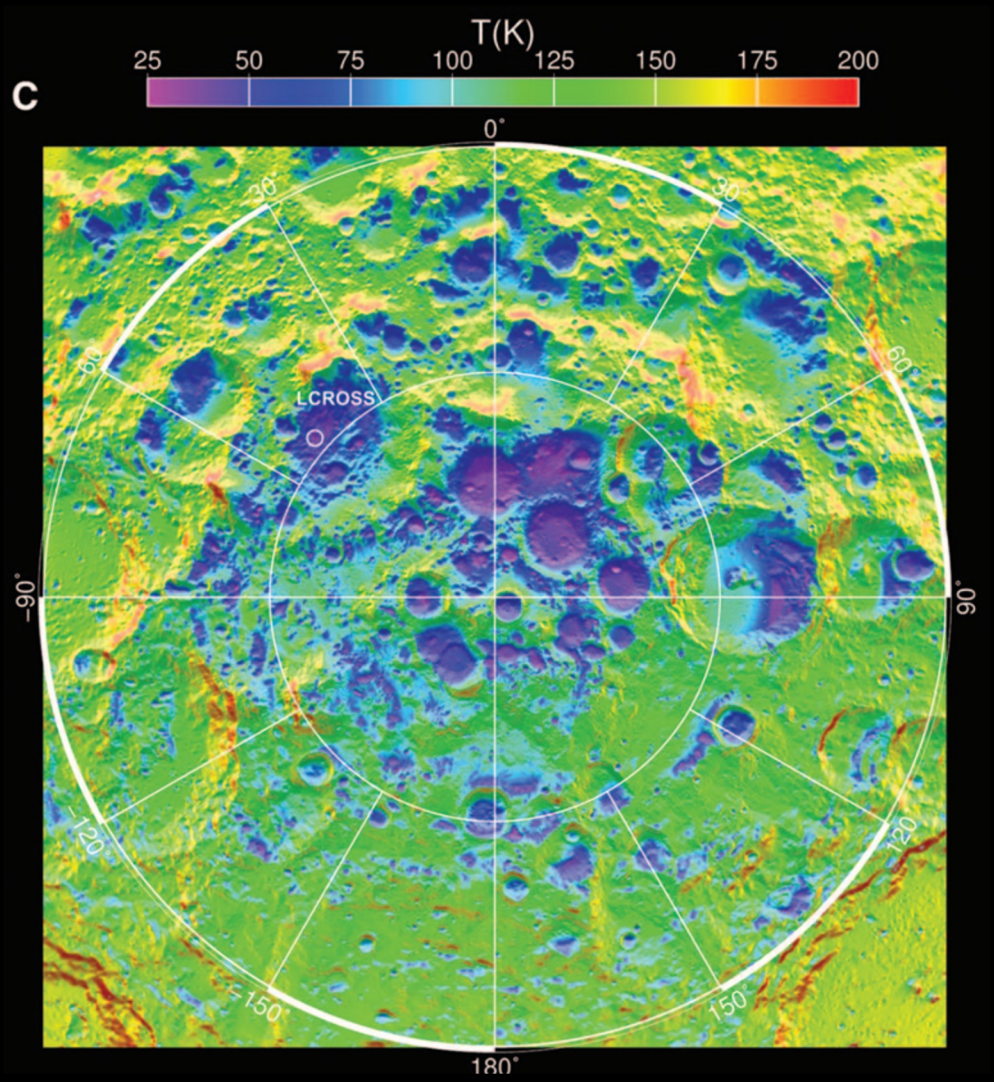

Simulated annual average near-surface temperatures
Paige et al., Science 330 (2010); www.sciencemag.org

Permanently Shadowed Regions

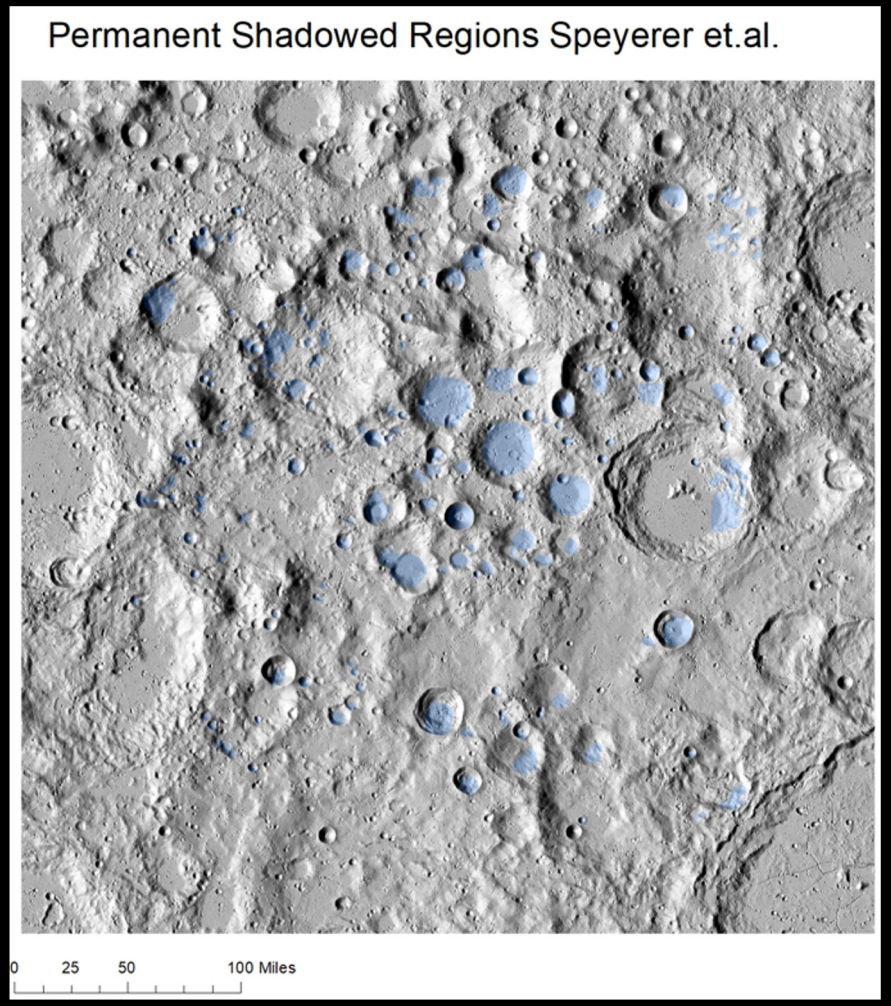

Speyerer E. J., S. J. Lawrence, J. D. Stopar, P. Gläser, M. S. Robinson, B. L. Jolliff (2016)
via http://lroc.sese.asu.edu

Adaptive Convolution Filter

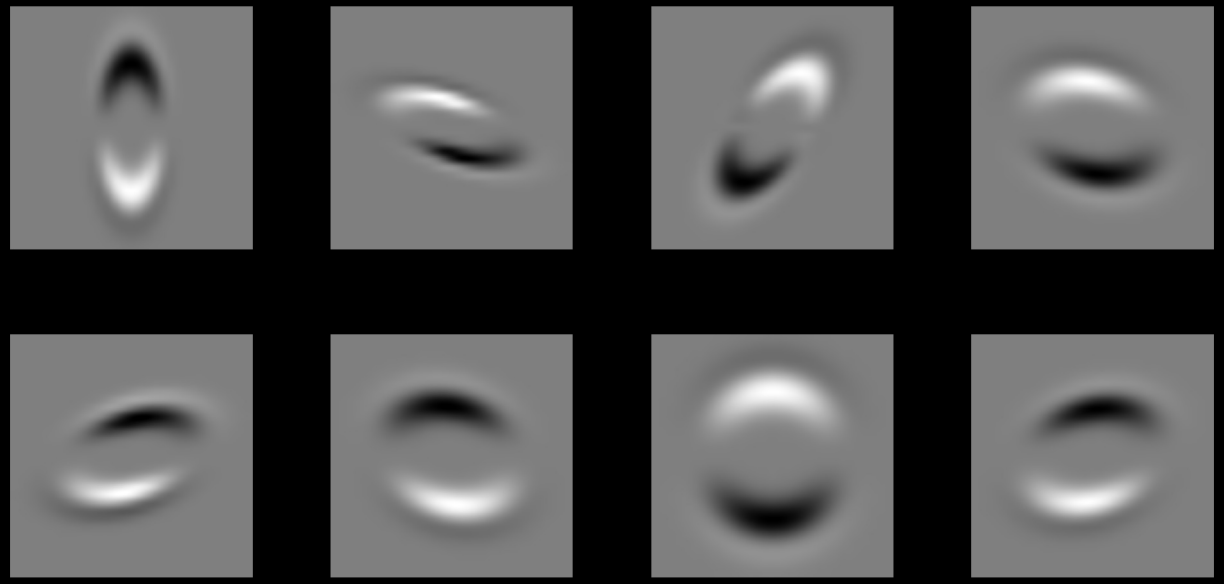

Represents a formulated baseline approach to crater detection.

2. Deep Learning Classifier

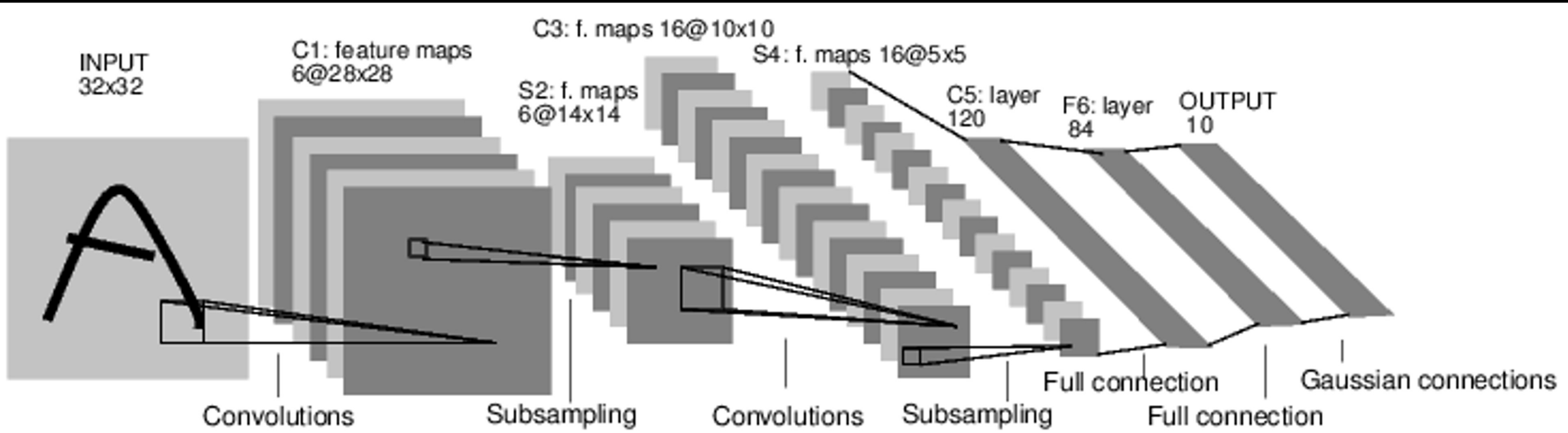

Automated Crater Detection

Accuracy Compared with Previous Work

Group	Vijayan et al.	Di et al.	Emani et al.	**FDL**
Year	2013	2014	2015	**2017**
Method	Pattern recognition	Pattern recognition	CNN	**CNN**
Precision (%) (Accuracy)	91	87	86	**98**
Error Rate (%)	9	13	14	**2**

Timing Comparison of Our Techniques

Group	Human	Single-Layer	**CNN**
Accuracy	-	Poor	**98.4%**
Time (1000 Images)	1-3 hours	10 hours	**1 minute**
Person-hours	1-3 hours	-	**-**

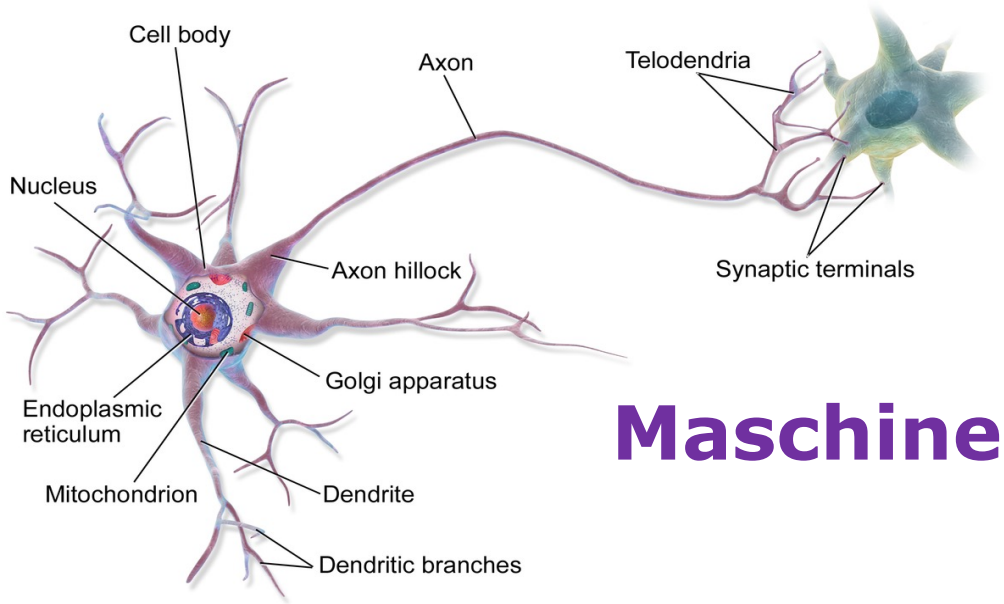

Auszug aus dem Vortrag, gegeben am
Kleiner Geodätentag, 7. Oktober 2022, Kaiserslautern
DVW-Rheinland Pfalz + Saarland, LAGG

Maschinelles Lernen in der automatischen Auswertung von Punktwolken: Beispiele der Erfahrungen an der Universität Luxemburg

Abdul Awal Md NURUNNABI und Felix Norman Teferle

Geodesy and Geospatial Engineering
Department of Engineering
University of Luxembourg

FEDER
FONDS EUROPÉEN
DE DÉVELOPPEMENT
RÉGIONAL
LUXEMBOURG

SOLSTICE

UNION EUROPÉENNE
Fonds européen de développement régional

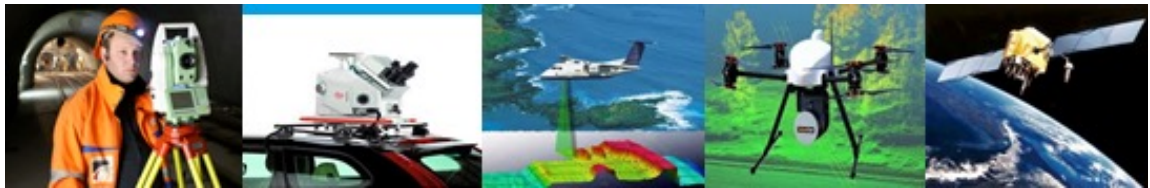

Was ist maschinelles Lernen ?

- **Machine learning** (ML) is the science that makes computer able to learn from data.
- A branch of artificial intelligence combined with statistical learning and computing technologies revolutionizes digital and data-intensive disciplines by producing tools and techniques to analyze and extract valuable information and knowledge from big data.

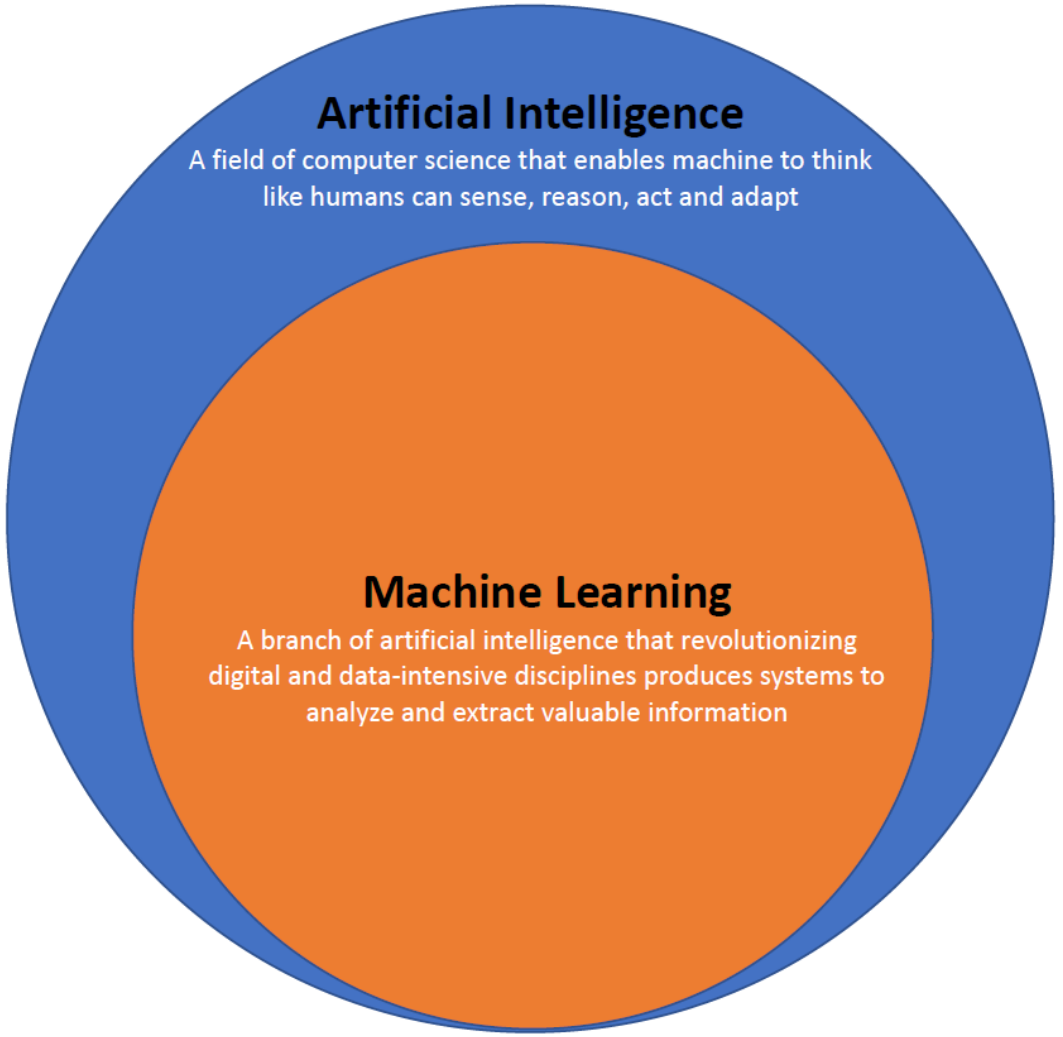

Typen von maschinellen Lernen und deren Anwendung

Supervised learning:

A model is trained based on the given input and output (the label of the input).

Unsupervised learning:

A model is trained only on the inputs, without their labels.

Semi-supervised learning:

A model is trained based on a small portion of labeled data and a large number of unlabeled data and make predictions on new data.

Reinforcement learning:

It is concerned with how intelligent agents ought to take actions in an environment in order to maximize the notion of cumulative reward.

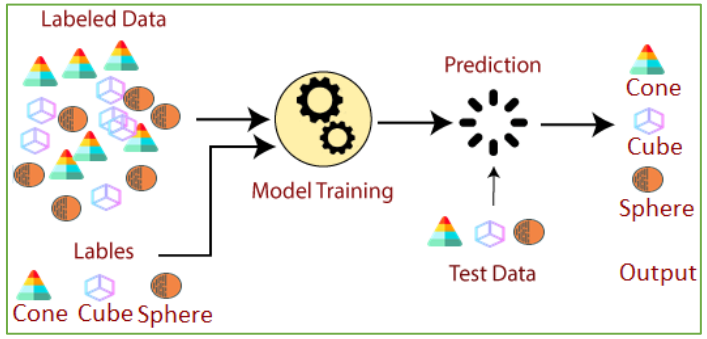

Supervised learning

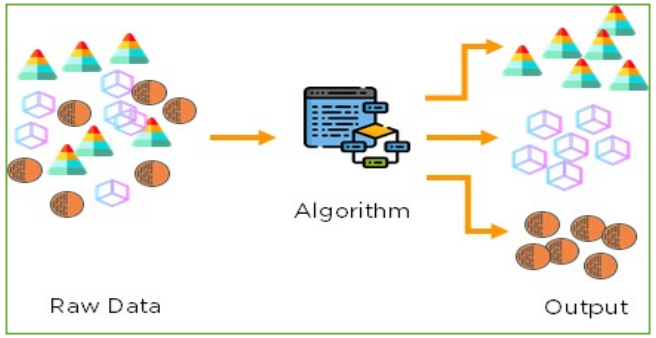

Unsupervised learning

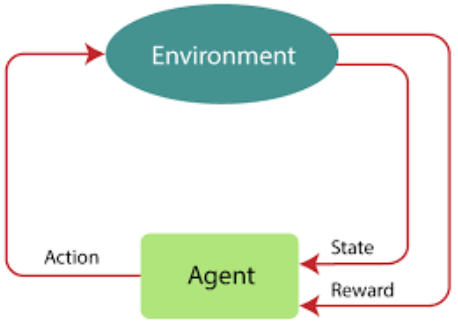

Reinforcement learning

Typen von maschinellen Lernen und deren Anwendung (2)

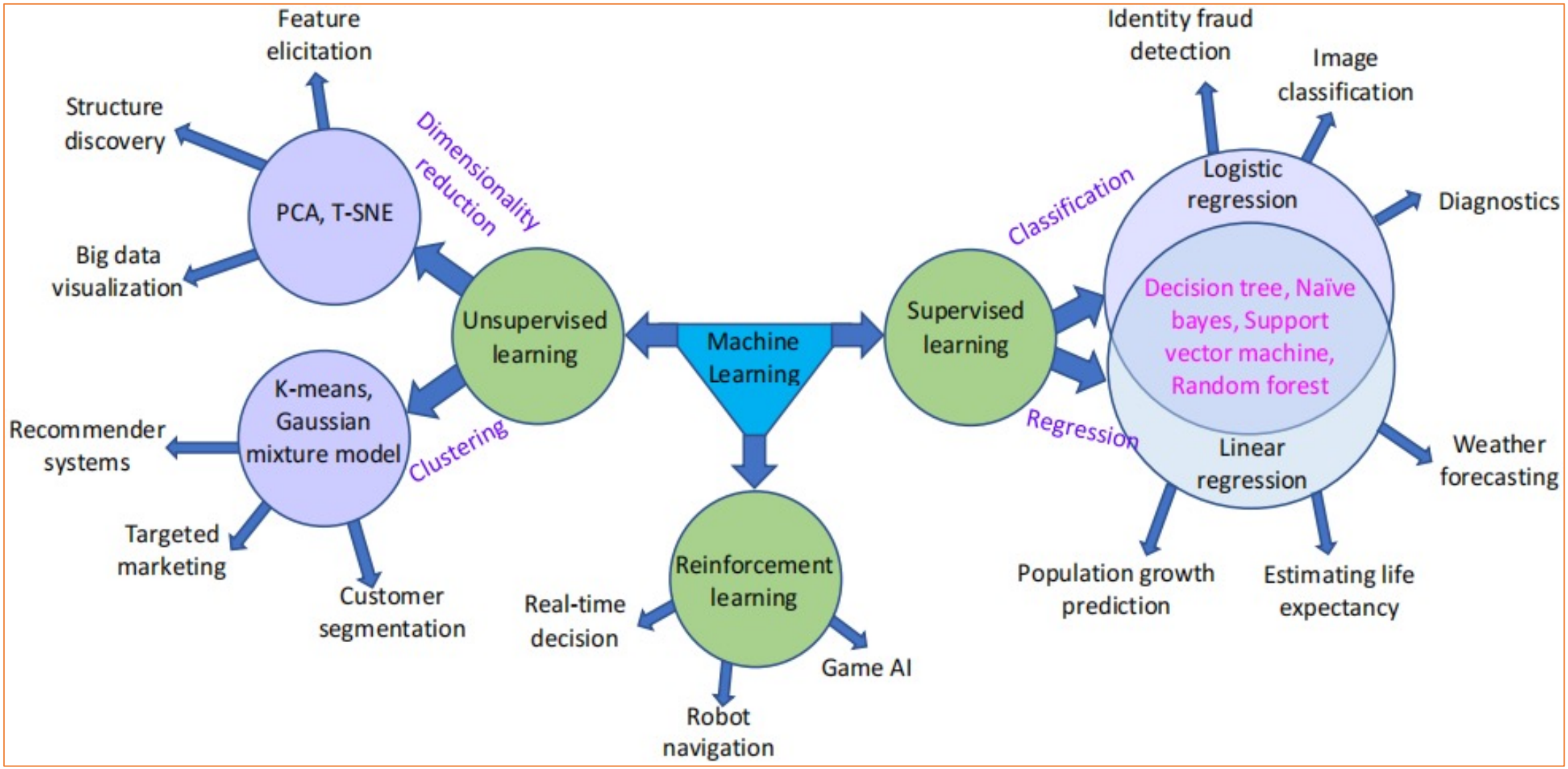

Was sind die grundlegenden Stufen des maschinellen Lernens?

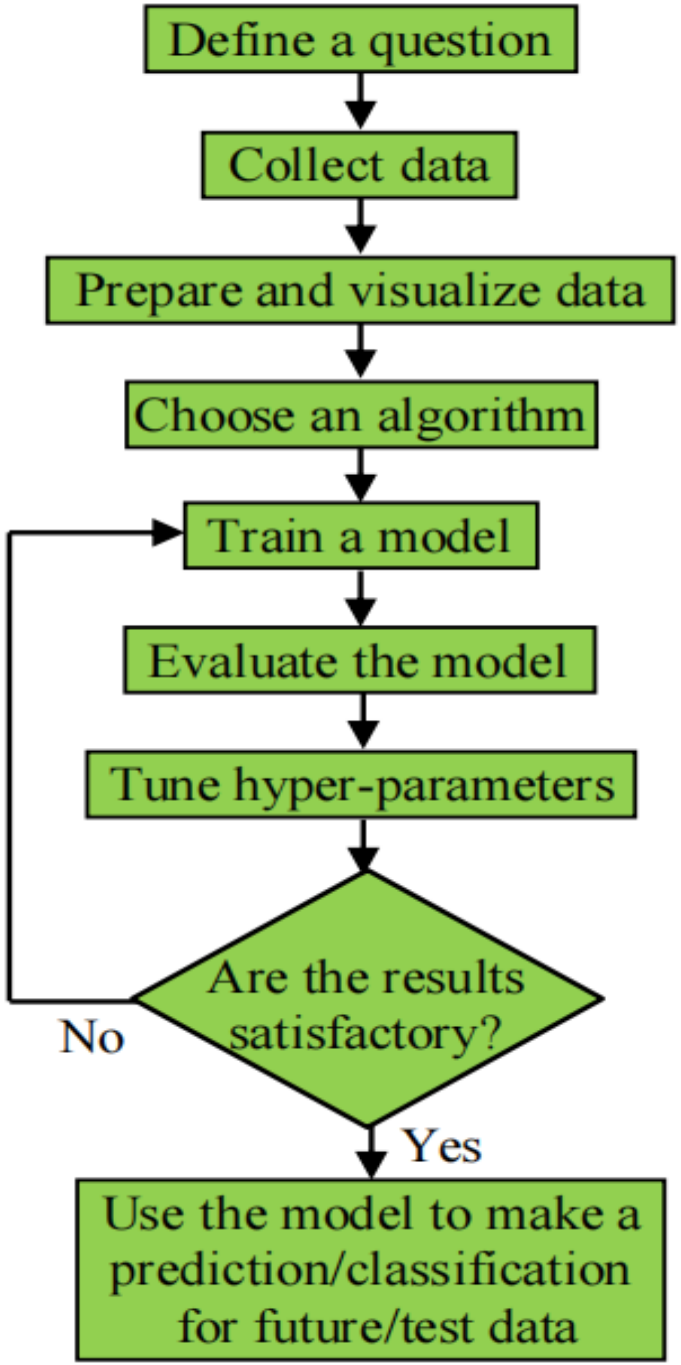

Figure. Machine learning workflow

Deep Learning

Deep learning (**DL**) is a form of machine learning techniques that *imitates the way human brain (neuron) acquire certain types of knowledge*. The term 'deep learning' refers to the artificial neural networks having many layers that enable learning from data (like human learns from experience).

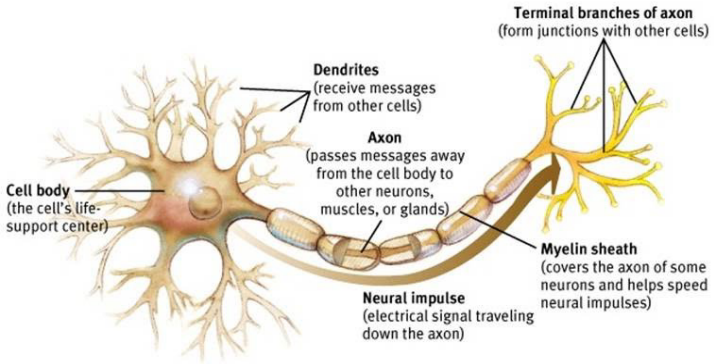

~ 86 billion neurons are in the human brain, each neuron connected to thousands of other neurons. A neuron receives a sufficient number of signals through synapses from other neurons within a few milliseconds, it fires its own signal. 1

Why DL ?

- DL methods are data-driven, sufficiently automatic, efficient, and intelligent for reliable processing of big (massive) data.
- They can detect and process non-linear complex phenomena.
- They are able to process multi-disciplinary and multi-modal data.

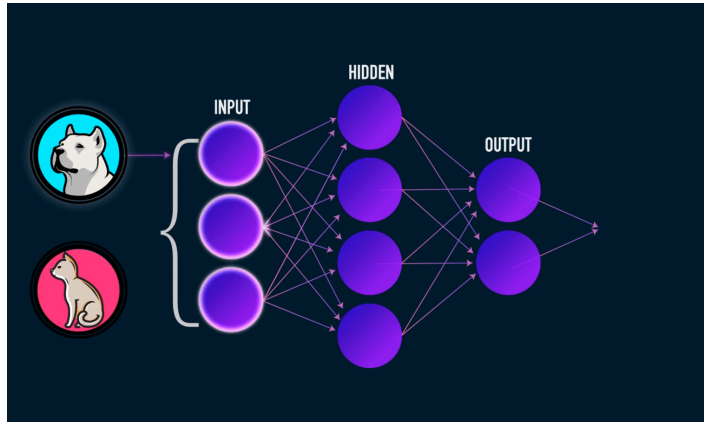

Artificial neural network [2]

Credit: 1, Stevenson; 2, James Liang, 2018.

Machine Learning Vs Deep Learning

- For normal/classical methods, we tell the computer very specific instructions what to do. Whereas for machine learning, we tell the computer how to figure out the answer itself, using the data we have.
- DL is a machine learning subfield that performs in an intelligent and automatic fashion, where features are trained by itself.
- DL algorithms attempt to learn (multiple levels of) representation by using a hierarchy of multiple layers.
- If we provide DL system with a lot of information/data, it begins to understand it and responds efficiently.

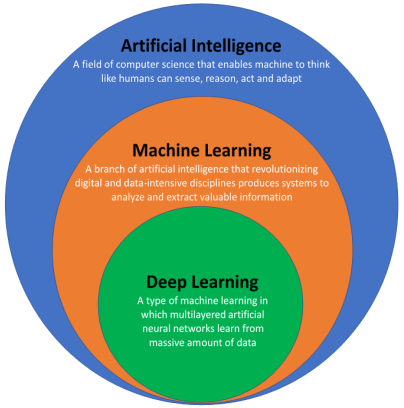

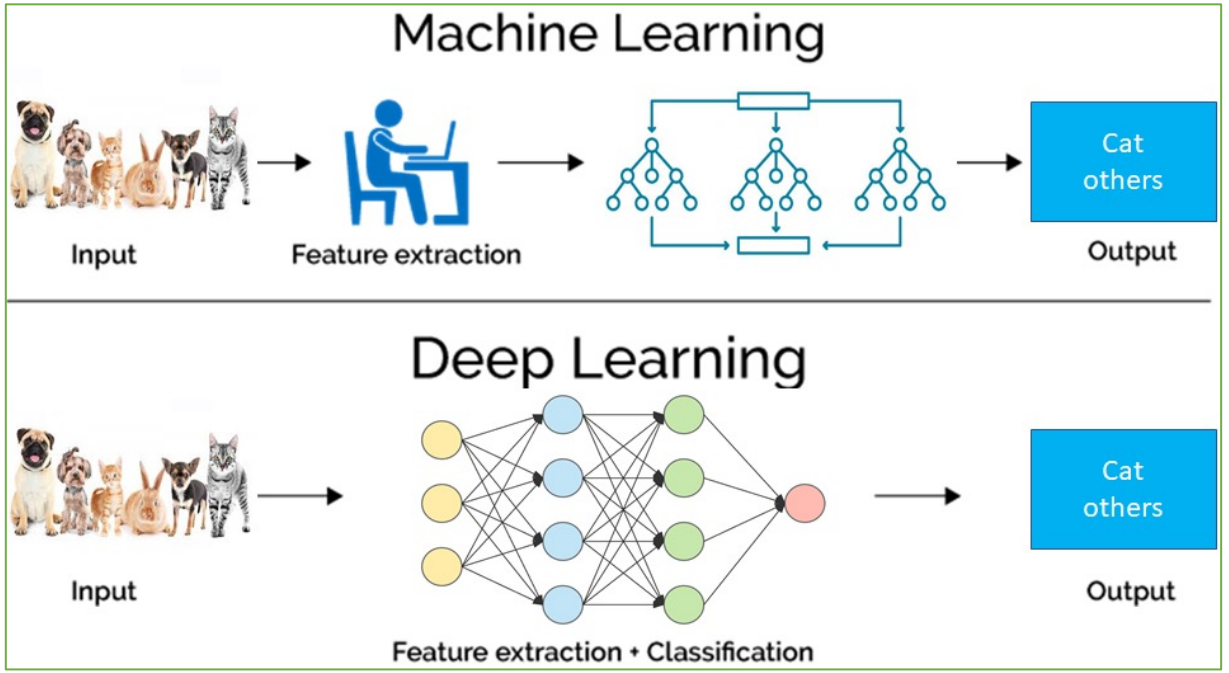

Wie beeinflussen ML/DL raumbezogene Big Data?

Geo/GIS science research can be characterized by massive (**big**) and multimodal-multidisciplinary sources of geolocated (**geospatial**) **data**, from which it is often crucial to extract high level information in the form of spatial semantics, spatial object relationships, trajectories, or more generally, numeric codes related to objects embedded in geographical coordinates.

Applications: city modelling, object detection, semantic segmentation, geometry generation, change detection, autonomous navigation, disaster monitoring, mapping, environment analysis, urban planning, weather forecasting, earth observation, ….

Punktwolken: Vorteile und Herausforderungen

Point cloud, collection of a large number of single spatial measurements of points that represent objects or space. These points usually defined by 3D vectors, the geometric coordinates (*x*, *y*, and *z*). Additional characteristics (e.g., color, intensity, return number, etc.) may be available.

Source: LiDAR, products from photogrammetry, structure from motion, etc.

Advantages:

- Point clouds can capture geometry of objects: shape, size, orientation, etc.
- Point clouds can avoid combinatorial irregularities and so easier to learn

Challenges:

- Unstructured
- Irregular/unordered data format
- Permutation-invariance
- Sparse
- Inhomogeneous data density
- Presence of data acquisition artefacts
- Presence of noise, occlusions, and outliers
- Huge data volume

DL zur Erkennung von Boden und nicht-Boden Flächen

- Precise ground surface topography is crucial for 3D city analysis, digital terrain modelling, natural disaster monitoring, high-density map generation and autonomous navigation, …
- Pointwise classification of ground and non-ground points in Aerial Laser Scanning (ALS) point clouds.

Figure: Workflow of the proposed algorithm.

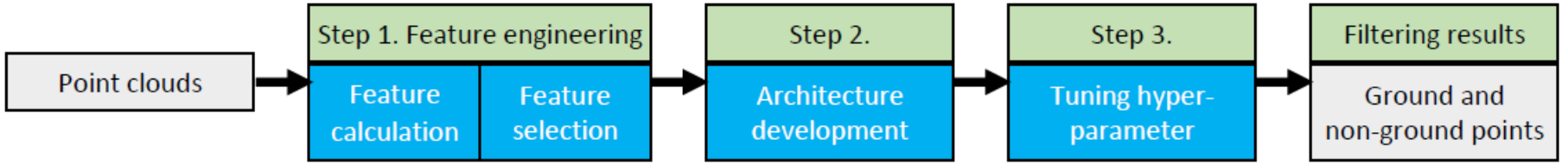

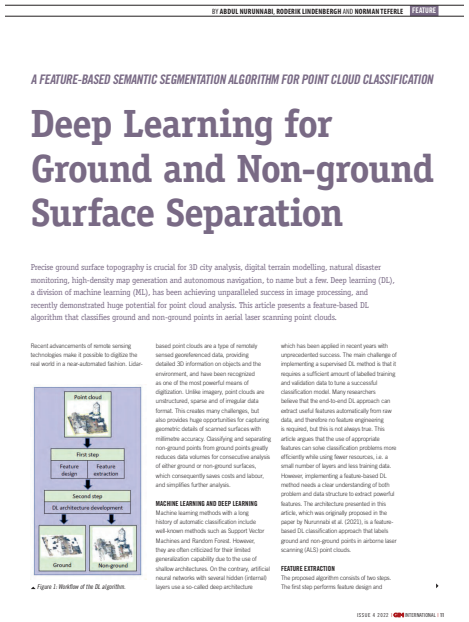

DL zur Erkennung von Boden und nicht-Boden Flächen (2)

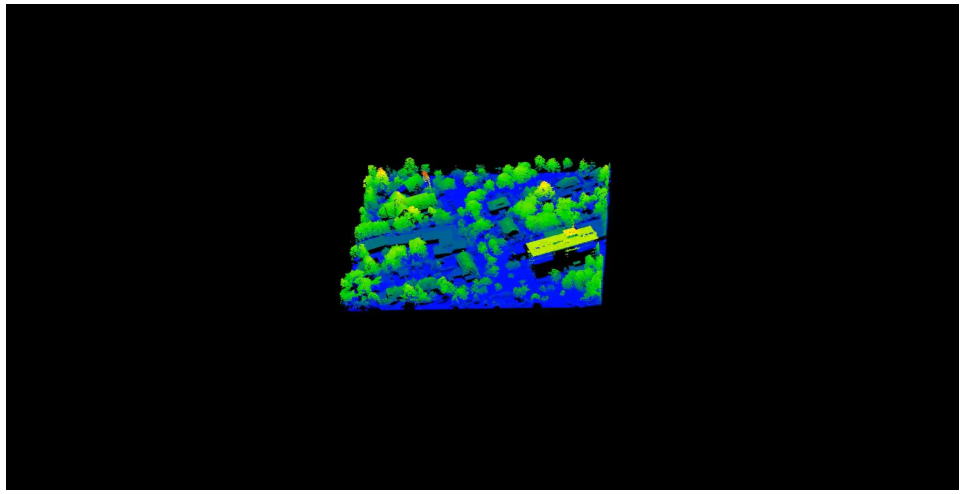

Training scene; Actueel Hoogtebestand Nederland data

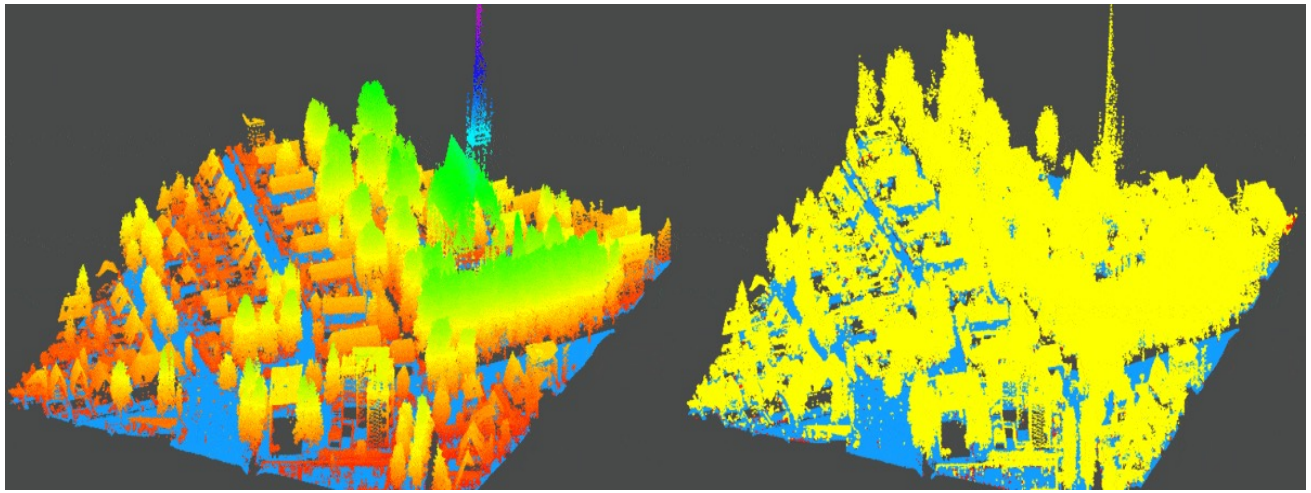

Test scene; Digital terrain modelling; ground (blue) and non-ground (yellow) surface extraction

- The feature-based ground point filtering algorithm follows a not end-to-end DL architecture.
- It needs less training data than end-to-end DL approach.
- It does not require multi-scale features.
- It performs well in the presence of steep slopes and height discontinuties in the terrain.
- New method achieves accuracy of 97% for per-point ground surface points classification.
- It requires clear understanding about underlying data structure, and the feature vectors.

*k*CV-B: Bootstrap mit Cross-Validierung für die DL Modelentwicklung, -prüfung und -auswahl

This study investigates the inability of train/test split and *k*-fold cross-validation methods to create training and validation data sets, and to achieve sufficient generality for supervised DL.

In response, the bootstrap is a computer based statistical resampling method that has been used efficiently for estimating the distribution of a sample estimator and to assess a model without having knowledge about the population.

This paper couples cross-validation and bootstrap to have their respective advantages in view of data generation strategy and to achieve better generalization of a DL model.

Contributions:

- Developing an algorithm for better selection of training and validation data sets,
- Exploring the potential of bootstrap for drawing statistical inference on the necessary performance metrics (e.g., mean square error), and
- Introducing a method that can assess and improve the efficiency of a DL model. The proposed method is applied for semantic segmentation and is demonstrated via a DL based classification algorithm, PointNet, through aerial laser scanning point cloud data.

Vorgeschlagene Methode

Training	Validation	Test

Figure. Train/test split method

Training	Training	Training	Training	Validation	Test
Training	Training	Training	Validation	Training	Test
Training	Training	Validation	Training	Training	Test
Training	Validation	Training	Training	Training	Test
Validation	Training	Training	Training	Training	Test

Figure. *k*-fold Cross Validation (*k*CV)

Training	Training	Training	Training	Validation	Test
Training	Training	Training	Validation	Training	Test
Training	Training	Validation	Training	Training	Test
Training	Validation	Training	Training	Training	Test
Validation	Training	Training	Training	Training	Test

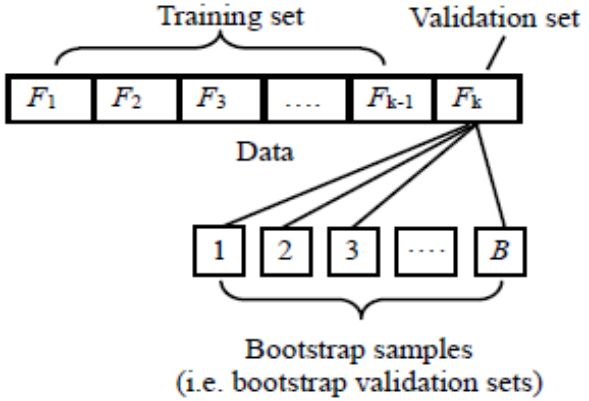

Figure. A schematic diagram; ***k*CV-B**: cross-validation couples with bootstrap to get B validations sets for each of k training sets. F_i is the ith (i =1,2,…,k) fold for a data set having k folds, where k-1 folds are used as a training set, and B bootstrap validations sets are used to validate the model developed by the training set.

Versuch mit dem ALS Datensatz

Class	Training points	Test points	Train/test split	Boot-strap	kCV	kCV-B
			F_1	F_1	F_1	F_1
uC	1,878,838	693,778	85.2	80.3	84.3	89.2
Ground	2,152,235	1,680,188	81.9	85.5	91.1	93.2
Building	1,441,483	902,834	78.9	82.9	89.9	89.2
Mean F_1			81.9	82.9	88.5	90.5
OA			81.6	83.5	89.2	91.1

Table. Classification results of an ALS test data set.

- The proposed bootstrap coupling with *k*CV has demonstrated to improve model quality.
- Using large values of *k* and *B* improve the generality and performance of a model, but there is a trade-off between generalization, accuracy and time to compete the process.
- Reasonably, *k*CV-B takes more time than the existing methods, but with high-powered computing facilities it can produce higher generalization power for the test and future data.

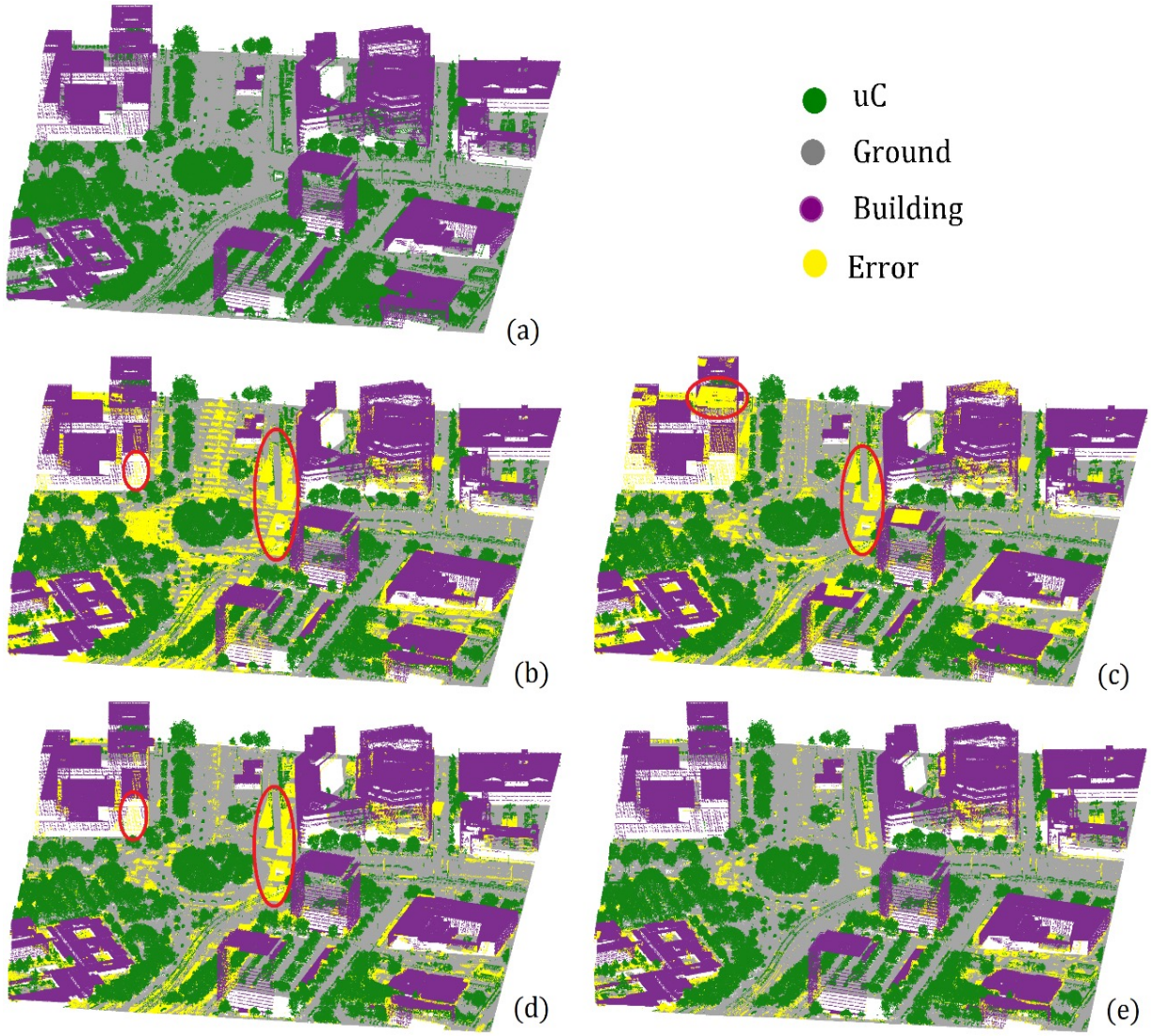

Figure. Classification results (misclassified points in yellow): (a) ground-truth, (b) train/test split, (c) bootstrap, (d) *k*CV, and (e) *k*CV-B. Many building and ground points are misclassified in red ellipses.

Robuste Methode zur Erkennung der Gebäudeausmaße

- The building footprint is crucial for a volumetric 3D representation of a building that is applied in urban planning, 3D city modeling, cadastral extraction, topographic map generation, and many more…
- Aerial laser scanning (ALS) has been recognized as the most suitable means of large-scale 3D point cloud data acquisition.
- Besides the presence of noise and outliers, data incompleteness and occlusions are two common phenomena for point clouds.
- Most of the existing methods for building footprint extraction employ classification, segmentation, voting techniques (e.g., Hough-Transform or RANSAC), or Principal Component Analysis (PCA) based methods, but most of them are not free from outlier effects and do not produce good results in the presence of data gaps.

This paper presents a novel algorithm that employs MCMD (maximum consistency within minimum distance), MSAC (a robust variant of RANSAC) and a robust regression to extract reliable building footprints in the presence of outliers, missing points and irregular data distributions. The algorithm is successfully demonstrated through ALS point clouds.

Vorgeschlagene Methode

Step 0: We employ RandLA-Net (a DL) approach to segment/label building points.

Step 1: Vertical surface (e.g., building walls) are separated from non-vertical surfaces (e.g., roofs) using surfaces points slope and height measurements based on MCMD algorithms.

Step 2: Projection of 3D points onto 2D plane, footprint-lines detection from 2D points using robust variant of RANSAC.

Step 3: Footprint-lines refinement using spatial segmentation.

Step 4: Footprint-lines fitting using robust regression.

Step 5: Final footprint extraction.

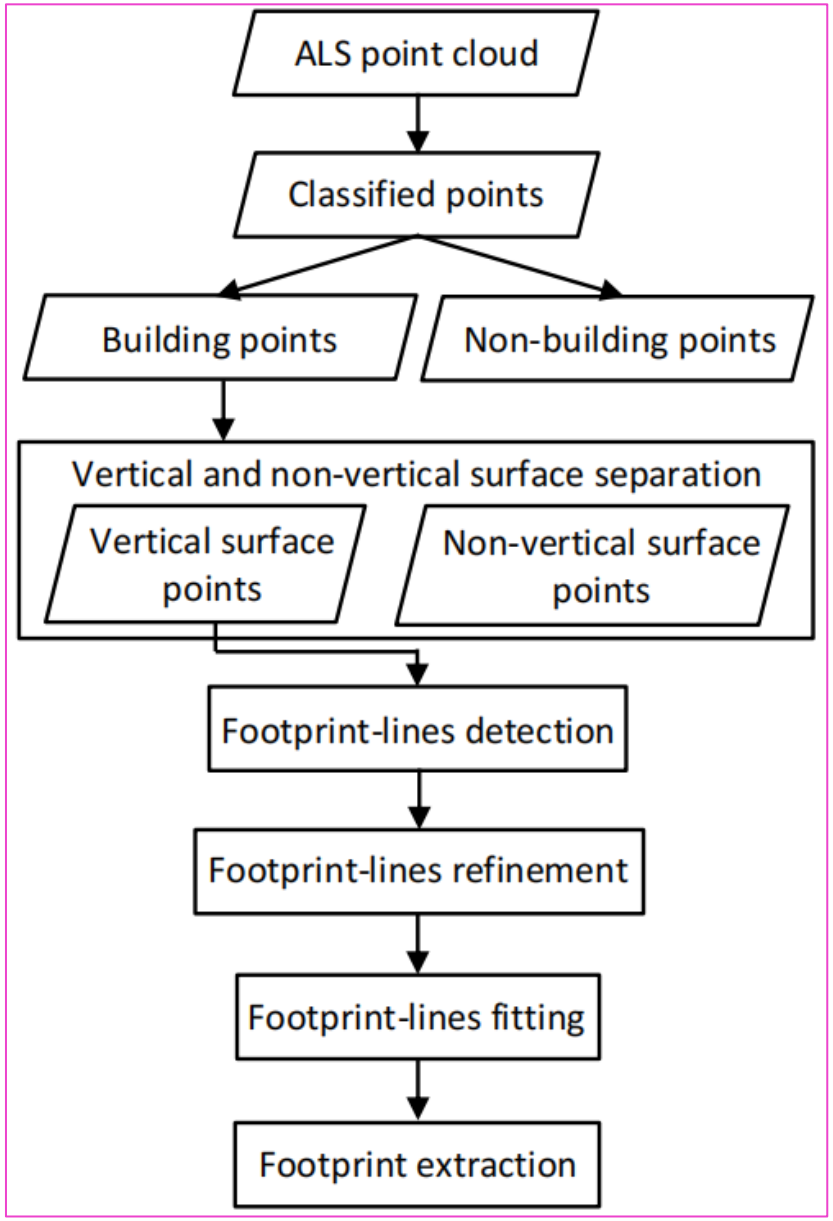

Figure. Flowchart of the proposed algorithm.

Versuch zur Erkennung von Gebäudeausmaßen

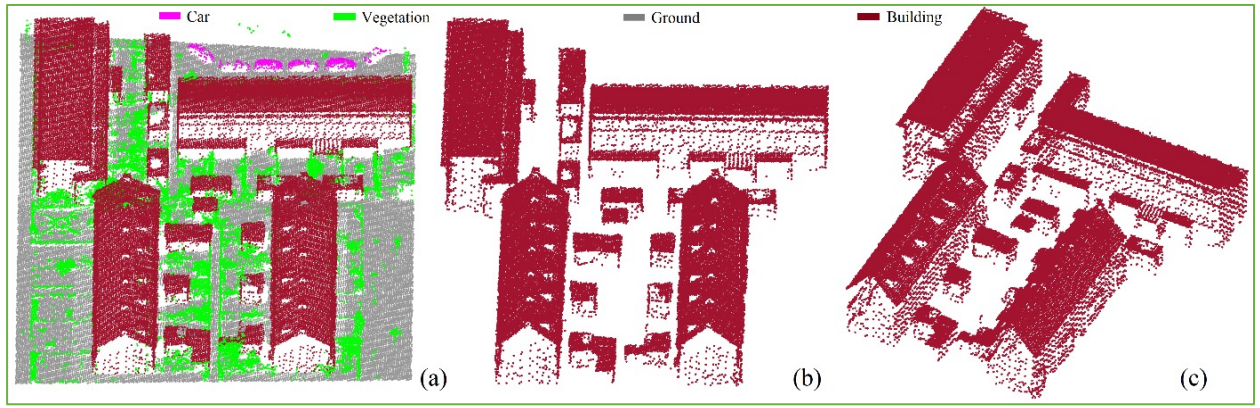

Figure. (a) Labelled AHN data set, (b) front-view of the buildings to extract footprint, (c) side-view of the buildings.

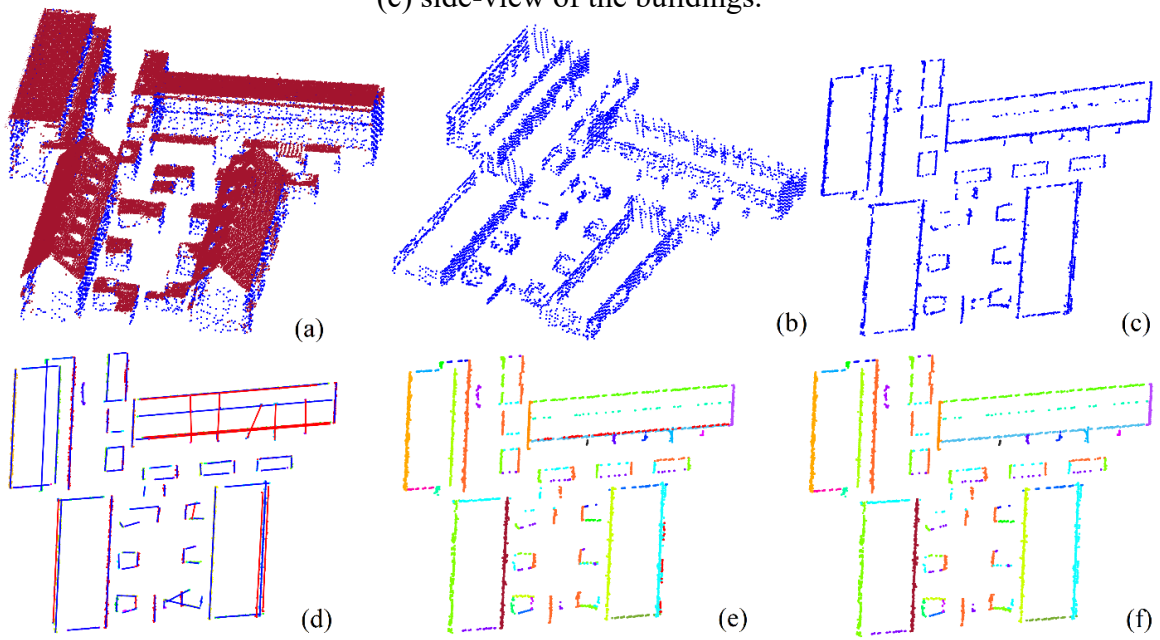

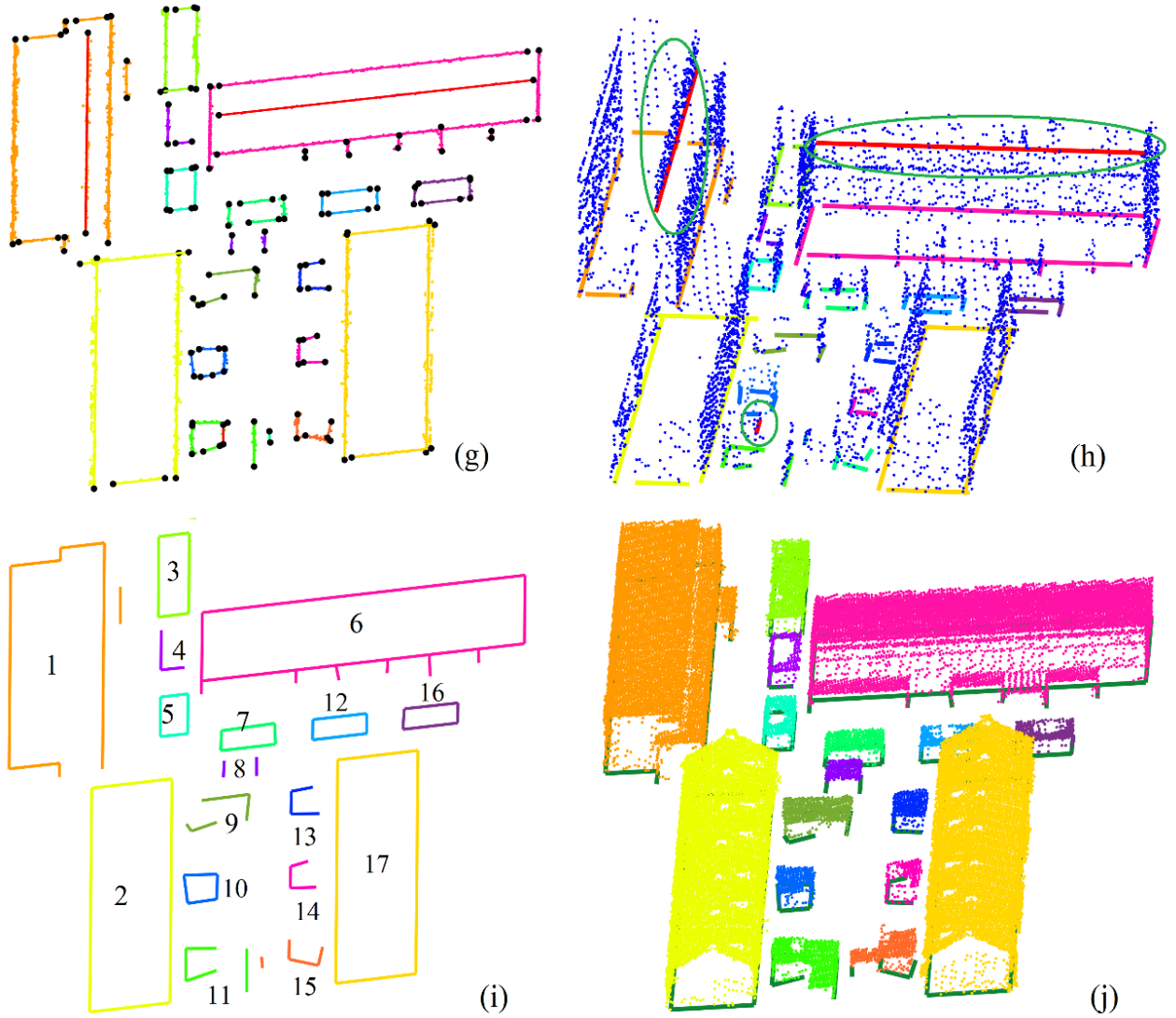

Figure. Building footprints extraction of AHN data set: (a) classification of vertical (blue) and non-vertical (maroon) surfaces, (b) 3D vertical surfaces (facades) below the roofs, (c) 2D (x, y) points for the vertical surfaces, (d) extracted lines using MSAC for the points in plot (c), (e) spatial segmentation for the 2D facades points in plot (d), (f) elimination of redundant/false (red) lines in (e); using $A_t = 5^0$, and nPT=10, (g) LTS regression lines for the points in plot (f); black dots are the end points of the lines, (h) footprint-lines for the buildings in 3D, red lines within the three green ellipses are from the hanging walls that have no ground connection, (i) final footprint-lines for the buildings, and (j) footprint (green)-lines aligned with the 3D buildings in plot (a).

Erkennung von Straßenflächen und Straßeninstallationen von mobilen Laserscanner Daten

- Road surface extraction is crucial for many applications including 3D city analysis and ensuring road safety.
- MLS (vehicle based mobile laser scanning) is the most appropriate mapping system for the road environment.
- Most of the existing methods for road surface extraction use classical approaches that do not relieve problems caused by the presence of noise and outliers.

Investigate problems of road surface extraction in the presence of noise and outliers, and to propose a statistically robust algorithm for road surface elements (road pavement, curb, divider/islands, and sidewalk) extraction using Mobile Laser Scanning (MLS) point clouds.

Vorgeschlagene Methode

Step 1:Slicing the raw point clouds along the road.

Step 2: Filtering ground and non-ground points using weighted robust regression technique.

Step 3: Slicing the stripes from Step 2 into small patches along the road width.

Step 4: Calculation of the range *Rz* of the patches, and find abnormal height values.

Step 5: Decision making using some prespecified criteria to identify road surface categories (components).

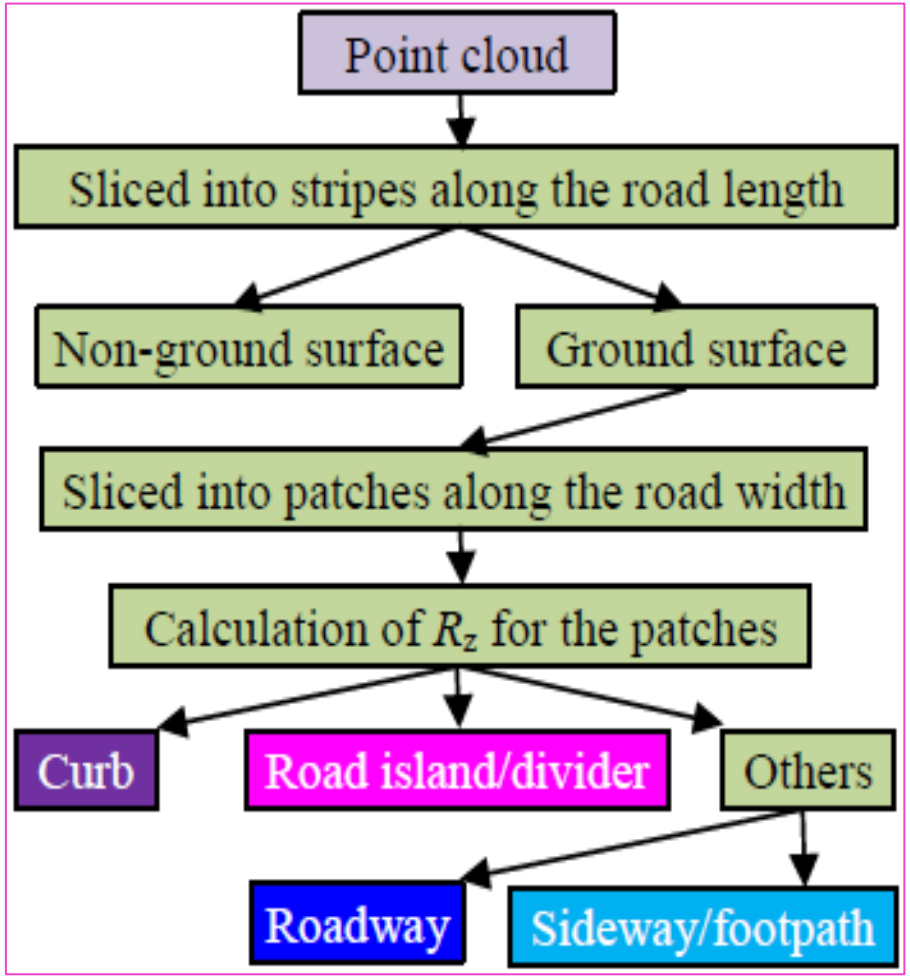

Figure: Workflow for the proposed method. *Rz* is the range of *z* (height) values within a patch points.

Versuch: Erkennung von Straßenflächen und Straßeninstallationen

MLS data:
Length = 53m
Total points: 1,112, 462
Stripes = 106, Patches = 100

Method	Point label	No. of points		Performance metrics		
		GT	D	P (%)	R (%)	MCC
Proposed method	Pavement	707,458	707,400	99.99	99.99	0.999
	Sideway	86,922	86,541	100.00	99.56	0.997
	Curb	14,928	15,346	**97.28**	100.00	**0.986**
Zhao et al. (2021)	Curb	14,928	16,663	**72.61**	81.05	**0.764**

Table. Road surface extraction results. Ground-truth (GT), and detected (D). P, R and MCC are for precision, recall and Matthews correlation coefficient, respectively.

(i) Proposed algorithm extracts road pavement, curb, road divider and sidewalk.

(ii) It produces robust results in the presence of noise and outliers.

(iii) It performs well in the presence of steep slopes, sharp edges, and corners.

(iv) It is successful for both straight and curved roads.

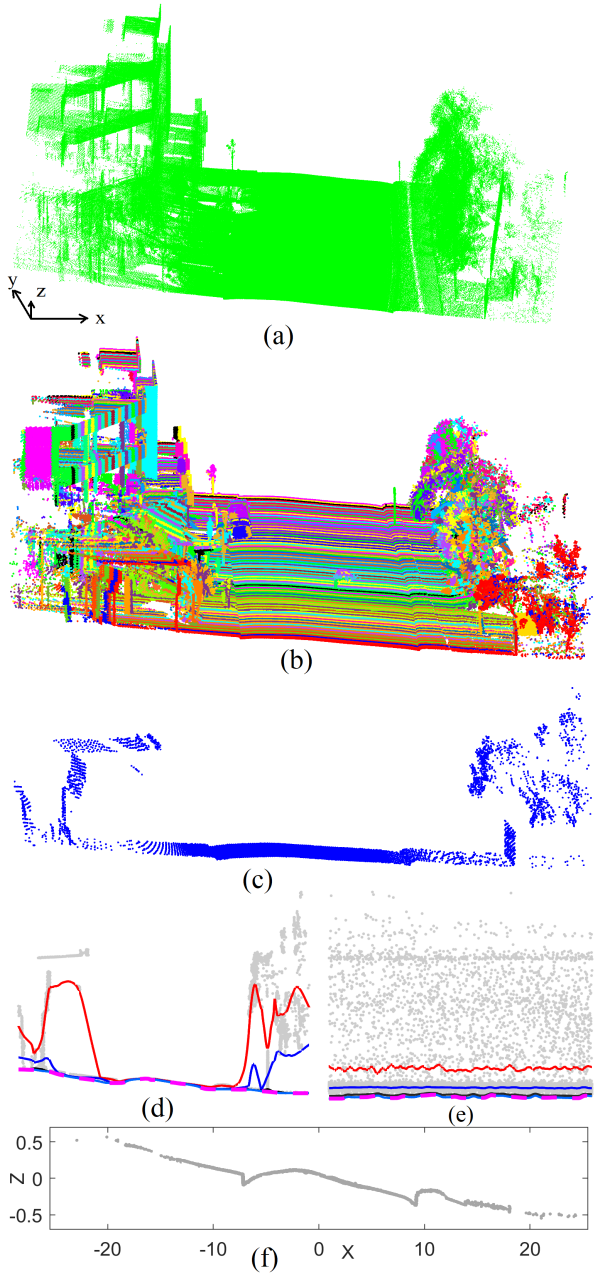

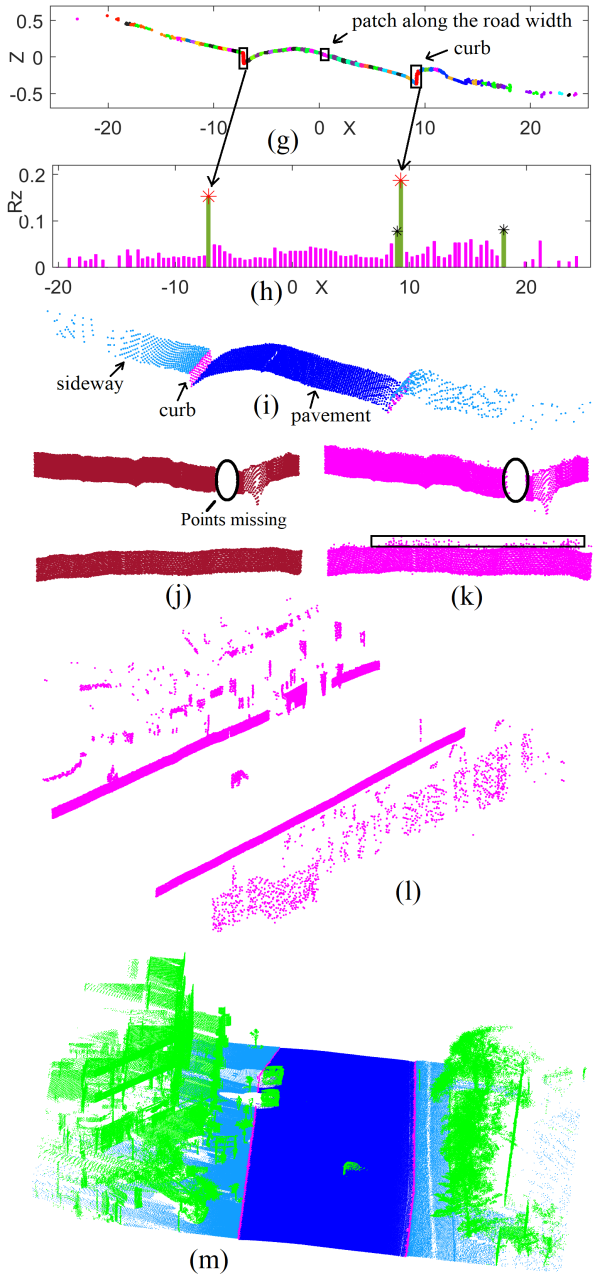

Figure. Road surface extraction: (a) road point cloud, (b) different stripes in different colors, (c) one selected stripe along the road length, (d) iterative fitting for ground filtering using RLWR on the x-z profile, (e) iterative fitting for ground filtering using RLWR on the y-z profile , (f) filtered ground points for plot (c), (g) patches along the road width, (h) bar diagram for the R_z values for the patches of plot (g), (i) classified road surface points for plot (c), (j) ground truth curb surface, (k) curb extracted by the proposed method, (l) curb extracted by Zhao et al. (2021), and (m) classified road and non-ground surfaces for the full data set.

Most Recent Developments

Two new FNR-Funded PhD projects

- **Improved Airborne Data Fusion for Advancing Automated 3D City Modelling (DF4CM)**
  - AFR Individual Grant
  - Sep 2022 – Aug 2026
  - Mr Shahoriar Parvaz

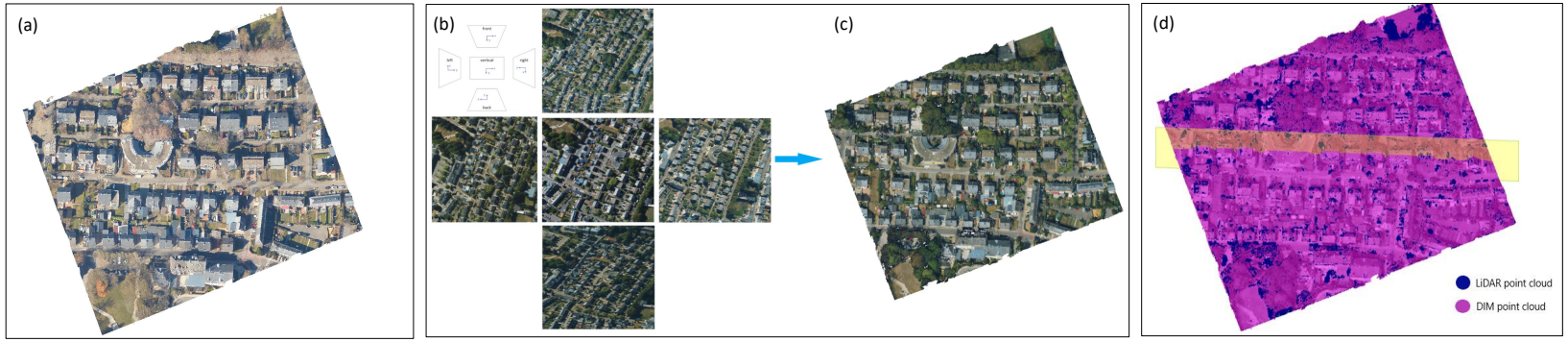

- **A High-Resolution Numerical Weather Prediction Model for Nowcasting Precipitation in the Grand-Duchy of Luxembourg (NWPLux)**
  - Industrial Fellowship with RSS-Hydro Sarl
  - Nov 2022 – Oct 2026
  - Mr Haseeb UR Rehman

Rosport was one of the most severely affected communes

Photo credit: Guy Jallay

Luxembourg Times

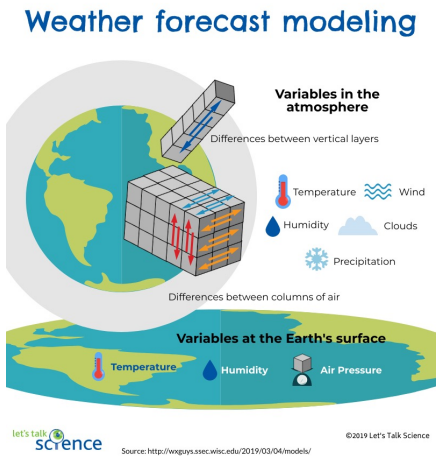

Experimental study:

A 3D analysis of dust pollution (PM10) accumulation in different urban scenarios of Luxembourg

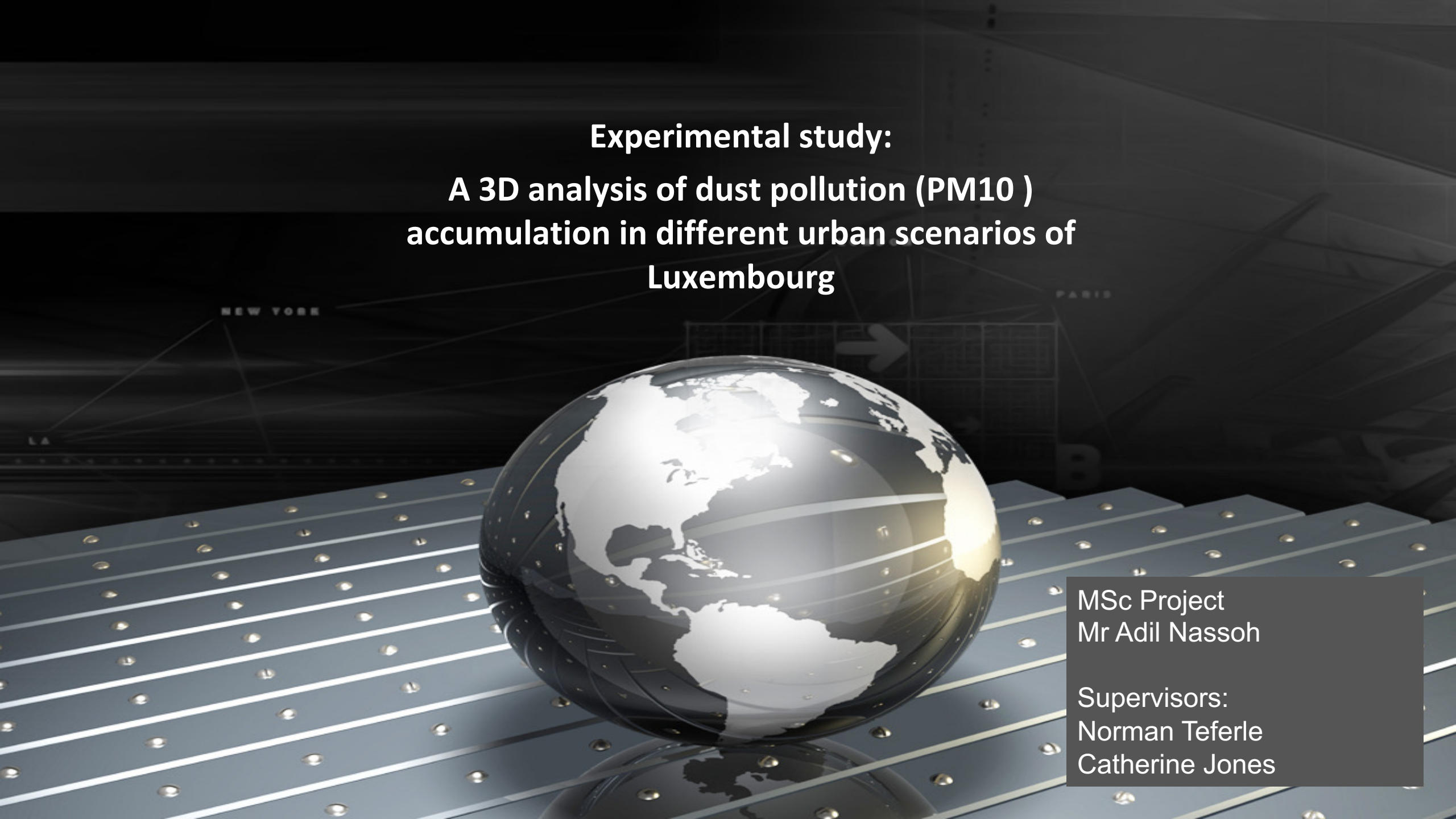

MSc Project
Mr Adil Nassoh

Supervisors:
Norman Teferle
Catherine Jones

Numerical Results

The **shading** renderer draws gradation on a specified section expressing the distributions of the wind speed, the concentration of diffusion materials *(Environmental GIS Laboratory 2018).*

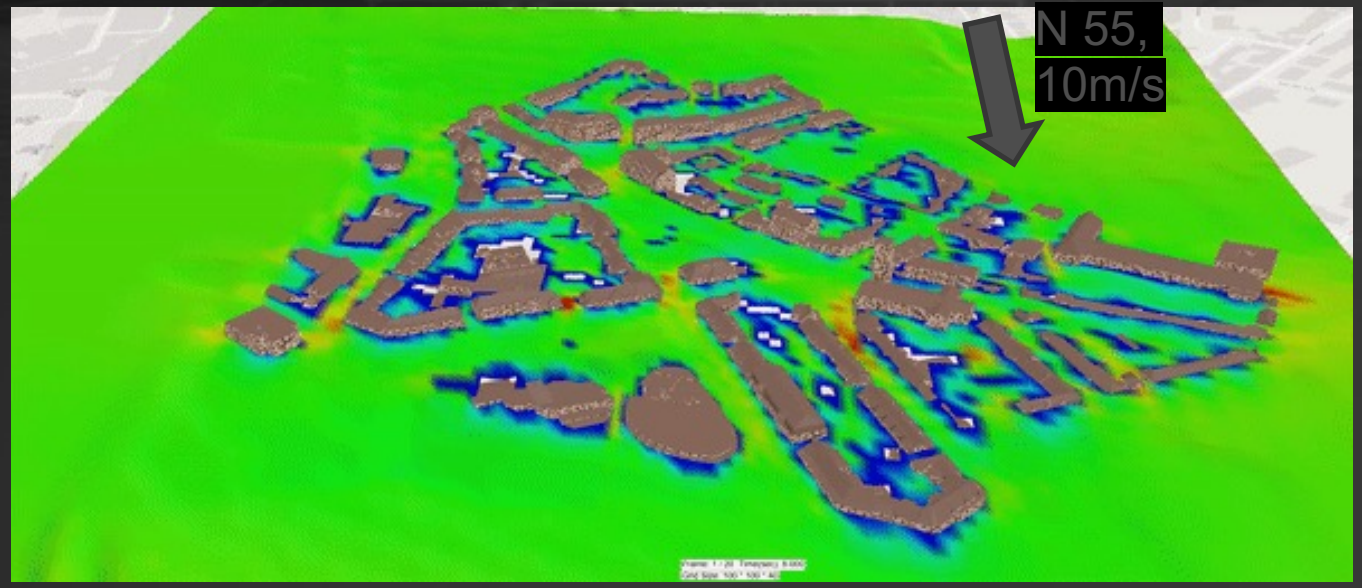

Figure 12 : Bonnevoie study area, North 55 direction and 10 m/s wind speed.

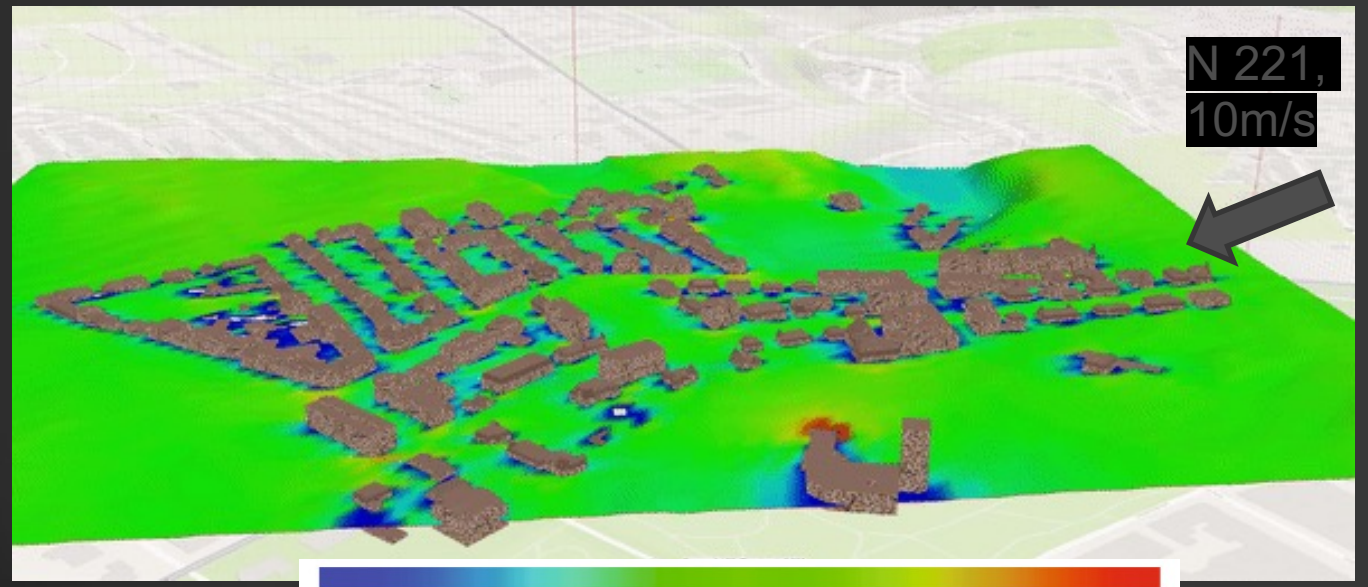

Figure 13: Place d'etoile study area, North 221 direction and 10 m/s wind speed.

Numerical Results

The **particle trace** renderer displays the trajectories of virtual particles that are released from arbitrary points in the computational grid *(Environmental GIS Laboratory 2018).*

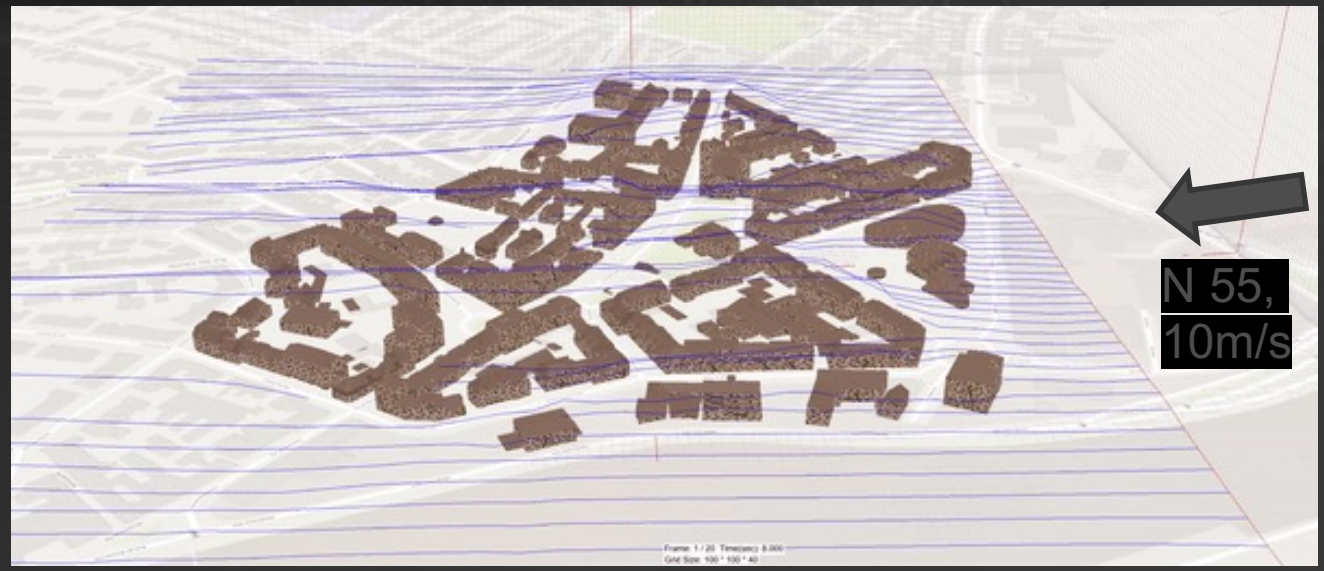

Figure 16: Bonnevoie study area, Nord 55 direction and 10 m/s wind speed.

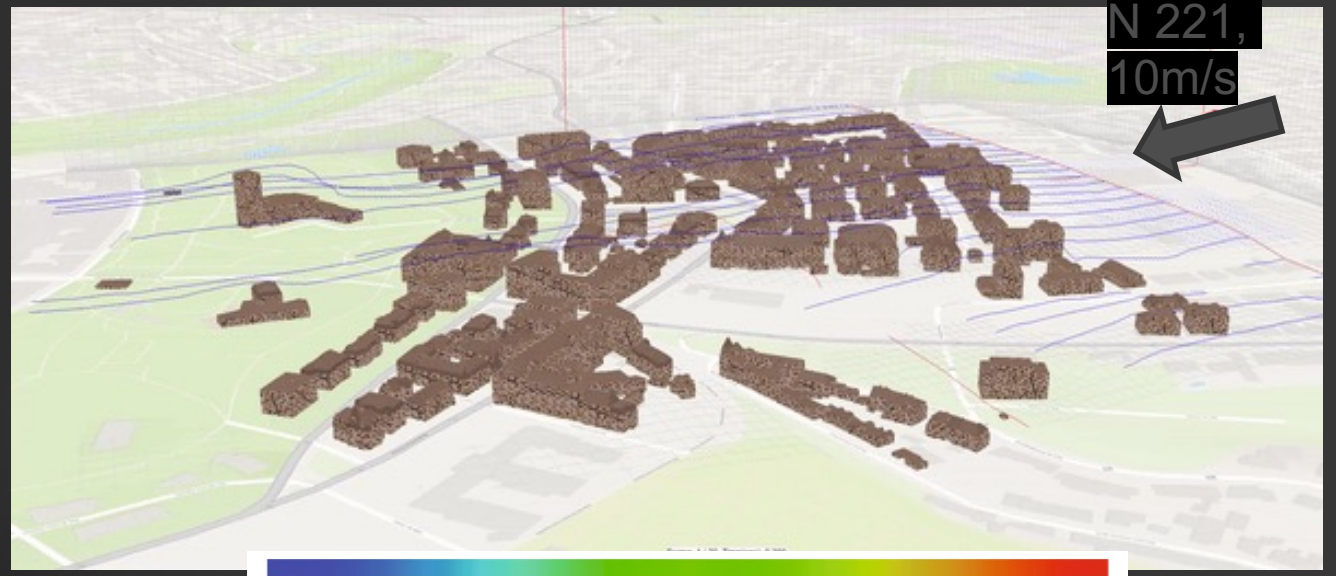

Figure 17 : Place d'etoile study area, Nord 221 direction and 10 m/s wind speed.

Discussion & Analysis

- Analysis of the results of the Airflow Analyst tool, based on meteorological conditions, urban form and air pollution.

Figure 20: Map displaying the possible wind accumulation scenarios in the Bonnevoie zone which is under the coverage of the telemetry station (Air quality station).

Figure 21: Map displaying the possible wind accumulation scenarios in the Churchill square zone which is under the coverage of the telemetry station (Air quality station).

Geodesy and Geospatial Engineering

GNSS & Positionning

Earth Observation

Reality Capture

Data Science, Informatics

Selected Collaborating and Supporting Institutions

University of Waterloo
USC
Fondazione Bruno Kessler
UNSW Australia
RMIT University
NYU
Karabük Üniversitesi
Universidade de Vigo
WAT
Le Gouvernement du Grand-Duché de Luxembourg – Administration du cadastre et de la topographie
UTIG
Leica Geosystems
DigitalGlobe Foundation
The University of Memphis – Center for Earthquake Research and Information
AIUB
RSS-Hydro
Le Gouvernement du Grand-Duché de Luxembourg – Ministère de l'Agriculture, de la Viticulture et du Développement rural
RWTH Aachen University
DigitalGlobe – A MAXAR COMPANY
TU Delft
Wrocław University of Environmental and Life Sciences
University of Nottingham – UK | CHINA | MALAYSIA
Luxembourg Institute of Science and Technology
LIST
ETH zürich
National Oceanography Centre – Natural Environment Research Council
GFZ Helmholtz-Zentrum Potsdam
cnes – Centre National d'Études Spatiales
Wuhan University
UCD Dublin
Fonds National de la Recherche Luxembourg
Chalmers University of Technology
FARO
British Antarctic Survey
Trimble
UCL
Bentley – Sustaining Infrastructure
PCI Geomatics
Hexagon Geosystems
MeteoLux
uni.lu – Université du Luxembourg

Belval goes Vegas !!!
or Maison du Savoir's Most Famous Moment

The results of our Reality Capture Exercise at Campus Belval where shown during Jürgen Dold's (CEO Leica Geosystems) Keynote at HxGnLive conference, Las Vegas, 2017.

Thank you for your attention!